2024-06-24

Brain Magnetic Resonance Spectroscopy: Advances and Applications to Chronic Pain in Knee Osteoarthritis

Leech, Samantha

UNIVERSITY OF CALGARY

Brain Magnetic Resonance Spectroscopy: Advances and Applications to Chronic Pain in Knee Osteoarthritis

by

Samantha Leech

A THESIS

SUBMITTED TO THE FACULTY OF GRADUATE STUDIES

IN PARTIAL FULFILMENT OF THE REQUIREMENTS FOR THE

DEGREE OF DOCTOR OF PHILOSOPHY

GRADUATE PROGRAM IN BIOMEDICAL ENGINEERING

CALGARY, ALBERTA

JUNE, 2024

Abstract

This dissertation investigates advancements in brain proton magnetic resonance spectroscopy (^{1}H-MRS) measures and their application to chronic pain in knee osteoarthritis. ^{1}H-MRS measures proton signals, which can be converted into absolute concentrations using the properties of water, brain tissue, and neurochemicals. These concentrations serve as markers of brain health or dysfunction. Current methods to quantify absolute neurochemical concentrations assume an equal distribution of neurochemicals between white matter (WM) and gray matter (GM), an assumption not thoroughly examined. To address this, I determined the distribution of six neurochemicals between WM and GM to establish correction factors to replace assumptions with calculated values. After validation using an independent dataset, I created an open-source tool to implement the calculated correction factors, improving ^{1}H-MRS accuracy by 30-55%.

I used quantitative synthetic imaging to measure water properties — relaxation rates (T1 and T2) and proton density (PD) — in different brain tissues of healthy adults. I assessed the impact of inter-individual differences in T1, T2, and PD on neurochemical concentration measures by comparing concentrations calculated using literature-based constants (as is typically performed) to concentrations calculated using individual measures from quantitative maps. In a young, healthy population, individual measures contributed to subtle yet significant variations in calculated neurochemical concentrations, suggesting that using uniform literature values may not be accurate for every individual. Sensitivity analyses indicated that these inaccuracies are likely greater across a wider age range or in individuals with clinical disorders.

Applying ^{1}H-MRS, I identified potential neurochemicals and brain regions associated with chronic pain in knee osteoarthritis to understand the brain's role in this condition. Knee osteoarthritis is a leading cause of chronic pain, with limited research on the specific

neurochemicals and brain regions involved. I compared neurochemical levels and their association with pain measures in four brain regions between patients with knee osteoarthritis and healthy controls as well as longitudinally in patients three months after total knee replacement surgery. I found opposing relationships in brain regions associated with pain's sensory and affective dimensions.

This dissertation enhances the accuracy of neurochemical concentration quantification and refines the understanding of the brain's contribution to knee osteoarthritis pain.

Preface

Chapter 1: A general introduction of the motivation, problem, hypotheses, and outline of this dissertation.

Chapter 2: A literature review of the relevant topics associated with this dissertation.

Chapter 3: A manuscript-based research chapter on developing tissue correction factors for improved accuracy of ^{1}H-MRS concentration measures. This chapter was submitted for publication in *Magnetic Resonance in Medicine*.

Chapter 4: This manuscript-based chapter measures water parameters in different brain tissues using quantitative synthetic imaging to quantify individually measured constants necessary for tissue correction. This chapter will be submitted to the *Journal of Magnetic Resonance Imaging* for publication.

Chapter 5: This manuscript-based research chapter applies ^{1}H-MRS to determine neurochemical alterations associated with pain in patients with knee osteoarthritis. This chapter will be submitted to *PAIN* for publication.

Chapter 6: A general discussion synthesizes the studies present in the context of this field of research and future directions that can build on this dissertation.

Acknowledgements

Completing this doctoral thesis would not have been possible without the support and guidance from numerous individuals. First and foremost, I extend my deepest appreciation to my co-supervisors, Dr. Ashley Harris and Dr. Sarah Manske, whose mentorship and encouragement have been instrumental throughout this four-year endeavor. Their willingness to embrace a civil engineering student's curiosity about brain imaging speaks volumes of their dedication to fostering interdisciplinary learning. Dr. Harris and Dr. Manske not only facilitated my transition into the realm of biomedical engineering but also granted me the autonomy to explore and lead my research endeavors. Their trust in my abilities has empowered me to evolve as a researcher and instilled a newfound confidence in my skills.

To my supervisory committee, Dr. Jeffrey Dunn and Dr. Richard Ng, thank you for graciously engaging with my work and consistently offering new and insightful perspectives.

To my esteemed co-collaborator, Dr. Paul Mullins, your generosity in sharing your expertise and insights has been invaluable, and your visit to Calgary remains a highlight of my graduate journey.

To the postdoctoral fellows with whom I've had the privilege of collaborating and learning from over the past four years: Dr. Tiffany Bell, I am deeply grateful for your willingness to work through challenges with me and for your patience in imparting your expertise in spectroscopy and beyond. Dr. Marilena DeMayo, thank you for always lending a listening ear and for being my steadfast companion during those early morning MRI scans. Dr. Justin Tse and Dr. Kirsten Bott, I extend my gratitude for your thoughtful feedback on scholarship applications and presentations. Each of you has played a significant role in my academic journey, and for that, I am truly thankful.

Graduate school would not have been the same without the support of my lab mates, who have not only been colleagues but also dear friends. To Hanna Bugler, Dr. Kate

Godfrey, Kayla Millar, Mehak Stokoe, Charley Hasselaar, Tadiwa “H” Waungana, Yousif Al-Khoury, Dr. Michael Kuczynski, Oyinda Oduba, Justen Saini, and Rachel Klassen – your encouragement and insightful feedback on my work have been invaluable. Thank you.

Special thanks to Lydia Cho and Dr. Parker La for being exceptional office mates. Parker, your provision of snacks and food deliveries during the intense periods of thesis writing quite literally fueled the completion of this dissertation. Additionally, I would like to thank the people who make Calgary home: Daphne Kaketsis and Dr. Ainsley Smith, my closest friends and unwavering supporters whom I met during graduate school. Their presence and support have made my time in Calgary truly memorable, and their encouragement has served as a constant source of motivation.

Thank you to Elder Doreen Spence, Elder Florence Kelly, Elder Roy Bear Chief, Dr. Pamela Roach, Dr. Lindsay Crowshoe, Holly Logan, Katrina Fras, and other members of the Indigenous Health Program and the Indigenous Primary Health Care and Policy Research (IPHCPR) Network for your support throughout graduate school. I am extremely grateful for the opportunities provided through these programs which have been fundamental to my growth personally and professionally.

Finally, thank you to my family – especially my parents, brother, and grandma – for your unwavering belief in me and constant encouragement.

To every individual who has played a part, no matter how big or small, in shaping my doctoral journey, I offer my sincerest appreciation. Your contributions have left a lasting mark, and for that, I am truly grateful.

Table of Contents

List of Tables

List of Figures

List of Abbreviations

Imaging Modalities and Neuromodulation Techniques

EEG	Electroencephalography
fMRI	Functional magnetic resonance imaging
^{1}H-MRS	Proton magnetic resonance spectroscopy
MR	Magnetic resonance
MRI	Magnetic resonance imaging
PET	Positron emission tomography
TMS	Transcranial Magnetic Stimulation
tDCS	transcranial Direct Current Stimulation

Spectroscopy Parameters and Acquisitions

CSDE	Chemical shift displacement errors
T1	Longitudinal relaxation time
T2	Transverse relaxation time
LASER	Localization by Adiabatic Selective Refocusing
NEX	Number of excitations
PRESS	Point RESolved Spectroscopy
RF	Radiofrequency
sLASER	Semi Localization by Adiabatic Selective Refocusing
SNR	Signal to noise ratio
STEAM	Stimulated Echo Acquisition Mode
TE	Echo time
TR	Repetition time

Pain-Related Terminology

CPM	Conditioned pain modulation
CPT	Cold pressor tolerance
IASP	International Association for the Study of Pain
MTS	Mechanical temporal summation
PPT	Pain pressure threshold
QST	Quantitative sensory testing

Neurochemicals

GABA	γ-aminobutyric acid
Glu	Glutamate
Glx	Glutamate + glutamine
Myo	Myoinositol
tCho	Total choline (choline + phosphocholine + glycerophosphocholine)
tCr	Total creatine (creatine + phosphocreatine)
tNAA	Total N-acetyl aspartate (N-acetylaspartate + N-acetyl-aspartyl-glutamate)

Medical and biological terminology

GM	Gray matter
KOA	Knee osteoarthritis
OA	Osteoarthritis
PD	Proton density
WM	White matter

Statistical Terminology

n	Sample size
p	P-value
IQR	Interquartile range
SD	Standard deviation
R	Correlation coefficient
R^2	Coefficient of determination

Units, symbols, and other

kg	Kilograms
cm	Centimetres
3D	Three-dimensional
L	Liters
mol	Moles
mmol	Millimoles
s	seconds
ppm	Parts-per-million
Hz	Hertz
α	Tissue correction factor
T	Tesla

CHAPTER ONE

※

Introduction

Chapter 1: Introduction

1.1 Motivation

Knee osteoarthritis (KOA), a prominent source of chronic pain worldwide (Neogi, 2013), poses challenges in pain management. Even after total knee arthroplasty (TKA), a common surgical intervention and final treatment option for advanced KOA, 15-40% of patients continue to report unresolved pain (Beswick et al., 2012; Bourne et al., 2010; Werner & Kongsgaard, 2014). Interestingly, pain severity shows poor association with structural knee damage (i.e., tissue damage shown on x-ray) (Cooper et al., 2000; Dieppe et al., 1997; Hannan et al., 2000). Emerging evidence suggests that this disparity between the extent of knee damage on x-ray and reported pain levels indicates that central (brain-driven) mechanisms may amplify KOA pain (Clauw & Hassett, 2017). As detected by proton magnetic resonance spectroscopy (^{1}H-MRS) in other chronic conditions (Fayed et al., 2010; Jung et al., 2021; Peek et al., 2020; Pomares et al., 2020), altered brain chemistry may be associated with dysfunctional pain processing in the brain (Foerster et al., 2012; Petrou et al., 2012; Z. Zhang et al., 2022). However, there is limited research on neurochemistry and pain in KOA. The complex nature of KOA pain makes it extremely difficult to develop effective pain management strategies.

^{1}H-MRS is the only method to measure multiple neurochemicals simultaneously, non-invasively, and without ionizing radiation. While innately quantitative, ^{1}H-MRS measures throughout the literature are reported in a variety of units, including signal ratio to a reference signal (typically creatine or water), or absolute concentrations in either molal (mmol/kg) or molar (mmol/L) units. While consensus recommendations in the field have attempted to standardize quantification methods and reporting (Near et al., 2021), the current recommended quantification model cannot be used to its fullest potential due to additional

variables that affect the quantification but are currently unaccounted for (Charles Gasparovic et al., 2018). Specifically, a correction factor that accounts for the differences in neurochemical concentrations between white matter (WM) and gray matter (GM) has yet to be explicitly determined and recommended for use. Consequently, researchers implicitly assume an equal distribution of neurochemicals in GM and WM, despite acknowledged differences. Additionally, the impact of inter-individual differences in constants for relaxation rates (T1 and T2) and proton density (PD) in the different tissue compartments of the brain (GM, WM, and cerebral spinal fluid, CSF) have yet to be determined. The use of various T1, T2, and PD constants from the literature may impact results across studies. For improved measurement accuracy and consistency, there is a need to establish tissue correction factors and determine if inter-individual differences in constants provide more accurate measures of absolute ^{1}H-MRS neurochemical concentrations.

1.2 Objectives

The motivating hypothesis of this dissertation is that the investigation of neurochemical alterations using ^{1}H-MRS can provide insight into the mechanisms and potential therapeutic targets for chronic pain in KOA. In parallel, I hypothesized that advancements in ^{1}H-MRS can lead to more accurate measures. As such, advanced ^{1}H-MRS methods were developed to apply in future studies of chronic pain. The following specific objectives address these hypotheses:

Objective 1 (Chapter 3): Establish correction factors (α) that address differences in neurochemical concentrations between WM and GM to improve the accuracy of ^{1}H-MRS concentration measures.

a. **Determine the distribution of neurochemicals between WM and GM in the brain:** Use ^{1}H-MRS in multiple brain regions with varying tissue compositions to determine the ratio of neurochemical concentrations between GM and WM, referred to as α, for six key neurochemicals in a healthy population.

b. **Validate correction factors for each neurochemical, using an independent dataset:** Verify the effectiveness of removing tissue dependencies with the correction factors (established in Objective 1a) by applying them to an independent dataset of healthy controls and comparing the corrected neurochemical concentrations with conventional estimates.

c. **Analyze the effects of different correction factors on neurochemical concentration estimates:** Calculate percent errors to investigate the impact of using different correction factors on the accuracy of neurochemical concentration estimates obtained from ^{1}H-MRS data, to assess the magnitude of improvement over conventional methods.

d. **Develop an open-source tool** to implement these correction factors for standardizing neurochemical concentration quantification.

Objective 2 (Chapter 4): Use quantitative synthetic imaging to measure individualized T1 and T2 relaxation rates, and proton density (PD) for improved ^{1}H-MRS quantification.

a. Determine the impact of inter-individual differences in T1, T2, and PD: Compare concentration measures quantified using individual in vivo T1, T2, and PD constants, obtained from each individual's quantitative T1, T2, and PD maps, with those quantified using literature values for T1, T2, and PD.

b. **Evaluate the impact of tissue relaxation constants on neurochemical quantification accuracy:** Perform variance-based sensitivity analyses to assess

the overall impact of varying ranges of T1, T2, and PD on concentration measures.

Objective 3 (Chapter 5): Identify neurochemical contributions to chronic pain in knee osteoarthritis using ^{1}H-MRS.

a. **Cross-sectional associations:** Determine whether neurochemical levels, measured using ^{1}H-MRS, are associated with measures of centralized pain (using quantitative sensory testing and questionnaires) in females with KOA and whether these differ from age-matched participants without KOA.
b. **Longitudinal associations:** Determine whether changes in neurochemical concentrations, measured using ^{1}H-MRS, change following TKA and whether these changes are associated with improvements in centralized pain following TKA in females with KOA.

1.3 Thesis Outline

This manuscript-based thesis consists of six chapters, three of which are manuscript-based and have either been published or are in the process of being published. **Chapter 1** introduces the motivation, knowledge gaps this thesis addresses, objective, outline, and contributions. **Chapter 2** provides background information on relevant topics and a review of current literature related to this thesis. **Chapter 3** describes the development of tissue correction factors for improved accuracy of ^{1}H-MRS concentration measures. This is the first report on whole brain correction factors for commonly measured neurochemicals and is accompanied by the first open-source tool to implement consensus-recommended tissue correction methods. This chapter was submitted for publication in *Magnetic Resonance in Medicine*. **Chapter 4** describes the analysis of the properties of water in different brain using quantitative synthetic MRI. This study applies individually measured T1, T2, and PD constants to quantify neurochemical concentrations (as opposed to mean literature values being applied to the entire sample) and assessed the impact of these constants on concentration measures. This is the first report of exploring the application of quantitative synthetic MRI for improved ^{1}H-MRS quantification. This chapter is in preparation for submission to the *Journal of Magnetic Resonance Imaging*. **Chapter 5** describes the application of ^{1}H-MRS to determine neurochemical alterations associated with pain in patients with knee osteoarthritis. This is the first report of single voxel ^{1}H-MRS acquired from multiple brain regions to study neurochemical alterations in KOA pain. Additionally, this is the first report of neurochemical associations with multiple centralized pain-related measures (i.e., multiple sensory tests and questionnaires asking about widespread pain rather than just localized knee pain). This chapter is being prepared for submission to *PAIN*. **Chapter 6** discusses the three studies presented in this thesis, emphasizes how this work has contributed to the field, recommends future directions, and final conclusions.

1.4 Contributions

Listed below are the published works I contributed to during the completion of this thesis.

1. **Leech SA**, Khaira A, Epp S, Schneider G, Werle J, Ng R, Harris AD, Manske SL. (2024). "Demographic, pain, and quality of life factors in unilateral and bilateral total knee arthroplasty: a population-based retrospective cohort study of 23,033 patients". *Journal of Science and Medicine*. https://doi.org/10.37714/josam.v4i1.114
2. **Leech, SA.** (2024). Magnetic Resonance Spectroscopy Absolute Concentration Quantification - Alpha Tissue Corrections. *Zenodo*. https://doi.org/10.5281/zenodo.10840451
3. **Leech SA**, Bell TK, Manske SL, Mullins PG, Harris AD. (2024). 1822 - Rethinking Neurochemical Distributions in White Matter and Grey Matter: Considerations for Improved Magnetic Resonance Spectroscopy Measures. *Proceedings of the International Society of Magnetic Resonance in Medicine*. Singapore. (May 4 – 9, 2024).
4. **Leech SA**, DeMayo MM, Bell TK, Batuyong E, Clark M, Schneider G, White N, Millar K, Hasselaar C, Ng R, Manske SL, Harris AD. (2024). 1827 - Investigating Cortical Neurochemical Concentrations in Painful Knee Osteoarthritis using Magnetic Resonance Spectroscopy. *Proceedings of the International Society of Magnetic Resonance in Medicine*. Singapore. (May 4 – 9, 2024).
5. **Leech SA**, DeMayo MM, Bell TK, Batuyong E, Clark M, Schneider G, White N, Millar K, Hasselaar C, Ng R, Harris AD, Manske SL (2024). 731 - Neurochemical Concentrations in the Brain in Knee OA using Magnetic Resonance Spectroscopy. *Osteoarthritis and Cartilage*, *32*, S502–S502. https://doi.org/10.1016/j.joca.2024.02.746

6. **Leech SA**, DeMayo MM, Bell TK, Ng R, Batuyong E, Clark M, Schneider G, White N, Hasselaar C, Manske SL, Harris AD. (2023). "Exploring the Role of GABA and Glutamate in Knee Osteoarthritis Pain". *Proceedings of the International Symposium on GABA and Advanced Magnetic Resonance Spectroscopy*. Bergen, Norway. (September 13 – 15, 2024).
7. **Leech SA**, Bell TK, Manske SL, Mullins PG, Harris AD. (2022). "Tissue effects on neurochemical quantification using single voxel magnetic resonance spectroscopy". *Proceedings of the Alberta Biomedical Engineering Conference*. (https://schulich.ucalgary.ca/sites/default/files/teams/1/23rd%20AB%20BME%20Conference%202022%20Long%20Program%20(1).pdf).
8. Manske SL, Khaira A, Epp S, **Leech SA**, Schneider G, Werle J, Ng R, Harris AD. (2021). "Pain outcomes following total knee replacement". *Osteoarthritis and Cartilage*. https://doi.org/10.1016/j.joca.2021.02.317.
9. **Leech SA**, Khaira A, Epp S, Schneider G, Werle J, Ng R, Harris AD, Manske SL. (2021). Pain outcomes in unilateral vs bilateral total knee arthroplasty patients. *Proceedings of the Canadian Arthritis Research Conference*. (https://arthritis.ca/getmedia/a194718a-2ce6-47ce-83b9-37c888c86ff6/CARC_PosterSession_Booklet_Feb10B_2021.pdf).
10. **Leech SA**, Desy NM, Ng R, Werle J, Schneider G, Manske SL, Harris AD. (2021). Protocol Development: Brain Spectroscopy and Quantitative Sensory Testing for Chronic Pain in Knee Osteoarthritis. *Proceedings of the Alberta Biomedical Engineering Conference.*

CHAPTER TWO

※

Literature Review

Chapter 2: Literature Review

2.1 Knee Osteoarthritis

Osteoarthritis (OA) is a degenerative joint disease, characterized by structural alterations in the articular cartilage, subchondral bone, ligaments, capsule, synovial membrane, and periarticular muscles. The knee is the most common site of OA. Pain is the dominant symptom that most often drives knee osteoarthritis (KOA) sufferers to seek medical attention (Neogi, 2013). Although cartilage loss is a fundamental component of OA, cartilage does not contain nerves. Thus, any pain associated with cartilage thinning is likely due to irritation of surrounding structures that are innervated (Morgan et al., 2022).

X-ray imaging is used for the diagnosis of KOA to identify the presence of peripheral tissue damage; however, the degree of damage shown on imaging is poorly associated with pain severity (Cooper et al., 2000; Dieppe et al., 1997; Hannan et al., 2000). Thus, KOA is also diagnosed based on symptoms such as pain, brief morning stiffness, functional limitations, and a physical examination that identifies popping or clicking joint sounds, restricted or painful movement, joint tenderness, and/or joint enlargement.

Treatments for KOA primarily include exercise, analgesics, and joint replacement surgery. Exercise therapy has been shown to significantly reduce pain when therapeutic goals focus on improving aerobic fitness, range of motion, strength, and reducing the risk of falls (Sharma, 2021). Analgesics (e.g., paracetamol, glucosamine sulphate, chondroitin sulphate, oral and topical nonsteroidal anti-inflammatory drugs (NSAIDs), steroid injections, and opioids) have small effect sizes on pain reduction (Bjordal et al., 2006; W. Zhang, 2004). Total knee replacement surgery, or total knee arthroplasty (TKA), provides adequate symptom relief in 60-85% of patients (Lewis et al., 2015; Werner & Kongsgaard, 2014) and is the last resort in treating OA. Therefore, TKA is typically reserved for patients who continue to experience chronic pain and functional limitations despite having exhausted other

non-surgical treatment options (Varacallo et al., 2022). The lack of a universally effective treatment for pain management in osteoarthritis demonstrates the need to better understand the mechanisms underlying osteoarthritis pain to provide evidence towards potential mechanism-tailored treatment targets (Clauw & Hassett, 2017; Hansson, 2002; Phillips & Clauw, 2011).

2.2 Mechanisms of Osteoarthritis Pain

Pain is defined as "*an unpleasant sensory and emotional experience associated with, or resembling that associated with, actual or potential tissue damage*" (International Association for the Study of Pain, 1994). However, this subjective, conscious experience is not always directly related to nociception (the body's process of detecting and signaling potential tissue damage) and does not always serve a protective function. As such, pain is difficult to assess, investigate, manage, and treat (Tracey & Mantyh, 2007). This is especially evident in OA, which has been described as a "mixed" pain state with both peripheral and central contributions (Clauw & Hassett, 2017). In OA, peripheral damage does not consistently correlate with pain severity, as evidenced by reports of severe pain in individuals with minimal peripheral damage and vice versa (Clauw & Hassett, 2017). This, along with the inefficacy of peripherally acting pain treatments in OA, has prompted a shift in the study of chronic pain in OA to include investigations of centralized (brain-mediated) pain in OA, similar to that observed in fibromyalgia (Clauw & Hassett, 2017). Such pain conditions are characterized by prominent involvement of the central nervous system in pain processing, and are marked by hyperalgia (increased sensitivity to painful stimuli), reduced pain thresholds, multifocal pain (in multiple bodily regions), somatic symptoms (i.e., fatigue, poor sleep, memory problems), comorbid mood and anxiety disorders, all indicating heightened central nervous system processing (Clauw & Hassett, 2017).

2.3 Measures of Pain

It is widely accepted that pain assessment requires consideration of multiple dimensions of pain, including sensory, affective, and cognitive (Fillingim et al., 2016). Chronic pain is typically evaluated through medical history, clinical examination, questionnaires, and behavioural measures, where stimulus-independent pain is a common symptom (Davis et al., 2017). Yet, the gold standard for assessing pain continues to be self-report. It is important to recognize that pain and nociception are distinct phenomena; while nociception involves sensory neuron activity, pain is a subjective experience influenced by biological, psychological, and social factors, emphasizing the need for validated subjective assessment tools such as questionnaires. Quantitative sensory testing (QST) offers an objective means to assess pain sensation by measuring responses to specific stimuli, including mechanical, vibration, and temperature (Siao & Cros, 2003). QST tests, detailed in **Chapter 5**, specifically target centralized pain in OA.

2.3.1 Neuroimaging

Brain imaging techniques such as electroencephalography (EEG), functional magnetic resonance imaging (fMRI), and positron emission tomography (PET), have offered insight into pain mechanisms (Davis et al., 2017). Briefly, EEG, fMRI, and PET can monitor the sequence of activity across multiple brain structures (using electrodes), blood flow, and metabolism, respectively, in response to pain. Although there is no standardized method to diagnose pain, the need for imaging biomarkers of pain stems primarily from the need for new pain management therapeutics (Mao, 2009). While EEG, fMRI, and PET are employed to study pain processing and to understand pain pathophysiology to aid the development of new treatments, each method has its limitations. EEG and fMRI can spatially localize and measure the activity levels of pain-associated brain regions but lack neurochemical

information that could potentially identify treatment targets. PET can detect changes in glucose metabolism, blood flow, neurotransmitter activity, and receptor density, but requires a radioactive tracer injection and separate scans for each chemical of interest. Alternatively, proton magnetic resonance spectroscopy (^{1}H-MRS) is a non-invasive means to measure the chemical composition of brain regions. As the demand for brain imaging tests grows to enhance our understanding of pain mechanisms, challenges persist in creating imaging biomarkers due to individual differences in pain perception and the lack of specificity of pain-related brain regions (Davis et al., 2017).

The perception of pain involves the recruitment of multiple brain regions that integrate sensations, emotions, and cognition. These interconnected regions integrate nociceptive stimuli into a painful experience. The pain matrix was previously conceptualized to define pain-related brain regions in terms of lateral (sensory-discriminatory) and medial (affective-cognitive evaluative) neuroanatomical components. This division was based on the most active regions identified during acute pain, including the primary and secondary somatosensory cortices, insular cortex, anterior cingulate cortex, prefrontal cortices, and thalamus. However, this model is now understood to be oversimplified, as there is no single brain region exclusively dedicated to processing pain. Instead, pain processing involves the coordinated activity and influence of multiple brain regions, reflecting the interconnected nature of pain perception and its modulation throughout the brain (Tracey & Mantyh, 2007).

Despite this oversimplification, categorizing brain regions into sensory and affective components remains useful for understanding their general functions. Sensory regions of the brain (such as the somatosensory cortex and posterior insula) play a crucial role in integrating sensory information from various body regions (Brooks et al., 2005; Frot et al., 2013)). In contrast, affective brain regions (such as the anterior cingulate cortex and anterior insula)

integrate emotional and motivational information following sensory processing (Bushnell et al., 2013; Wiech & Tracey, 2009)).

Furthermore, several brain regions have been implicated in chronic pain. A meta-analysis of structural imaging studies highlights alterations primarily in brain regions associated with nociceptive processing, including the amygdala, thalamus, hippocampus, insula, anterior cingulate cortex, and inferior frontal gyrus (Henn et al., 2023). Furthermore, chronic pain treatment has been shown to induce changes in brain function and metabolism, potentially mitigating these alterations. fMRI studies have demonstrated decreased activity within regions such as the somatosensory cortex, thalamus, insula, and anterior cingulate cortex post-treatment, while PET studies have shown increased glucose uptake and blood flow within similar regions, both suggesting brain reorganization in response to treatment (Kim et al., 2021).

Neurochemical alterations in pain-related brain regions, as determined by ^{1}H-MRS, offer insights into chronic pain conditions. Studies have shown that elevated or depleted levels of neurochemicals such as total N-acetylaspartate (tNAA), total creatine (tCr), total choline (tCho), myoinositol (Myo), glutamate (Glu), glutamate + glutamine (Glx), and gamma-aminobutyric acid (GABA) in areas including the primary and secondary sensory cortices, insular cortex, and anterior cingulate cortex may indicate centralized pain (Foerster et al., 2012; Peek et al., 2020; Petrou et al., 2012; Z. Zhang et al., 2022). For example, greater glutamate levels and reduced GABA, myoinositol, and choline levels have been observed in the brains of fibromyalgia patients (Fayed et al., 2010; Jung et al., 2021; Pomares et al., 2020). Specific associations with pain including correlations between glutamate levels and pain severity/sensitivity in chronic low back pain and fibromyalgia (Cirstea, 2011; R. E. Harris et al., 2008, 2009), as well as negative correlations between GABA and pain severity in OA (Reckziegel et al., 2016), highlight the potential role of these neurochemicals in

chronic pain and suggest they may be treatment targets for managing chronic pain conditions such as OA.

2.4 Magnetic Resonance Spectroscopy (^{1}H-MRS)

2.4.1 Principles of Magnetic Resonance

When brain tissue is exposed to an externally applied magnetic field (B_0, in Tesla), protons within the tissue precess about the field at the Larmor frequency (f_0, in MHz) given by **Equation 2.1**, where the gyromagnetic ratio (γ) is a constant for the nuclear species of interest (e.g., for hydrogen $\gamma_H = 267.522 \ \frac{rad \cdot MHz}{T}$ for ^{1}H-MRS).

$$f_0 = \frac{\gamma}{2\pi} B_0 \tag{2.1}$$

In magnetic resonance (MR) experiments, a radiofrequency (RF) pulse (B_1) is applied to a defined volume of tissue to tip the net magnetization vector (the combined magnetic moment of all hydrogen nuclei aligned with the B_0) away from the direction of B_0. Once B_1 is removed, a RF signal can be detected as the net magnetization vector re-aligns with B_0 (a process called relaxation). This relaxation of the net magnetization vector from the transverse plane to the longitudinal axis causes regrowth of the vector's longitudinal component (T1) and decay of its transverse component (T2). T1 refers to the relaxation of the longitudinal component of the net magnetization vector, whereas T2 refers to relaxation of the transverse magnetization component. T1 and T2 weighting can be controlled by set parameters of repetition time (TR, used to define when the next RF pulse should be applied) and echo time (TE, defines the time between the RF pulse and the when the signal is sampled), respectively.

Imaging parameters, such as voxel size, TR, TE, and number of excitations (NEX) are chosen to optimize the trade-offs between spectral resolution, acquisition time, and neurochemical visibility. The signal-to-noise ratio (SNR) measures the contribution of detectable signal relative to noise in a spectrum.

2.4.2 ^{1}H-MRS versus MRI

^{1}H- MRS is a method to measure tissue chemistry using a standard MRI scanner. ^{1}H-MRS acquisitions are designed to measure the chemical composition of tissues rather than generate a structural MRI image. Both structural MRI and ^{1}H-MRS, however, are based on principles of proton nuclear magnetic resonance (NMR) which exploits the intrinsic spin properties of proton nuclei within tissues to gain information about the body. The proton nucleus is the most sensitive nucleus for NMR and produces the best SNR because of its high gyromagnetic ratio and high abundance in the body (>99.9%). In structural MRI, the imaging signal comes from water protons to generate an anatomical image. In single voxel ^{1}H-MRS, a tissue region of interest is selected, and the abundant water signal is suppressed since it is several orders of magnitude greater than the proton signals originating from low-concentration neurochemicals.

2.4.3 ^{1}H-MRS Theory

^{1}H-MRS records an electromagnetic signal in the time domain (i.e., amplitude vs time) called the free induction decay (FID). This signal is then converted to the frequency domain (i.e., amplitude vs frequency) via a mathematical function (Fourier Transformation) to generate a spectrum, as shown in **Figure 2.1**.

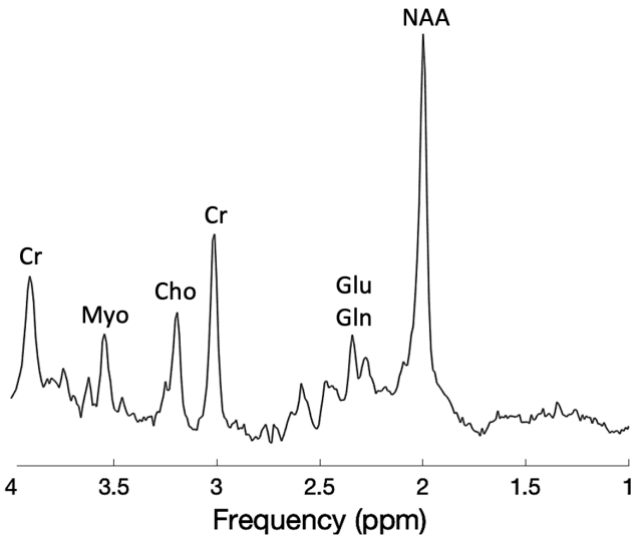

Figure 2.1 *Typical ^{1}H-MRS spectrum from a healthy human brain acquired at 3T (TE/TR = 0.035/3s). Prominent peaks show creatine (Cr), myo-inositol (Myo), choline (Cho), N-acetyl aspartate (NAA), glutamate (Glu), and glutamine (Gln).*

^{1}H-MRS is able to differentiate between different neurochemical signals because they occur at different frequencies due to chemical shifts. Chemical shifts occur due to electron shielding of the nuclei, causing slightly different resonance frequencies. Two otherwise identical nuclei will exhibit frequency differences within a spectrum because the measured resonant frequency experienced by the local field experienced by the nucleus (B_n) is reduced by an opposing magnetic field generated by the surrounding electron environment (B_e), in addition to the externally applied magnetic field (B_0), given by **Equation 2.2**. Thus, the resonant frequency of the nucleus is given by **Equations 2.3**.

$$B_n = B_0 + B_e \tag{2.2}$$

$$f = \frac{\gamma}{2\pi} B_n \tag{2.3}$$

Using these equations, frequency is dependent on external magnetic field strength (B_0), hindering comparison capabilities between other laboratories and studies. Thus, to remove the dependence of frequency on B_0, they are typically expressed in parts per million (ppm) relative a reference standard, as shown in **Equation 2.4**.

$$\delta = \frac{f - f_{reference}}{f_{reference}} \cdot 10^6 \quad (2.4)$$

Thus, in a spectrum, neurochemical peaks are identified by their characteristic frequency shifts (typically in ppm) relative to a frequency standard, which is am an internal reference signal from a neurochemical or compound that is present in the sample (voxel) and is used to calibrate the spectrum. While tetramethylsilane is widely accepted as having a frequency of 0 ppm, it is not found in vivo therefore it cannot be used as an internal reference. Thus, the methyl resonance of N-acetyl aspartate (2.01 ppm) is typically used as an internal reference for ^{1}H-MRS.

2.4.4 Voxel Localization

Point RESolved Spectroscopy (PRESS), Stimulated Echo Acquisition Mode (STEAM), and Localization by Adiabatic SElective Refocusing (LASER), as well as its preferred variation, semi-LASER (sLASER), are approaches to localize a single volume of interest (voxel) to acquire signal from high concentration neurochemicals using ^{1}H-MRS. The most commonly used localization approach to date is PRESS, in which voxel localization is achieved using three radio-frequency pulses (90°, 180°, 180°) with slice-selective gradients (a variation in magnetic field strength used to spatially encode signals) in three orthogonal planes. The overlapping area of the orthogonal planes defines the voxel for signal measurement, as shown in **Figure 2.2**.

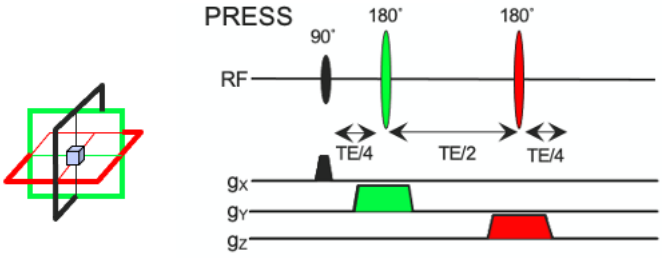

Figure 2.2 *PRESS single-voxel localization acquisition sequence consisting of a slice-selective 90° excitation pulse (black) and two 180° slice-selective refocusing pulses (green and red). Figure adapted from* (H. Zhu & Barker, 2011).

STEAM relies on a stimulated echo (signal produced from three RF pulses) following three 90° RF pulses (**Figure 2.3**). Although STEAM allows for the detection of short T2 neurochemicals because shorter TEs can be achieved, use of 90° pulses (as opposed to 180° refocusing pulses used in other localization methods) results in decreased refocusing and lower signal compared to spin-echo approaches (refocused signal produced from a 90° RF pulse followed by a 180° RF pulse).

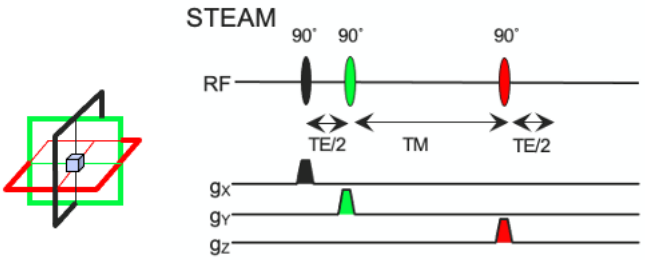

Figure 2.3 *STEAM single-voxel localization acquisition sequence consisting of three 90° slice-selective pulses with orthogonal localization gradients, shown in black, green, and red respectively. Figure adapted from* (H. Zhu & Barker, 2011).

LASER uses adiabatic pulses (a type of RF pulse that uniformly excites spins despite magnetic field inhomogeneities) that sweep through a range of frequencies by simultaneously modulating both amplitude and frequency. LASER uses a non-slice-selective adiabatic 90°

pulse for excitation and three pairs of 180° adiabatic refocusing pulses that are applied with orthogonal gradients for localization (**Figure 2.4**). The pairs of the adiabatic refocussing pulses are needed because a single 180° adiabatic pulse with a slice-selection gradient yields a large variation in phase. The second 180° adiabatic pulse within the pair cancels out the phase variation. However, the large number of RF pulses used in LASER results in high levels of power deposition in tissue.

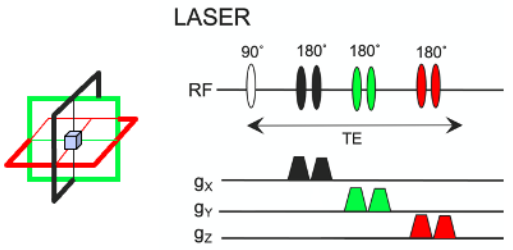

Figure 2.4 *LASER single-voxel localization acquisition sequence consisting of a 90° non-slice-selective adiabatic excitation pulse (white), followed by three pairs of adiabatic 180° refocusing pulses with localization gradients (black, green, and red). Figure adapted from* (H. Zhu & Barker, 2011).

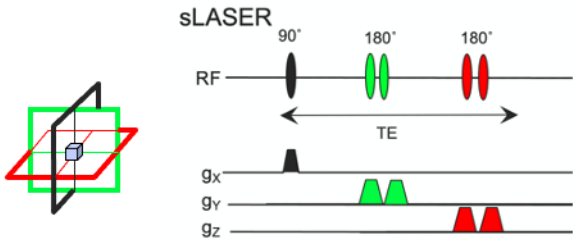

Figure 2.5 *sLASER single-voxel localization acquisition sequence consisting of a slice-selective 90° excitation pulse (black) and two pairs of adiabatic 180° refocusing pulses (green and red). Figure adapted from* (H. Zhu & Barker, 2011).

To address this problem, semi-LASER (sLASER), a simplified variation of LASER was developed. sLASER consists of a non-adiabatic, conventional 90° slice-selective pulse followed by two pairs of 180° adiabatic pulses for refocusing (**Figure 2.5**). The advantage of sLASER is the reduced chemical shift displacement errors (CSDE, misalignment of signals due to magnetic field variations), compared to PRESS, by producing a more uniform excitation profile due to the large bandwidths of the adiabatic pulses while maintaining a high SNR (H. Zhu & Barker, 2011) (**Figure 2.6**).

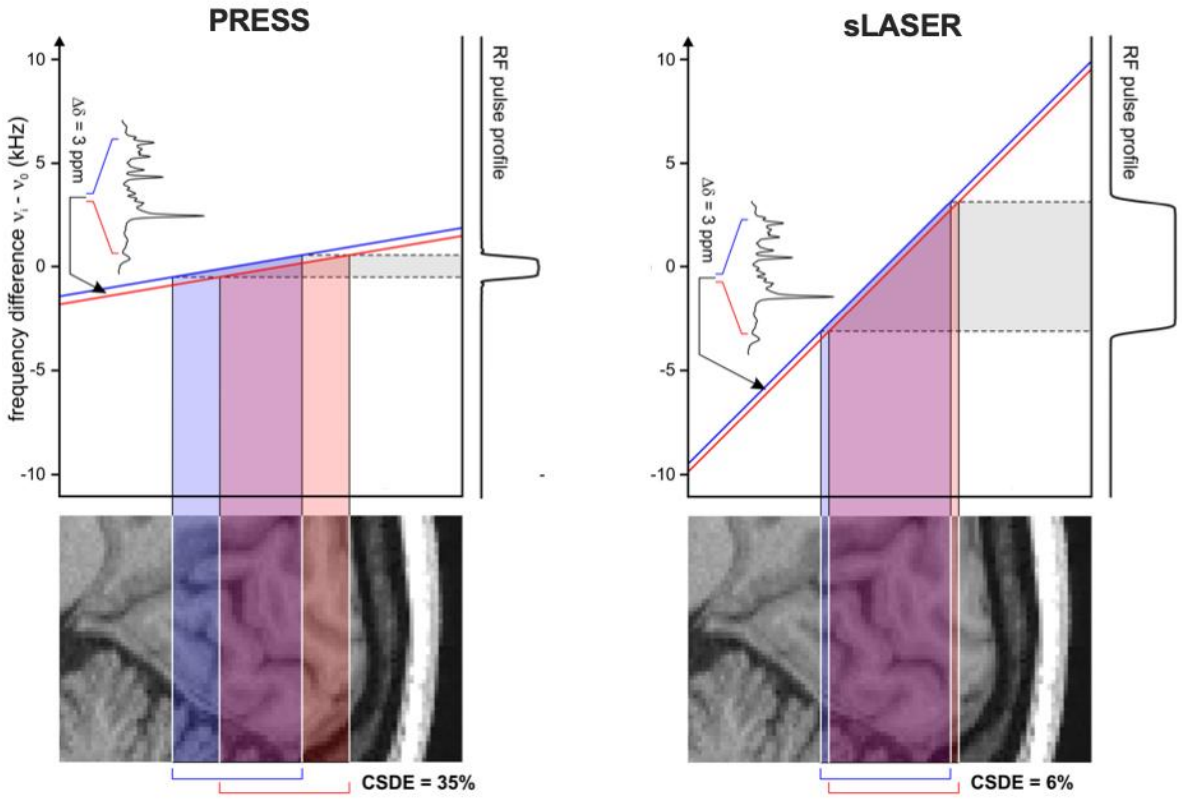

Figure 2.6 *Spatial dependences of resonance frequencies for two resonances separated by 3 ppm (blue and red lines) showing 35% chemical shift displacement effect (CSDE) per 3 ppm for a typical PRESS 180° pulse (left). The increased bandwidth of the adiabatic 180° pulse in sLASER reduces the CSDE to 6% per 3 ppm. Figure adapted from* (Öz et al., 2021).

2.4.5 Acquisition for Low Concentration Neurochemicals

To measure neurochemicals that exist in lower concentrations (and are overlapped by more abundant neurochemicals), spectral editing that relies on spin-spin coupling (e.g., MEGA as developed by Mesher and Garwood) is used to remove the overlapping peaks. MEGA is then paired with a localization approach, most typically PRESS. To measure GABA, MEGA-PRESS specifically aims to isolate the GABA peak at 3 ppm which is overlapped by a large creatine peak. Because the GABA peak at 3 ppm is coupled to the peak

at 1.9 ppm and the 3 ppm creatine peak is not, a frequency selective editing pulse applied at 1.9 ppm will modulate the 3 ppm GABA peak without influencing the creatine. This is referred to as the "Edit-On" spectrum. An "Edit-Off" spectrum is also acquired where no editing pulse is applied, and the GABA peak is unaffected (in fact, an editing pulse is applied but far away from the portion of the spectrum being analyzed and any coupled resonances). A difference spectrum is then obtained by subtracting the "Edit-Off" spectrum from the "Edit-On" spectrum, resulting in the removal of the creatine signal (**Figure 2.7)**.

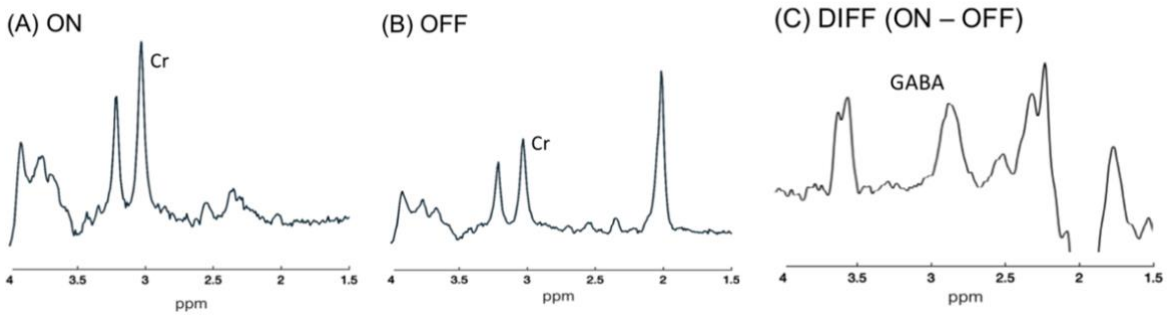

Figure 2.7 *(A) MEGA-PRESS "Edit-On" spectrum with editing pulse applied at 1.9 ppm (ON). (B) MEGA-PRESS "Edit-Off" spectrum (with an editing pulse applied far away). (C) Difference spectrum obtained by subtracting the "Edit-Off" spectrum from the "Edit-On" spectrum. Figure adapted from* (Tiffany Kay Bell et al., 2019).

There are macromolecules (i.e., large molecules such as lysine and arginine) with coupled peaks at 1.7 ppm and 3 ppm. Because the MEGA-PRESS editing pulse applied at 1.9 ppm is not perfectly selective, the GABA peak is contaminated by macromolecules. Specifically, approximately 45% of the GABA signal acquired using MEGA-PRESS is signal from macromolecules. To achieve a more specific GABA signal without macromolecule contamination, macromolecule-suppressed GABA editing can be used. This method places the "Edit-Off" pulse at 1.5 ppm, symmetrically about the macromolecule peak at 1.7 ppm. In

this approach, the macromolecules at 1.7 ppm are equally modulated by the ON and OFF editing pulses thus in the difference spectrum they are removed.

2.4.6 Quantification

The area under the spectral peak of a neurochemical is proportional to the neurochemical's concentration. To analyze a spectrum, the most common approach is linear combination modelling. In this approach, a model spectrum of each individual neurochemical in the data, is scaled and combined to best model the raw data (**Figure 2.8**).

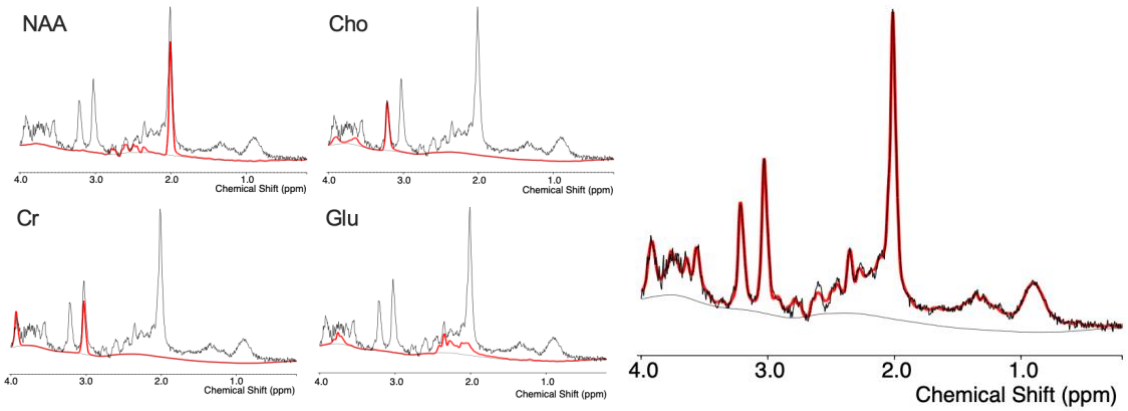

Figure 2.8 *Models for individual neurochemicals present in the data (left figure in red) are scaled to fit the raw data (black). These sub-spectra are then summed to achieve a model of the raw spectrum (right).*

In the past, ^{1}H-MRS studies have typically presented neurochemical data as ratios relative to a reference, often creatine or the unsuppressed water signal. These ratios provide insight into neurochemical differences, yet they pose limitations for comparing changes across subjects and studies because it is unclear which part of the ratio is varying—the neurochemical of interest or the reference (Near et al., 2021). To overcome this challenge, absolute concentrations can be quantified using an unsuppressed water signal and several parameters of water, including the concentration of water in tissue and different tissue-

specific effects of relaxation. Concentrations can be expressed in molarity (moles of neurochemical and water per volume of tissue) or molality (moles of neurochemical per kg of water). Reporting concentration in units of molality is advantageous as it can be reported independent of the following considerations: temperature, barometric pressure, and the contributions of other compounds. As such, the derivation of the established equation that quantifies concentrations (in units of molality) by accounting for tissue-specific properties is presented in **Appendix A**.

CHAPTER THREE

※

Tissue Effects on Neurochemical Concentrations

Chapter 3: Tissue Effects on Neurochemical Concentrations

This chapter is being presented as a journal submission:

> **Leech SA**, Bell TK, Serrano Huaman R, Manske SL, Mullins PG, Harris AD. *Considerations for Improved Partial Volume Correction of ^{1}H-MRS Data during Absolute Quantification.*

Conceptualization, study design, data analysis, and write-up of this chapter was completed by the lead author, with support from co-authors.

There may be some overlap with materials and methods presented in previous chapters.

Supplementary tables and figures for this chapter are presented in **Appendix A**.

3.1 Abstract

Purpose: To improve the accuracy of estimates of brain neurochemical concentrations using proton magnetic resonance spectroscopy (^{1}H-MRS) by developing a tissue correction factor (α) that accounts for differences in neurochemical concentrations between gray matter (GM) and white matter (WM).

Methods: A revised tissue correction equation was proposed to minimize tissue fraction dependencies. Human ^{1}H-MRS data were collected from six brain voxels with varying WM and GM voxel compositions to determine the WM-to-GM concentration ratio (α) for total N-acetylaspartate (tNAA), total creatine (tCr), total choline (tCho), myoinositol (Myo), glutamate (Glu), and glutamate + glutamine (Glx). Regional variation in α was assessed by comparing anterior and posterior brain voxels. Recommended α were validated with an independent dataset. A sensitivity analysis evaluated the impact of varying α on concentration estimates. An open-source tool was developed to integrate this tissue correction factor.

Results: Recommended α values for tNAA (α = 0.8), tCr (0.7), tCho (1), Myo (0.7), Glu (0.5), and Glx (0.5) effectively capture regional variations in neurochemical concentrations, improving ^{1}H-MRS measures by 30-55% compared to the conventional assumption of 1.

Conclusion: We improved the accuracy of tissue-corrected ^{1}H-MRS concentration measures by recommending neurochemical-specific α values from in vivo data, validating these with an independent dataset, and integrating these into an open-source tool for future studies.

3.2 Introduction

Single voxel, proton magnetic resonance spectroscopy (^{1}H-MRS) is a non-invasive technique used to quantify neurochemical concentrations *in vivo* within a 3D volume, or voxel, of tissue. Neurochemical concentrations are used to assess and characterize various pathologies and disorders, including tumors (Brandão & Castillo, 2016), psychiatric disorders such as major depressive disorder, schizophrenia, and bipolar disorder(Brandt et al., 2016; Diederichs et al., 2021), developmental disorders such as autism spectrum disorder (ASD) and attention-deficit/hyperactivity disorder (ADHD) (DeMayo et al., 2021; A. D. Harris et al., 2021; He et al., 2021; Puts et al., 2017), as well as chronic pain (T. Bell, Stokoe, Khaira, et al., 2021; Pigott et al., 2023).

Absolute neurochemical concentrations measured with ^{1}H-MRS are typically quantified using water as a reference. However, voxels typically contain a mixture of gray matter (GM), white matter (WM) and cerebrospinal fluid (CSF), each with distinct properties that differentially affect the water signal. Tissue correction methods, utilizing tissue-specific water and neurochemical properties such as relaxation rates and proton densities, can be used to account for differences in signal between GM, WM, and CSF (Barker et al., 1993; Charles Gasparovic et al., 2006, 2018; Gussew et al., 2012; A. D. Harris et al., 2015; Near et al., 2021). The current consensus recommended tissue correction approach attempts to address tissue relaxation rates and concentration differences between GM and WM (Near et al., 2021). However, this correction relies on the ratio of the neurochemical concentration of GM (cGM) to WM (cWM), denoted as α = cWM/cGM, which has not been systematically determined for commonly reported brain neurochemicals (tNAA, tCho, tCr, Myo, Glu and Glx). As such, there is an inherent assumption that the distribution of neurochemicals between GM and WM is equal. This

assumption, as demonstrated in a prior study of GABA, can significantly impact data interpretations (Porges et al., 2017). Specifically, using current methods, voxels with greater fraction of GM yield greater uncorrected concentration estimates because there is a greater concentration of neurochemicals in GM than WM. Correcting for concentration differences between these tissues is crucial to ensure that observed neurochemical differences genuinely reflect variations in neurochemical quantities, rather than being influenced by voxel tissue composition discrepancies. This is particularly important in scenarios involving changes in voxel composition, such as studies with brain atrophy or inconsistent voxel positioning (Porges et al., 2017).

Harris et al. (2015) formulated an equation to correct for the higher concentration of gamma-aminobutyric acid (GABA) in GM compared to WM using α to represent the ratio of WM-to-GM GABA concentration. However, this has not yet been effectively studied for other important neurochemicals (A. D. Harris et al., 2015). Furthermore, regional variations in neurochemical ratios between GM and WM likely exist due to the unique cellular compositions and functional demands of different brain regions (Zachlod et al., 2022).

To improve the accuracy of concentration measures using ^{1}H-MRS, we systematically determined α for several neurochemicals of interest (tNAA, tCr, tCho, Myo, Glu and Glx) and compared our findings to those obtained by assuming that these concentrations are equal in GM and WM. First, we used *in vivo* data to determine each α, and then validated our values using a second, independent dataset. We then determined the degree to which α varies regionally in the brain, and the impact of this regional variation on measurement variability. We also created an open-source tissue correction tool for easy implementation of our correction method.

3.3 Methods

Ethics approval for the primary dataset was obtained from the Conjoint Health Research Ethics Board at the University of Calgary. Ethics approval for the validation dataset was approved by the research committee of the School of Human and Behavioural Science at Bangor University. All the study participants provided informed, written consent prior to study participation.

3.3.1 Data Acquisition

3.3.1.1 Primary Dataset

From 27 healthy participants (aged 18-40 years), data were collected using a 3 Tesla Discovery MR750W MRI scanner equipped with a 32-channel head coil (GE Healthcare, Waukesha, WI). T1-weighted structural images were acquired using a BRAVO sequence (TR/TE=7.4ms/2.7ms, 1mm^3 isotropic voxels) for voxel placement and tissue segmentation. A Semi-Localization by Adiabatic SElective Refocusing (sLASER) acquisition (TR/TE=3000ms/35ms, voxel size 20x20x20 mm^3, 96 averages, and VAPOR water suppression) was used to collect ^{1}H-MRS data from six voxels (three anterior and three posterior), as shown in **Figure 3.1**. For both the anterior and posterior regions, voxel placement included one primarily WM voxel, one primarily GM voxel, and one mixed voxel.

3.3.1.2 Validation Dataset

An independent dataset from 14 healthy participants (ages 20-30 years), referred to as the validation dataset, was collected using an Ingenia Elition 3.0T X MRI scanner equipped with a 32-channel heal coil (Philips, Amsterdam, The Netherlands). T1-weighted structural images were acquired using a 3D five-echo MP-RAGE sequence (TE = 3.5, 10.5, 20.5, 30.5, 40.5 ms;

TR = 45 ms, TI = 1150 ms; 1 mm^3 isotropic voxels, SENSE = 2). The five echoes were averaged to produce a single image for voxel placement and tissue segmentation. ^{1}H-MRS data were also acquired using sLASER with the same acquisition parameters as the primary dataset.

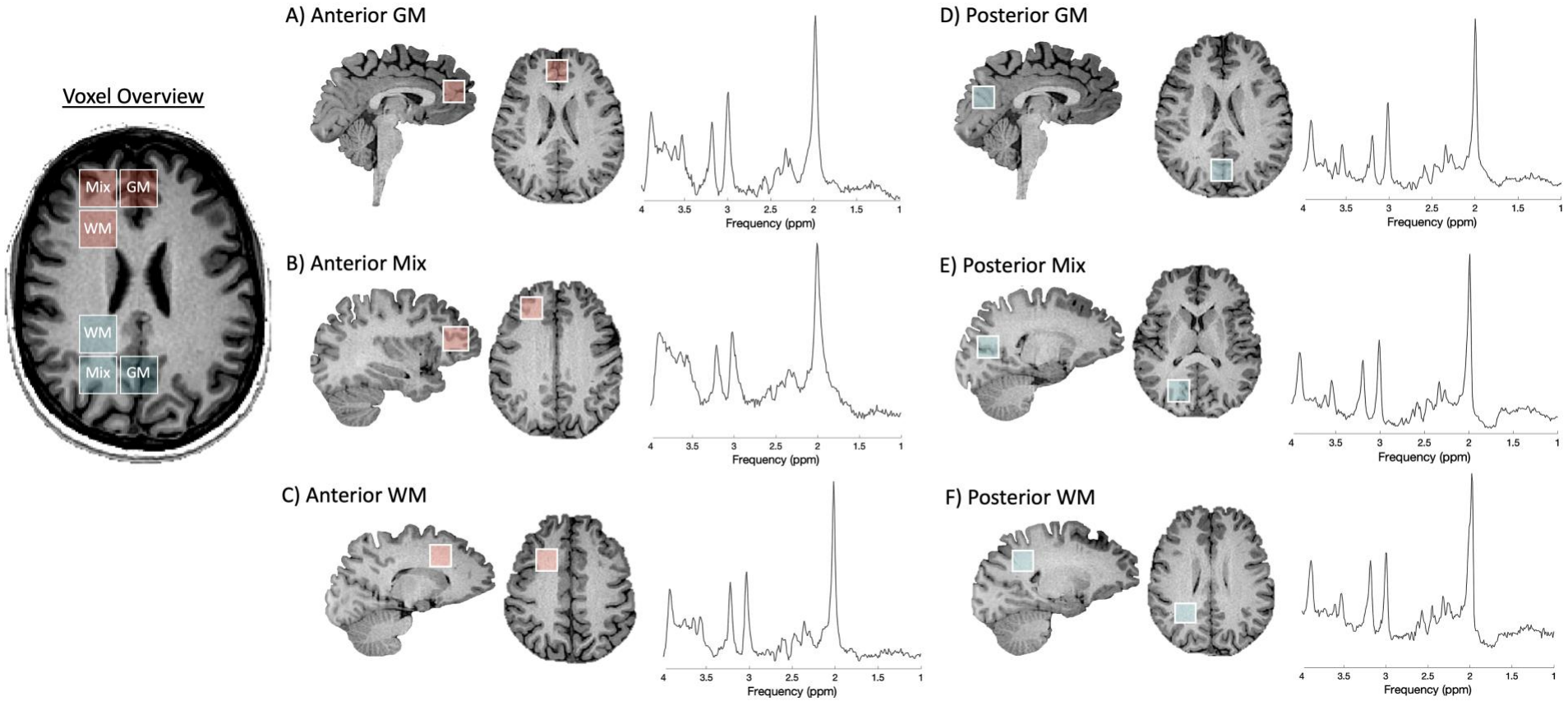

Figure 3.1. *Example placement of six 2x2x2cm^3 voxels in the brain (three anterior, red and three posterior, blue) with corresponding example spectra. Voxels were either predominantly GM, predominantly WM, or a mixture of GM and WM.*

3.3.2 Data Analysis

All data were preprocessed using a MATLAB based open-source software for processing ^{1}H-MRS data, *FID Appliance (FID-A)* (Simpson et al., 2017). This automated preprocessing pipeline included coil combination, removal of bad averages, frequency drift correction, and zero-order phase correction. Outputs from *FID-A* were analyzed using *LCModel* software (v 6.3) (Provencher, 2001). Basis sets were simulated using *FID-A*, based on sequence timings and the shape of radiofrequency pulses for each scanner, and included alanine, aspartate, choline, glycerophosphocholine, phosphocholine, creatine, phosphocreatine, GABA, glutamate, glutamine, lactate, inositol, N-acetylaspartate, N-acetylaspartylglutamate, scyllo-inositol, glutathione, glucose, taurine, β-hydroxybutyrate, citrate, ethanol, glycine, and phosphoethanolamine. LCModel default macromolecule basis sets were also included. Data were corrected for differing water density and relaxation constants differences between WM, GM, and CSF, using literature values (Near et al., 2021) (detailed in the **Appendix A**). All absolute neurochemical concentrations are reported in molal units (moles per kg of tissue water), as recommended in the field (Near et al., 2021).

3.3.3 WM-to-GM Concentration Ratio (α) Calculation

The WM-to-GM concentration ratio (α) was determined for N-acetylaspartate + N-acetyl-aspartyl-glutamate (tNAA), creatine + phosphocreatine (tCr), choline + phosphocholine + glycerophosphocholine (tCho), myo-inositol (Myo), glutamate (Glu), and glutamate + glutamine (Glx) for the primary dataset using linear regression between the neurochemical concentrations and the voxel GM volume fractions. This was performed using R (v4.2.3) and RStudio (v2023.06.1+524). To calculate concentrations within GM and WM, the GM volume fraction (f_{GM}, the independent variable) was set to either 1 for a purely GM voxel or 0 for a purely WM voxel, which was then used to determine α for each

neurochemical. Three values of α were determined to investigate the impact of voxel placements across brain regions on the quantification of neurochemicals: 1) pooled α, using all the six voxels pooled, (2) anterior α, using just the three anterior voxels pooled, and (3) posterior α, using just the three posterior voxels pooled.

3.3.4 Quantification Methods

To apply α, **Equation 3.1** was proposed. This equation integrates corrections for differing relaxation rates between GM and WM (first bracket, as per Gasparovic et al 2018) and normalizes the neurochemical of interest to a voxel of pure GM for improved comparability (second bracket, as per Harris et al 2015).

$$[M]_{molal} = c_{raw}\left(\frac{\sum_i^{GM,WM,CSF} f_i \times R_{H2O_i}}{R_{M_{WM\_GM}}}\right)\left(\frac{1}{f_{GM}+\alpha f_{WM}}\right) \quad (3.1)$$

Equations 3.1a, 3.1b, 3.1c, 3.1d define variables within **Equation 3.1** where c_{raw} (**Equation 3.1a**) is the raw signal ratio of the neurochemical (or metabolite, denoted as M to be consistent with other literature) to internal tissue water (typical output from ^{1}H-MRS quantification software, such as LCModel):

$$c_{raw} = \frac{S_{M_{obs}}}{S_{H2O_{obs}}} \times \frac{2}{\#H_M} \times [H_2O] \quad (3.1a)$$

$S_{M_{obs}}$is the neurochemical signal intensity, $S_{H2O_{obs}}$is the water signal intensity, $\#H_M$ is the number of protons in the neurochemical of interest, and $[H_2O]_{molal}$ is the concentration of water (typically assumed as 55510 mmol/kg for molal units).

f_i (**Equation 3.1b**) is the mole fraction of water in each tissue compartment relative to total water in the voxel, where i indicates the tissue compartment (GM, WM, or CSF):

$$f_i = \frac{f_{i_{vol}} \times d_i}{f_{GM_{vol}} \times d_{GM} + f_{WM_{vol}} \times d_{WM} + f_{CSF_{vol}} \times d_{CSF}} \quad (3.1b)$$

$f_{i_{vol}}$ are the volume fractions estimated from image segmentation. d_i are the relative water densities (i.e., the ratio of signals from tissue water to total water) where $d_{CSF} = 0.97$, $d_{GM} = 0.78$, and $d_{WM} = 0.65$. R_{H2O_i} (**Equation 3.1c**) is the signal attenuation factor that corrects for the longitudinal (T1) and transverse (T2) relaxation of water to recover signal that was lost from not acquiring the signal under ideal/fully relaxed conditions:

$$R_{H2O_i} = e^{\left(-\frac{TE}{T_{2_{H2O_i}}}\right)}\left(1 - e^{\left(-\frac{TR}{T_{1_{H2O_i}}}\right)}\right) \tag{3.1c}$$

$R_{M_{WM\_GM}}$ (**Equation 3.1d**) weights the neurochemical signal fractions in GM and WM by different relaxation factors:

$$R_{M_{WM\_GM}} = \frac{f_{GM} \times R_{M_{GM}} + \alpha f_{WM} \times R_{M_{WM}}}{f_{GM} + \alpha f_{WM}} \tag{3.1d}$$

Where R_{M_i} is the signal attenuation factor that corrects for the longitudinal (T1) and transverse (T2) relaxation of neurochemicals to recover signal that was lost from not acquiring the signal under ideal/fully relaxed conditions: $R_{M_i} = e^{\left(-\frac{TE}{T_{2M,i}}\right)}\left(1 - e^{\left(-\frac{TR}{T_{1M,i}}\right)}\right)$. f_i is again, the mole fraction of water in each tissue compartment relative to total water (as per **Equation 3.1d**). The full derivation of this equation is detailed in **Appendix A**.

3.3.5 WM-to-GM Concentration Ratio (α) Selection

The values of α as determined using the primary dataset were applied to the validation dataset to determine the α ratio (anterior, posterior, or pooled) that best removed the contribution of tissue voxel composition to neurochemical concentration on the tissue voxel composition, compared to traditional CSF correction (i.e., α = 1) (Charles Gasparovic et al., 2018). To choose the best α, linear regressions of concentration versus tissue GM fraction with non-significance of p-values, slopes close to 0, and low R^2 values were interpreted as supporting evidence that concentration was independent of tissue composition. Therefore, the

α for the regression line that most effectively indicated an independent relationship between concentration and GM fraction was selected.

3.3.6 Sensitivity Analysis

A sensitivity analysis was performed to evaluate the impact of varying α values on quantification of neurochemical concentrations. To isolate the effect of changing α values, all other variables in **Equation 3.1** were held constant. The α values were varied across an observable range of 0 to 3. Typical reported uncorrected signal measures (c_{raw}) for each neurochemical were sourced from the literature: 12 IU for tNAA, 8 IU for tCr, 1 IU for tCho, 6 IU for Myo, 9 IU for Glu, and 10 IU for Glx(Joyce et al., 2022). Standard voxel fractions were maintained at 45% GM, 45% WM, and 10% CSF. Percent errors (**Equation 3.2**) between the recommended and tested α were determined,

$$\%\ Error = \frac{[M]-[M]_{recommended}}{[M]_{recommended}} \times 100\% \quad (3.2)$$

where $[M]$ is the neurochemical concentration calculated with α ranging from 0 to 3, and $[M]_{selected}$ is the molal neurochemical concentration calculated with the empirically selected α (one per neurochemical). In other words, the percent errors were calculated with our recommended α as a reference to determine the error in neurochemical concentration estimates when using other α values, including the commonly assumed α = 1 as in CSF-correction. The threshold for acceptable errors was predefined as ±10%.

3.3.7 Open-Source Software Tool

An open-source tool to calculate absolute neurochemical concentrations using the recommended α values was written in *Python* (v 3.9.0) using *Jupyter Notebook* (v 6.1.4).

3.4 Results

3.4.1 Descriptive Statistics and Data Quality

In the primary dataset, out of the 27 participants, 19 were female and the mean age was 29.1 years (SD 4.6). No data were excluded from the primary dataset. One participant was removed from the validation dataset because of improper data rendering, resulting in a sample size of n=13. The signal-to-noise (SNR) ratio was greater than 25 for each dataset, and the full width at half maximum (FWHM) of the NAA peak was less than 0.07 ppm for all spectra. Tissue fractions and data quality measures reported for each of the six voxels are shown in **Table 3.1**.

Table 3.1. *Summary of the mean GM, WM, and CSF fractions, mean linewidth (reported as the full width half maximum, FWHM, of the NAA peak) and mean signal to noise ratio (SNR) for each of the six voxels. Measures are reported as the mean and standard deviation.*

	Anterior			***Posterior***		
	GM voxel	**WM voxel**	**Mixed voxel**	**GM voxel**	**WM voxel**	**Mixed voxel**
GM fraction	0.61 ± 0.04	0.24 ± 0.05	0.26 ± 0.05	0.74 ± 0.05	0.21 ± 0.06	0.39 ± 0.07
WM fraction	0.09 ± 0.04	0.74 ± 0.06	0.72 ± 0.06	0.11 ± 0.04	0.77 ± 0.08	0.58 ± 0.08
CSF fraction	0.31 ± 0.04	0.02 ± 0.02	0.02 ± 0.01	0.15 ± 0.06	0.02 ± 0.02	0.03 ± 0.02
FWHM (Hz)	0.036 ± 0.01	0.031 ± 0.00	0.043 ± 0.01	0.032 ± 0.00	0.027 ± 0.00	0.031 ± 0.00
SNR	37.26 ± 4.14	38.41 ± 3.93	33.52 ± 5.63	45.44 ± 4.35	42.35 ± 3.36	48.26 ± 4.97

3.4.2 WM-to-GM Concentration Ratio (α) Calculation

Generally, as levels of GM increased, uncorrected levels of the neurochemical also increased, indicating there is more of each neurochemical in GM compared to WM. This strong, positive, linear relationship between concentration and GM fraction pooling both regions together was found for all neurochemicals (R^2 range, 0.42-0.75), except for tCho (R^2 = 0.0023) (as shown in **Figure 3.2**). The slope for tCho approached 0, indicating nearly equal concentrations of tCho in GM and WM. We found that the goodness of fit improved for all neurochemicals including tCho (R^2 range, 0.25-0.91), when we separated the analyses by

anterior and posterior voxels (**Figure 3.3**), indicating α varies between the anterior region and the posterior region.

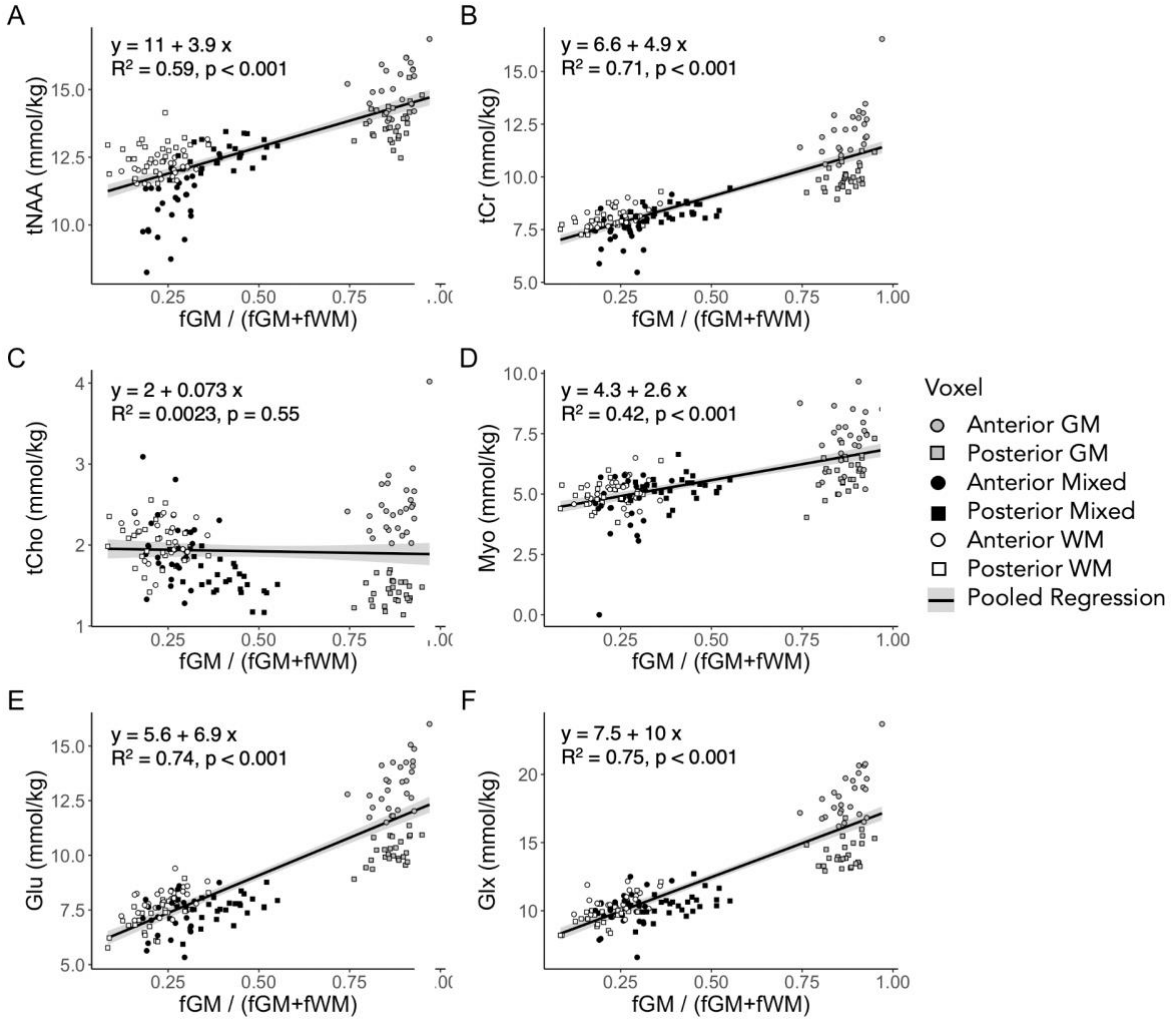

Figure 3.2. *Concentrations of A) N-acetyl aspartate (tNAA), B) creatine (tCr), C) choline (tCho), D) myoinositol (Myo), E) glutamate (Glu), F) glutamate + glutamine (Glx) versus GM tissue fraction. Data from all 6 voxels were pooled for the linear fit, the equation of the fit is shown on each of the graphs (standard error shown in gray). Voxels include GM anterior (grey circle), GM posterior (grey square), Mixed anterior (black circle), Mixed posterior (black square), WM anterior (white circle), and WM posterior (white square).*

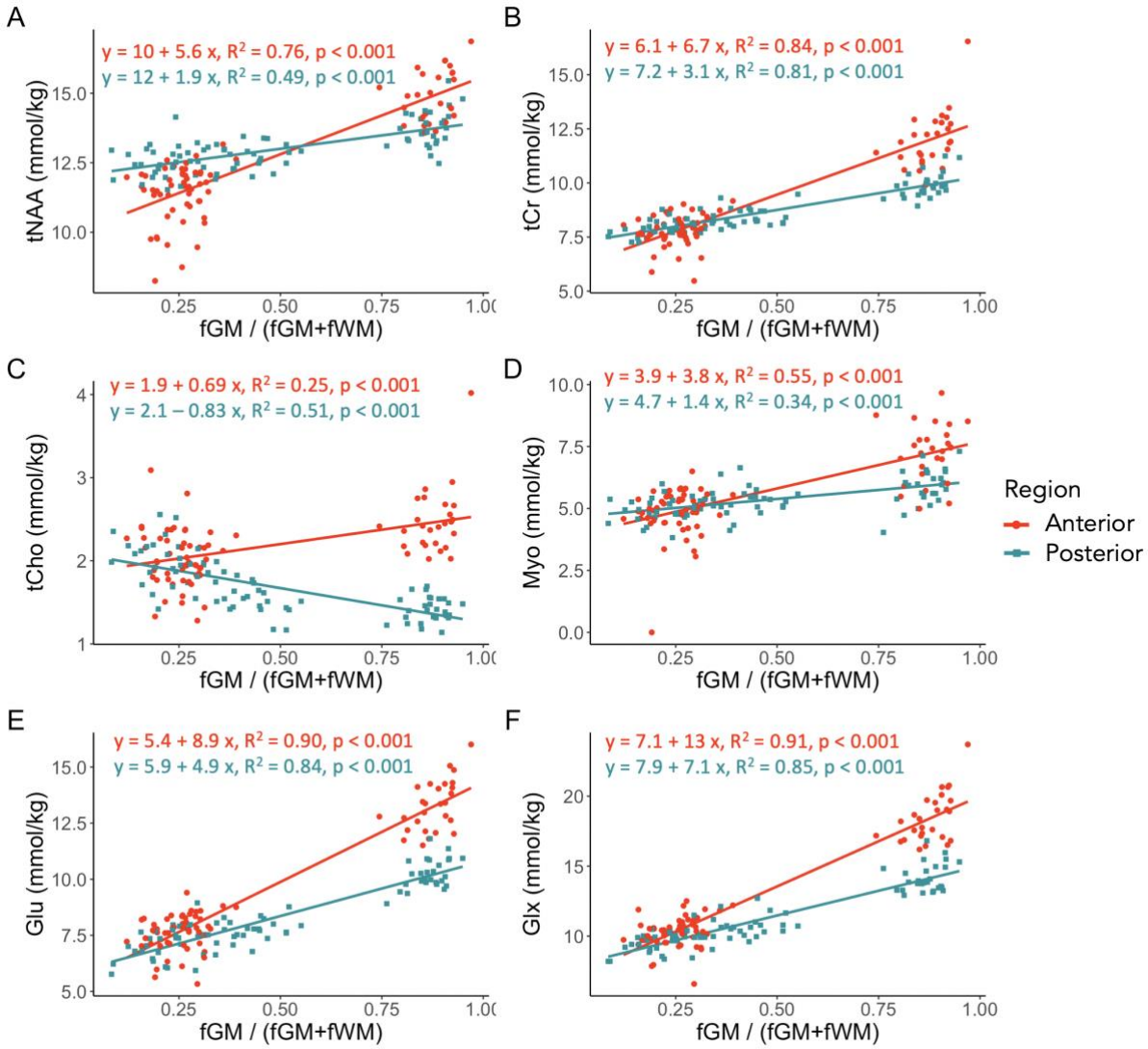

Figure 3.3. *Concentrations of A) N-acetyl aspartate (tNAA), B) creatine (tCr), C) choline (tCho), D) myoinositol (Myo), E) glutamate (Glu), F) glutamate + glutamine (Glx) versus GM voxel fraction. Data were pooled by region for the linear fit (with anterior voxels shown in red circles and posterior voxels shown in blue squares, standard error shown in gray), the equation of the fit is shown on each of the graphs.*

3.4.3 WM-to-GM Concentration Ratio (α) Selection

For each neurochemical, four α values were compared; anterior α, posterior α, pooled α (i.e., anterior and posterior regions pooled), and α = 1 (**Figure 3.4**). The regression results show that the posterior ratios best achieved independence of concentration from tissue composition for tNAA, tCr, Myo and Glx. For tCho and Glu, the pooled α best achieved independence. Based on these findings, the α ratio corresponding to the regression line with the most robust indication of independence between concentration and GM fraction was selected. Based on these results, a recommended α has been determined; all α values are shown in **Table 3.2**.

Table 3.2. *Summary of α values for total N-acetyl aspartate (tNAA), total creatine (tCr), total choline (tCho), myoinositol (Myo), glutamate (Glu), and glutamate + glutamine (Glx) for all data pooled, the anterior region and posterior region and the recommended α.*

	WM-to-GM Concentration Ratios (α)				
	Pooled	**Anterior**	**Posterior**	**Recommended**	**Interpretation**
tNAA	0.74	0.64	0.86	0.8	1.25x more tNAA in GM than WM
tCr	0.57	0.48	0.70	0.7	1.4x more tCr in GM than WM
tCho	1.04	0.73	1.66	1	Equal tCho in GM and WM
Myo	0.62	0.51	0.76	0.7	1.4x more Myo in GM than WM
Glu	0.45	0.38	0.55	0.5	2x more Glu in GM than WM
Glx	0.43	0.35	0.53	0.5	2x more Glx in GM than WM

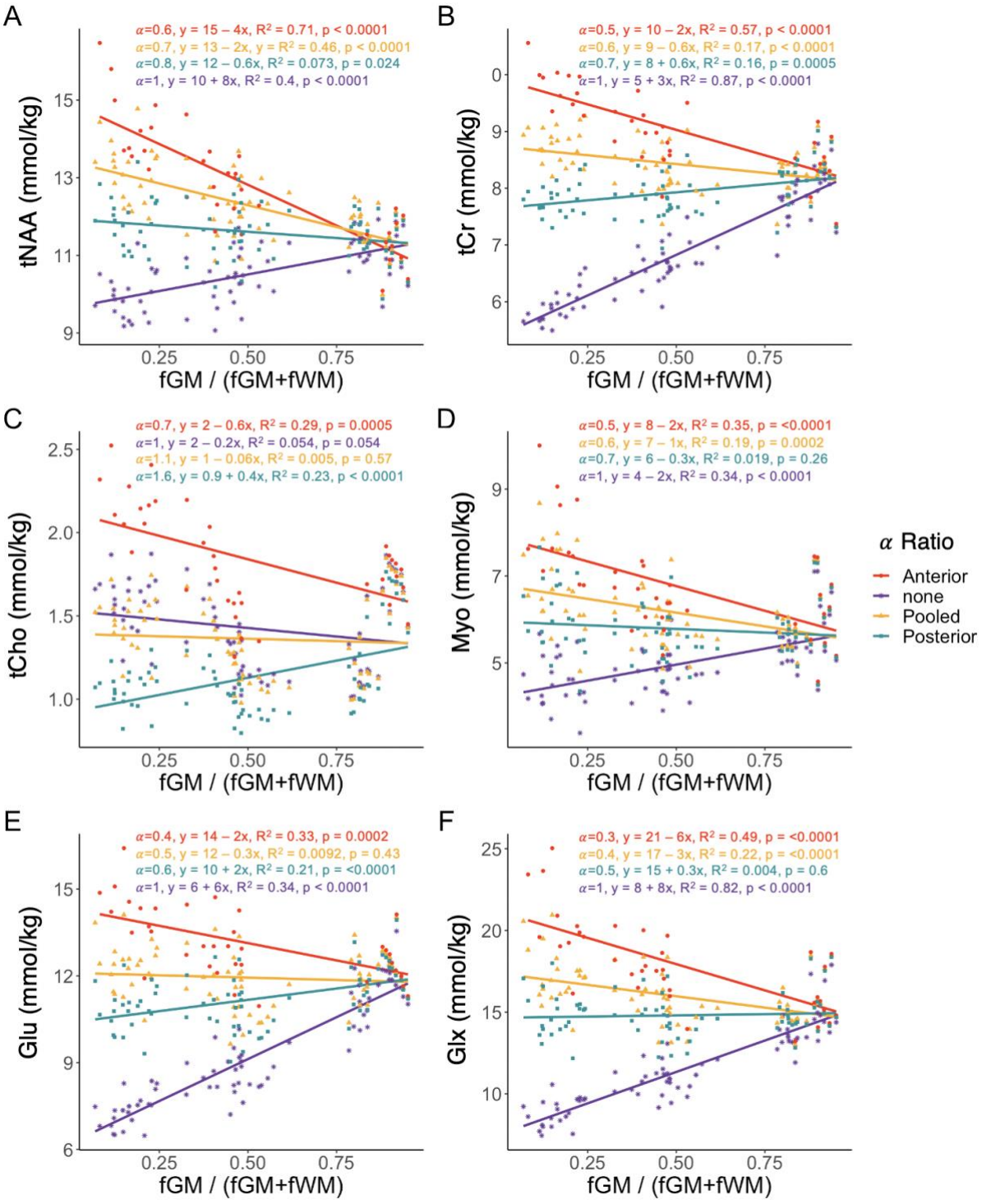

Figure 3.4. *Concentrations of A) N-acetyl aspartate (tNAA), B) creatine (tCr), C) choline (tCho), D) myoinositol (Myo), E) glutamate (Glu), F) glutamate + glutamine (Glx) versus GM tissue fraction calculated using anterior (red circle), none (purple star), pooled (yellow triangle), and posterior (blue square) α ratios.*

3.4.4 Sensitivity Analysis

Figure 3.5 shows that voxels with high GM content are less sensitive to variations in α (when normalizing to a pure GM voxel), whereas voxels with low GM content are highly sensitive to variations in α, yielding percent errors of up to 55% for the assumption of a 1:1 α ratio in a voxel of 10% GM. As acceptable limits are typically predefined as ±10% error, the current assumption α = 1 is insufficient used for all regions and all voxel compositions.

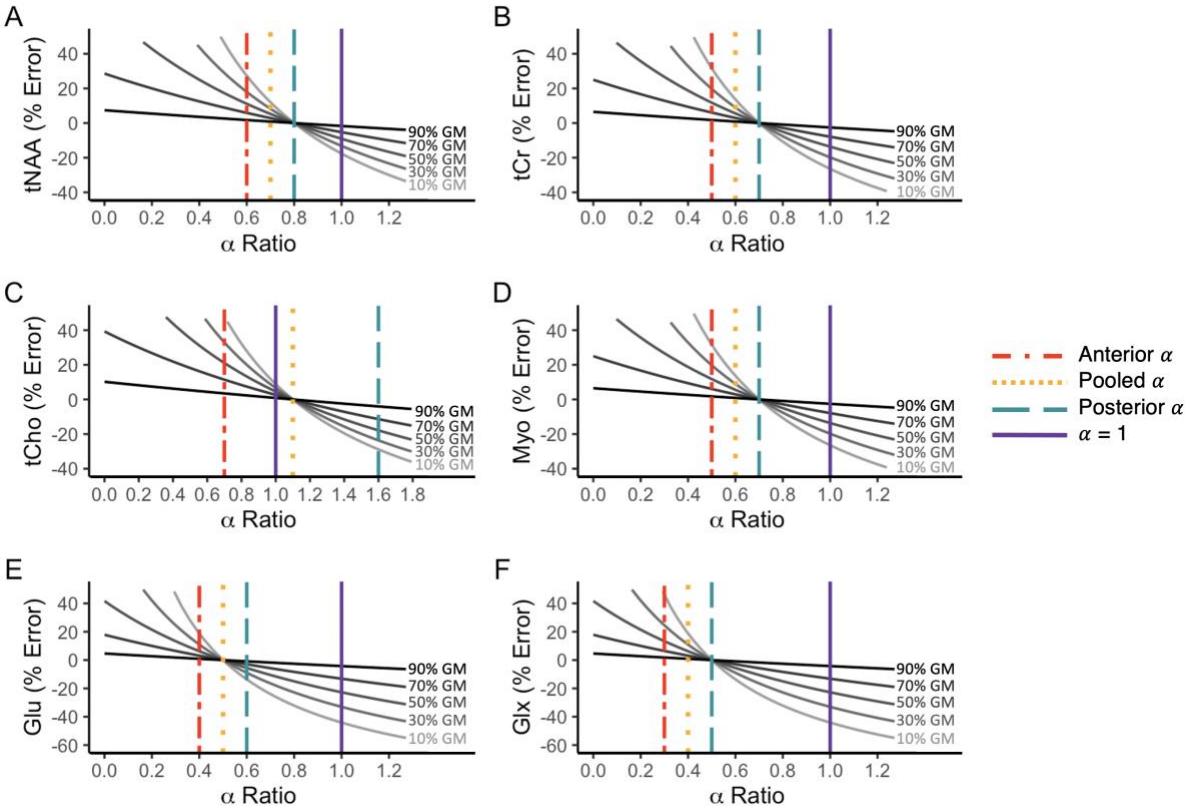

Figure 3.5. *Percent error in concentrations plotted against a range of α ratios for simulated voxels with 90% GM, 70% GM, 50% GM, 30% GM, 10% GM, using the selected ratio as a reference. The dashed vertical lines (from left to right) indicate the anterior (two-dashed, red), pooled (dotted, yellow), and posterior (long dashed, blue) α ratios while the solid vertical line (purple) indicates the prevalent assumption of a 1:1 ratio.*

3.5 Discussion

We determined α, the WM-to-GM concentration ratio, for tNAA, tCr, tCho, Myo, Glu, and Glx in a cohort of healthy, young adult participants. Although the presence of differences in neurochemical concentrations between GM and WM are generally accepted, the implications of these differences for data quantification, analysis, and interpretation have largely been overlooked by the ^{1}H-MRS community. Gasparovic et al. (2018) developed an equation to correct for relaxation differences between GM and WM, but this does not account for the actual proportion of tissue in the voxel. Harris et al. (2015) formulated an equation for correcting GABA concentration differences between GM and WM (i.e., determined α for GABA to be 0.5), but a similar correction has not yet been effectively integrated for the quantification of more standard ^{1}H-MRS-measured neurochemicals (namely, tNAA, tCr, tCho, Myo, Glx and Glu). By applying the α ratios calculated in this study, both relaxation and concentration differences between GM and WM are accounted for, offering a more representative reporting of neurochemical levels. If not corrected for appropriately, these bulk tissue changes may erroneously appear as concentration changes.

The concentration differences between anterior and posterior brain regions are significant, yet neurochemical concentration ratios between white matter (WM) and gray matter (GM) (α) are comparable across these regions. For instance, α ratios for Glx are 0.3, 0.4, and 0.5 in anterior, pooled, and posterior regions, respectively. A sensitivity analysis showed that a 0.1 difference in α between these regions is insignificant, with errors < ±10%. Similarly, across vendors (GE and Philips), though concentration differences exist(Tiffany K. Bell et al., 2022; Považan et al., 2020), α ratios remain comparable. For example, while Glx α ratios on GE were 0.4 and 0.5 for pooled and posterior regions, respectively, the α representing pooled Glx on Philips was 0.5. Despite slight differences, sensitivity analysis

confirms they are not significant (< ±10% errors), allowing for cross-vendor data correction using these ratios.

Generally, we observed higher α values in posterior brain regions, indicating that there are higher neurochemical concentrations in GM relative to WM in anterior brain region compared to the posterior brain region. Only one other study has specifically calculated α, and this was done in the putamen(Gogishvili et al., 2023). Generally, their α values were aligned with our recommended α and most close to the posterior α values.

Interestingly, tCho demonstrates regional differences in WM/GM tissue concentrations; in the anterior region there is higher tCho in GM and in the posterior region there is higher tCho in WM. However, for both anterior and the posterior regions, the difference between GM and WM are subtle. We therefore recommend an $\alpha = 1$ for tCho as this generalizes for all voxels and removes the effect of tissue, as seen in the validation data set.

The scope of this study was to improve absolute neurochemical concentration measures by applying a mathematical correction factor (α) to obtain a tissue-corrected concentration estimate. It should be noted that two alternative approaches are commonly used to report concentrations: using tissue composition parameters as covariates in statistical analyses or reporting measured signals as a ratio to a reference signal (typically tCr). Including covariates is beneficial for studies with large sample sizes, such method can reduce the power to detect changes in small sample sizes. In contrast, absolute neurochemical concentration measures are particularly useful for exploratory studies with small sample sizes. Reporting signals as a ratio to a reference signal relies on the stability of the reference across age, gender, pathology, and other factors, as it is difficult to attribute changes to the neurochemical signal of interest if the reference is also changing. Although similar concerns apply to α in yielding confidence in a representative α, α corrections facilitate the detection of

changes in small-scale studies, allowing larger studies to investigate the underlying causes in more detail.

One limitation of absolute quantification is its reliance on many assumptions, including the ratio of neurochemical concentrations within GM and WM (α), relaxation times of water and neurochemicals within GM, WM, and CSF (T1 and T2), and the relative density of water within GM, WM, and CSF (d_i). This manuscript aimed to test the assumed ratio of neurochemical concentrations within GM and WM while keeping all other standard assumptions constant. Although these assumptions are likely representative of our young, healthy adult population, they may not be sufficient for all populations. It is essential to test and improve one assumption at a time when refining absolute quantification methods. As such, each assumption should be tested separately in each population of interest (e.g., across different ages and pathologies) to ensure confidence in these methods.

In reporting neurochemical concentrations, we have opted to use a full GM voxel as the reference. This decision was made to ensure consistent and straightforward comparisons across studies, despite the non-representative nature of a fully GM voxel in vivo. We acknowledge that a 50-50 WM/GM voxel or using sample averages, as suggested by Harris et al. (2015)(A. D. Harris et al., 2015), could be alternative approaches. However, these methods also have limitations due to variability across samples and arbitrary selection criteria. By standardizing on a full GM voxel, we aim to provide a clear and easily comparable benchmark for future studies.

This study found that the conventional assumption of equal neurochemical concentrations in WM and GM in ^{1}H-MRS may cause up to 55% error in concentration estimates. Thus, we recommend the use of absolute concentrations calculated with the proposed equation and α ratios summarized in **Table 2** for improved accuracy. While there may be approximately 25% error associated with this generalized selection of the pooled α

ratio depending on voxel composition and voxel placement within the brain when normalizing to a pure GM voxel, the associated error will be approximately 35% less than simply assuming $\alpha = 1$. While we recognize these recommended α values are imperfect, incorporating these best estimate α values within the tissue correction will enhance the accuracy of ^{1}H-MRS neurochemical concentration measures, especially in cohorts where tissue content may vary, such as in brain atrophy. Alternatively, including the tissue fraction of GM as a covariate is a different approach to statistically account for differences in neurochemical concentrations between WM and GM; however, this is at the expense of statistical power which is often limited in ^{1}H-MRS studies.

3.6 Conclusion

In this study we have demonstrated the ability to improve the accuracy of tissue corrected ^{1}H-MRS concentration measures by incorporating neurochemical-specific α (WM-to-GM neurochemical concentration ratios), which were determined from *in vivo* data. The utility of these α values is to improve tNAA, tCr, tCho, Myo, Glu, and Glx concentration measures, which was validated using a second, independent dataset. We also confirmed that α varies regionally in the brain, to differing degrees for individual neurochemicals and demonstrated the impact this can have on measurement variability. Despite this variability, we are able to recommend an α for each neurochemical that minimizes any tissue fraction dependencies. These recommended α values have been incorporated into an open-source tool that implements this extension of the α and tissue correction methodology of Harris et al (2015) and Gasparovic et al (2018) in future studies.

3.7 Data Availability Statement

An open-source tool was created to calculate absolute neurochemical concentrations using the recommended α ratios. Users can easily import processed ^{1}H-MRS signal measures

and segmented tissue volume fractions to automatically calculate α corrected absolute neurochemical concentrations. The markdown format of the code allows users to easily understand each equation. The tool also creates a visualization of the performance of absolute neurochemical concentrations calculated with the recommended α correction normalized to different voxel compositions in comparison to current consensus recommended methods using CSF correction (Gasparovic et al. 2018). The tool is publicly available on Zenodo: 10.5281/zenodo.10840451 and updates can be downloaded at: https://github.com/HarrisBrainLab/alpha.

CHAPTER FOUR

※

Quantitative Synthetic Imaging for Improved ^{1}H-MRS Quantification

Chapter 4: Quantitative Synthetic Imaging for Improved ^{1}H-MRS Quantification

This chapter is being presented as a journal submission:

> **Leech SA**, Bell TK, Manske SL, Mullins PG, Harris AD. *Inter-Individual Differences in T1, T2, and PD using Quantitative Synthetic Imaging for ^{1}H-MRS Quantification.* (In preparation for submission).

Conceptualization, study design, data analysis, and write-up of this chapter was completed by the lead author, with support from co-authors.

There may be some overlap with materials and methods presented in previous chapters.

Supplementary tables and figures for this chapter are presented in **Appendix B**.

4.1 Abstract

Quantification of absolute neurochemical concentrations using single-voxel proton magnetic resonance spectroscopy (^{1}H-MRS) necessitates correction for mixed tissue composition including tissue-specific T1 and T2 relaxation times and proton density across various tissues. Typically, T1, T2, and proton density (PD) are assumed from literature values, often overlooking inter-individual variability due to age and certain pathologies, potentially compromising the accuracy of neurochemical concentration estimates. In this study, we utilized quantitative synthetic imaging to directly measure T1, T2, and PD within a single acquisition. Comparisons of neurochemical concentrations for tNAA, tCr, tCho, Myo, Glu and Glx calculated using these measured parameters versus literature constants demonstrated a consistent overestimation when employing literature values (e.g., mean difference of 0.3 mmol/kg for tCho to 1.8 mmol/kg for tNAA). While interindividual differences in tissue parameters contribute minimally to variation in neurochemical concentration estimates among young, healthy adults, sensitivity analyses suggest that wider parameter ranges, as observed in aging and clinical disorders, could significantly affect neurochemical concentration estimates. This underscores the necessity of considering individually measured T1, T2, and PD values for precise neurochemical quantification across diverse populations and pathological conditions.

4.2 Introduction

Quantification of brain neurochemicals using single-voxel proton magnetic resonance spectroscopy (^{1}H-MRS) requires correction for mixed tissue composition within the voxel, as water within different tissues (WM, GM and CSF) has different T1 and T2 (longitudinal and transverse tissue relaxation times, respectively), and proton density (PD) (Charles Gasparovic et

al., 2018). Typically, these values are obtained from published literature values; however, this disregards interindividual differences as well as possible variation across anatomy. For example, it is well known that T1, T2, and PD vary non-linearly with age (Canales-Rodríguez et al., 2021; Hagiwara et al., 2021; Knight et al., 2016; Kumar et al., 2011, 2012; Nürnberger et al., 2017). These values can also be influenced by changes in tissue, such as increased collagen content, decreased water content, increased iron deposition (Gelman et al., 1999; Vymazal et al., 1999), or other changes with clinical conditions (Gracien et al., 2017; Wearn et al., 2020), potentially leading to errors in absolute neurochemicals concentration quantification . For example, NAA concentration has been reported to decrease with aging (Brooks et al., 2001), while relaxation times, such as T2, also typically decrease with age (Kumar et al., 2012), which may confound observations of changing neurochemical concentrations.

A more accurate approach is to explicitly measure these constants in the tissue comprising the spectroscopy voxel (C. Gasparovic et al., 2009). To do so with traditional magnetic resonance (MR) methods several acquisitions would be required to obtain T1, T2, and PD, substantially increasing scan time. More recently, multi-contrast acquisitions have been developed such that these parameters can be quantified within a single acquisition, mitigating the time burden associated with their measurement (Tanenbaum et al., 2017). This sequence optimizes time efficiency by reading previously encoded slices to eliminate the waiting periods following saturation pulses (Nunez-Gonzalez et al., 2022; Warntjes et al., 2007, 2008). Quantitative maps for T1, T2 and PD can then be generated (using mathematical models and algorithms) based on these T1, T2, and PD values to depict the distribution of tissue relaxation times (T1 and T2) and PD across the imaged volume, providing a representation of tissue properties that is not directly captured by traditional MRI techniques (SyntheticMR AB, 2021).

In this study of healthy young adults, we compare neurochemical concentrations quantified using individually measured T1, T2 and PD from quantitative synthetic images to concentrations calculated from constants assumed from the literature (as is typically performed) to determine the impact of inter-individual parameters in neurochemical quantification. Additionally, we examine the sensitivity of our results to assess the impact of varying these interindividual parameters on neurochemical concentration measurements.

4.3 Methods

4.3.1 Participants

Data were collected at 3T (GE 750W, 32-channel head coil) from 26 participants (ages 18-40 years). Participants were in good health (i.e., no physical or mental impairments that would impact their ability to consent to, or participate in, an MRI scan). They were free from contraindications to MRI (e.g., not pregnant, no metallic implants). Ethics approval was obtained from the Conjoint Health Research Ethics Board at the University of Calgary (REB22-0738), and all the study participants provided informed consent upon enrollment.

4.3.2 Acquisition

First, a standard T1-weighted structural image was acquired (TR/TE=7.4ms/2.7ms and 1mm^3 isotropic voxels) for voxel placement and tissue segmentation. ^{1}H-MRS data were collected in six voxels, as shown in **Figure 4.1**.

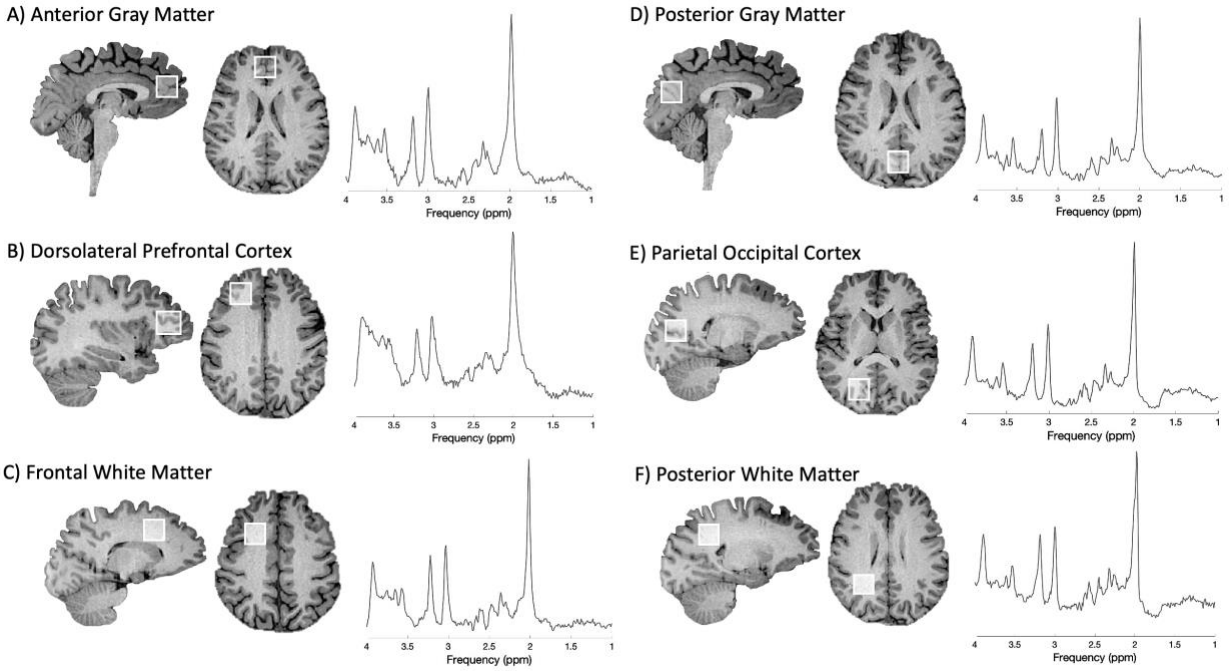

Figure 4.1. *Example placement of six 2x2x2cm^3 voxels in the brain with corresponding example spectra.*

Voxels were placed to encompass a variety of tissue compositions, with the goal of defining with primarily WM, primarily GM, and mixed WM and GM in the anterior and posterior of the brain. Semi-Localization by Adiabatic SElective Refocusing (sLASER) was used to collect ^{1}H-MRS data (TR/TE=3000ms/35ms, voxel size 20x20x20 mm^3, 96 averages, and VAPOR water suppression) as well as unsuppressed water data for quantification.

The multiple-contrast acquisition 3D-MAGiC (3D MAGnetic resonance image Compilation); a proprietary sequence developed by GE Healthcare, was used to develop T1, T2 and PD maps. 3D MAGiC was acquired with the following scan parameters: axial acquisition; TR/TE/TI, 7.2/2.8/100 msec (automatic minimum TE selection was used to provide the shortest possible TE times without setting a fractional TE); field of view (FOV) = 24 cm^2; matrix size = 256 × 256; slice thickness = 1.4 mm; flip angle = 4°; bandwidth = 244.14 Hz/pixel; acquisition time = 4 min 38 sec. Multichannel parallel imaging to correct for non-uniform receiver coil profiles was performed using GE's PURE (Phased array Uniformity Enhancement) method.

ARC (Autocalibrating Reconstruction for Cartesian imaging) was used with phase = 2.0 and slice=1.0. HyperSENSE acceleration with a factor of 1.5 was applied.

4.4 ^{1}H-MRS Fitting

The ^{1}H-MRS data underwent preprocessing using *FID-A* (Simpson et al., 2017), an open-source software written in MATLAB. This automated preprocessing pipeline includes all recommended preprocessing steps (Near et al., 2021): coil combination, elimination of poor-quality averages, frequency drift correction, and zero-order phase correction. Subsequently, the outputs from *FID-A* were fit using *LCModel* software (Version 6.3) (Provencher, 2001). The basis set was generated using *FID-A*, considering the sequence timings and radiofrequency pulse shapes, and included the following neurochemicals: alanine, aspartate, choline, glycerophosphocholine, phosphocholine, creatine, phosphocreatine, GABA, glutamate, glutamine, lactate, inositol, N-acetylaspartate, N-acetylaspartylglutamate, scyllo-inositol, glutathione, glucose, taurine, β-hydroxybutyrate, citrate, ethanol, glycine, and phosphoethanolamine. Additionally, *LCModel* default macromolecule basis sets were included.

4.5 ^{1}H-MRS Quantification

For traditional analysis of spectroscopy data (i.e., using literature values for T1, T2 and PD), the standard T1-weighted structural image was segmented into WM, GM, and CSF using *SPM12* software (The FIL Methods Group, London, UK). ^{1}H-MRS voxel masks were generated using the "CoRegStandAlone" co-registration function in *Gannet 3.3.1* (A. D. Harris et al., 2015), a MATLAB based open-source software package, implemented using MATLAB version 2022b. Each neurochemical (tNAA, tCr, tCho, Glx and Glu) was quantified following the

consensus recommended tissue correction approach, detailed in **Equation 4.1** (Charles Gasparovic et al., 2018; Near et al., 2021).

$$[M]_{molal} = c_{raw}\left(\frac{f_{GM}\times R_{H2O_{GM}} + f_{WM}\times R_{H2O_{WM}} + f_{CSF}\times R_{H2O_{CSF}}}{R_M}\right)\left(\frac{1}{1-f_{CSF_{vol}}}\right) \quad (4.1)$$

The mole fraction of water in each of the three tissue compartments (i: GM, WM, CSF) is expanded in **Equation 4.1a**.

$$f_i = \frac{f_{i_{vol}}\cdot \boldsymbol{PD_i}}{\left(f_{GM_{vol}}\cdot \boldsymbol{PD_{GM}}\right)+\left(f_{WM_{vol}}\cdot \boldsymbol{PD_{WM}}\right)+\left(f_{CSF_{vol}}\cdot \boldsymbol{PD_{CSF}}\right)} \quad (4.1a)$$

The signal attenuation factor of water in each of the three tissue compartments (i: GM, WM, CSF) is expanded in **Equation 4.1b**.

$$R_{H2O_i} = \left(e^{-TE/\boldsymbol{T2_{H2O_i}}}\right)\left(1 - e^{-TR/\boldsymbol{T1_{H2O_i}}}\right) \quad (4.1b)$$

Neurochemical concentrations were calculated using either T1, T2, and PD constants (bolded in the above equation) found in literature or explicitly measured in this study. To ensure representative literature constants for ^{1}H-MRS quantification were used, T1, T2 and PD were compiled from common ^{1}H-MRS preprocessing and quantification software packages, specifically Osprey (Oeltzschner et al., 2020), Gannet (Edden et al., 2014), and FSL-MRS (Clarke et al., 2021) which were acquired from studies by (Ethofer et al., 2003), (Charles Gasparovic et al., 2009), (Lu et al., 2005), (Piechnik et al., 2009), (Posse et al., 2007), (Rooney et al., 2007), (Spijkerman et al., 2018), (Stanisz et al., 2005), (Vymazal et al., 1999), and (Wansapura et al., 1999) and typically used PD values acquired from (Kreis et al., 1993), as summarized in the **Appendix B**.

To acquire individualized T1, T2 and PD values, quantitative T1, T2, and PD maps (**Figure 4.2**) from the MAGiC acquisition were extracted using SyMRI (Hagiwara et al., 2017). Using *FSL FLIRT* (FMRIB's Linear Image Registration Tool) (Jenkinson et al., 2012), the T1-

weighted structural image (acquired for ^{1}H-MRS voxel placement) and the voxel masks for GM, WM, and CSF (extracted using CoRegStandAlone) were simultaneously registered to the quantitative T1, T2, and PD maps to ensure all data were analyzed within a common spatial reference frame. The mean T1, T2, and PD values for GM, WM, and CSF within each voxel were determined using "fslstats" (FSL).

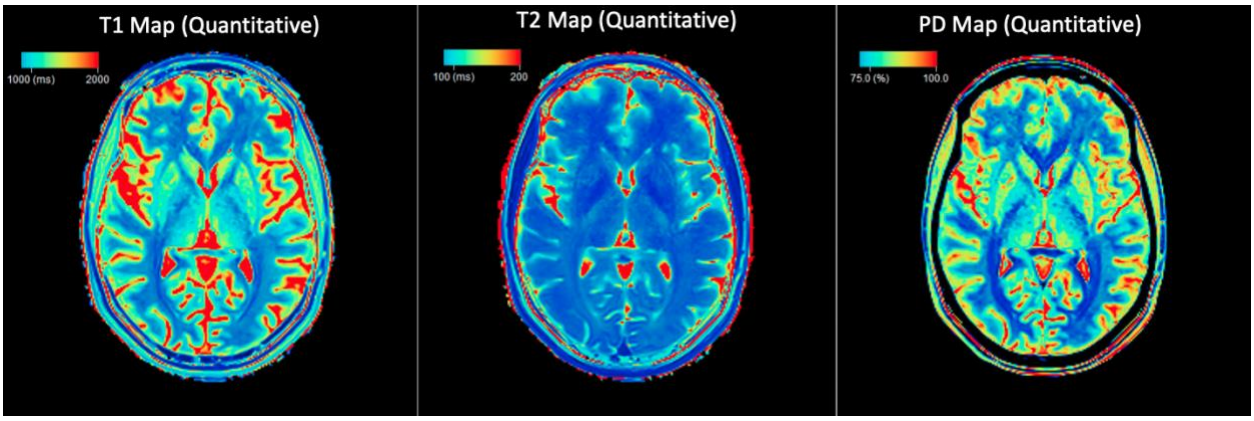

Figure 4.2. *Quantitative T1, T2, and PD maps from a single participant generated in SyMRI. These synthetic images depict the quantitative values of tissue relaxation times (T1 and T2) and proton density (PD).*

4.6 Statistical Analysis

Pearson correlations and Bland-Altman plots were used to compare absolute concentration measures of tNAA, tCr, tCho, Myo, Glu, and Glx from all six voxels calculated using individually measured water T1, T2, and PD constants versus concentrations calculated using literature values. This was performed using R (v4.2.3) and RStudio (v2023.06.1+524).

A variance-based sensitivity analysis, specifically a Sobol sensitivity analysis (X. Zhang et al., 2015), was conducted in Python (v 3.9.0) to assess the overall impact of varying ranges of T1, T2, and PD on concentration measures. This sensitivity analysis varied all continuous input parameters simultaneously over the entire parameter space to evaluate the relative contributions of each individual parameter as well as the interactions between parameters to the model output

variance. The model evaluated was the current consensus recommended tissue correction model (Charles Gasparovic et al., 2018; Near et al., 2021) with fixed input parameters of TE = 0.035 s, TR = 3 s, and $M_{GM}/M_{WM} = 1$ (the ratio of neurochemical concentrations in GM to WM assumed as 1 for simplicity), as well as T1s and T2s of neurochemicals in GM and WM (summarized in the **Appendix B**). Continuous input parameters: water T1, T2, PD, volume fractions of GM, WM, and CSF, and c_{raw} (raw water-referenced signal measure), were varied within the ranges measured from the quantitative synthetic maps (detailed in Error! Reference source not found.). A total of 8192 model evaluations were performed (using Saltelli's method) (X. Zhang et al., 2015). Sensitivity indices greater than 0.05 are typically considered to significantly contribute to model output (X. Zhang et al., 2015).

Four sensitivity analyses were performed to determine the *variance contributions to* absolute neurochemical concentrations based on:

1) input ranges within our observed metrics for all 6 voxels

2) input ranges within our observed metrics for a single voxel with consistent tissue fractions

This analysis is more representative of typical ^{1}H-MRS analyses where voxels are analyzed independently and therefore tend to have consistent tissue-volume fractions. As a result, this analysis is less likely to be largely driven by tissue fractions (f_{GM}, f_{WM}, f_{CSF}), as can occur in the primary sensitivity analysis.

3) a larger input T2 range from a meta-analysis

This sensitivity analysis was performed with T2 measures observed over a larger range [0.04 to 0.72s] from a meta-analysis evaluating 12 studies that measured T2 of water in the human brain, spanning a large age range (18 – 80 years) as well as within healthy brains and various clinical conditions (including Alzheimer's disease and mild cognitive impairment)(Gudmundson et al., 2023). This analysis was performed to determine the impact of extremes that may be measured *in vivo.* While we acknowledge that T2 values for different tissue types may not fall within the same ranges, this limitation arises from utilizing values obtained through meta-analysis, where tissue types were not consistently reported across the included studies. The purpose of applying an exaggerated T2 range to all three compartments was to test the sensitivity analysis limits within observable ranges, potentially overestimating the impacts of ranges observed in pathological conditions.

4) input values ranging to 0 in the CSF compartment (i.e., f_{CSF}, and consequently PD_{CSF}, $T1_{CSF}$, $T2_{CSF}$ ranging to 0)

This sensitivity analysis was performed to determine the impact of having no CSF compartment (i.e., the volume fraction of CSF, $f_{CSF} = 0$). This is important in ^{1}H-MRS studies as we typically try to minimize the volume of CSF in the voxel since there are negligible amounts of neurochemicals in CSF. Therefore, it is not uncommon to have no CSF in a voxel. During the ^{1}H-MRS voxel mask registration to the quantitative synthetic maps, if the CSF voxel mask is non-existent (due to a volume fraction of 0), $T1_{CSF}$, $T2_{CSF}$, and PD_{CSF} values cannot be extracted, resulting in null values in the CSF compartment. This is not a limitation of the method because when f_{CSF} is 0, it cancels the entire CSF term in **Equation 4.1**. Therefore, $T1_{CSF}$, $T2_{CSF}$, and PD_{CSF} values are not needed when f_{CSF} is 0. Thus, this tertiary sensitivity analysis tests input values ranging from 0 to the observed maximums (from **Error! Reference source not found.**) for f_{CSF}, $T1_{CSF}$, $T2_{CSF}$, and PD_{CSF}.

4.7 Results

Of the 27 participants, 19 were female and the mean age was 29.1 years (SD 4.6). No data were excluded due to data quality. The signal-to-noise (SNR) ratio was greater than 25 for every measurement, and the full width at half maximum (FWHM) of the NAA peak was less than 0.07 ppm for each spectrum. Tissue fractions and data quality measures reported for each of the six voxels can be found in **Table 4.1**.

Table 4.1. *Summary of voxel content and spectral quality (linewidth, reported as the full width half maximum, FWHM, of the NAA peak and signal to noise ratio, SNR). Measures are reported as the mean and standard deviation.*

	Anterior GM	**Anterior WM**	**DLFC**	**Posterior GM**	**Posterior WM**	**POC**
GM fraction	0.61 ± 0.04	0.24 ± 0.05	0.26 ± 0.05	0.74 ± 0.05	0.21 ± 0.06	0.39 ± 0.07
WM fraction	0.09 ± 0.04	0.74 ± 0.06	0.72 ± 0.06	0.11 ± 0.04	0.77 ± 0.08	0.58 ± 0.08
CSF fraction	0.31 ± 0.04	0.02 ± 0.02	0.02 ± 0.01	0.15 ± 0.06	0.02 ± 0.02	0.03 ± 0.02
FWHM (ppm)	0.036 ± 0.01	0.031 ± 0.00	0.043 ± 0.01	0.032 ± 0.00	0.027 ± 0.00	0.031 ± 0.00
SNR	37.26 ± 4.14	38.41 ± 3.93	33.52 ± 5.63	45.44 ± 4.35	42.35 ± 3.36	48.26 ± 4.97

GM: gray matter; WM: white matter; CSF: cerebral spinal fluid; DLFC: dorsolateral prefrontal cortex; POC: posterior occipital cortex.

4.7.1 Literature and Measured Values for T1, T2, PD

The measured ranges compared to ranges reported in literature of water T1, T2, and PD, as well as volume fractions of GM, WM, and CSF, are shown in **Table 4.2**. A compilation of commonly used literature values for water and neurochemical T1, T2, and PD are detailed in the **Appendix B**.

Table 4.2. *Measured ranges of continuous input parameters used for the sensitivity analysis: T1, T2, PD, volume fractions of GM, WM, and CSF. These metrics were measured from each voxel's synthetic PD, T1, T2 maps and are reported as the mean [minimum, maximum] values observed within the sample.*

	Measured Ranges **Mean [Min, Max]**	***Literature Ranges*** **Typically Used [Min, Max]**
$T1_{GM}$ (sec)	1.470 [1.265, 1.759]	1.331 [1.304, 1.820]
$T1_{WM}$ (sec)	0.844 [0.767, 0.940]	0.832 [0.660, 1.11]
$T1_{CSF}$ (sec)	2.880 [1. 680, 4.085]	3.817 [3.817, 4.472]
$T2_{GM}$ (sec)	0.073 [0.065, 0.090]	0.110 [0.093, 0.110]
$T2_{WM}$ (sec)	0.063 [0.057, 0.074]	0.0796 [0.069, 0.0796]
$T2_{CSF}$ (sec)	0.137 [0.089, 0.448]	0.503 [0.503, 2.47]
PD_{GM}	0.836 [0.776, 0.890]	0.65
PD_{WM}	0.708 [0.671, 0.737]	0.78
PD_{CSF}	0.948 [0.842, 1.000]	0.97
f_{GM}	0.415 [0.098, 0.812]	–
f_{WM}	0.469 [0.015, 0.896]	–
f_{CSF}	0.110 [0.001, 0.440]	–

4.7.2 Concentrations Calculated with Literature vs Measured Values

The correlation coefficients between concentrations calculated using *in vivo* and literature-acquired constants range from r = 0.992 (for tCr) to r = 0.998 (for tNAA), indicating strong agreement (**Figure 4.3**). Concentrations calculated from literature values were consistently higher than concentrations calculated from individual measures, demonstrating a systematic bias. Proportional biases were also observed as shown by the increasing deviation from unity (dotted line) as concentrations increase.

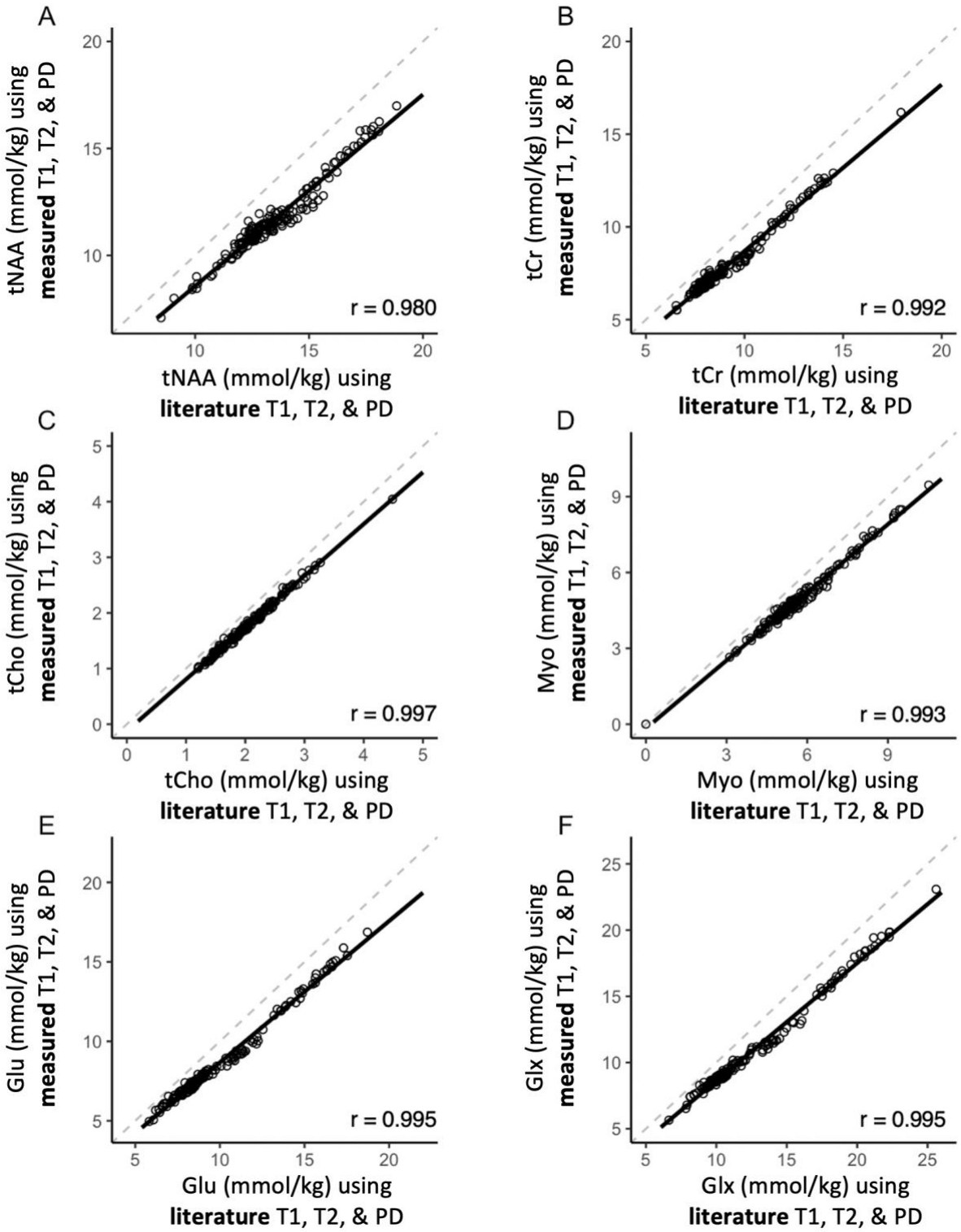

Figure 4.3. *Pearson correlations of A) tNAA, B) tCr, C) tCho, D) Myo, E) Glu, and F) Glx concentrations calculated using individual measures (i.e., T1, T2, and PD of water measured in vivo for each individual using a multi-echo MAGiC) versus concentrations calculated using literature constants for water. The dotted line indicates the line of unity.*

Both systematic and proportional biases were also observed in the Bland-Altman plots (**Figure 4.4**). A few data points fall outside the 95% limits of agreement in the Bland-Altman plots (mean difference ± 1.96 standard deviation), suggesting that a few individuals have noticeably different values when concentrations are calculated using the two sets of constants. The limits of agreement do not encapsulate 0 and show that concentrations calculated from literature values are significantly higher than concentrations calculated from individual measures. For tNAA, Glu, Glx, and tCr, as the concentration difference increases, the mean concentration (x-axis) increases for lower concentrations, indicating a proportional bias at lower concentrations. Despite this slight bias, overall, concentrations calculated with in vivo and literature measures demonstrate agreement.

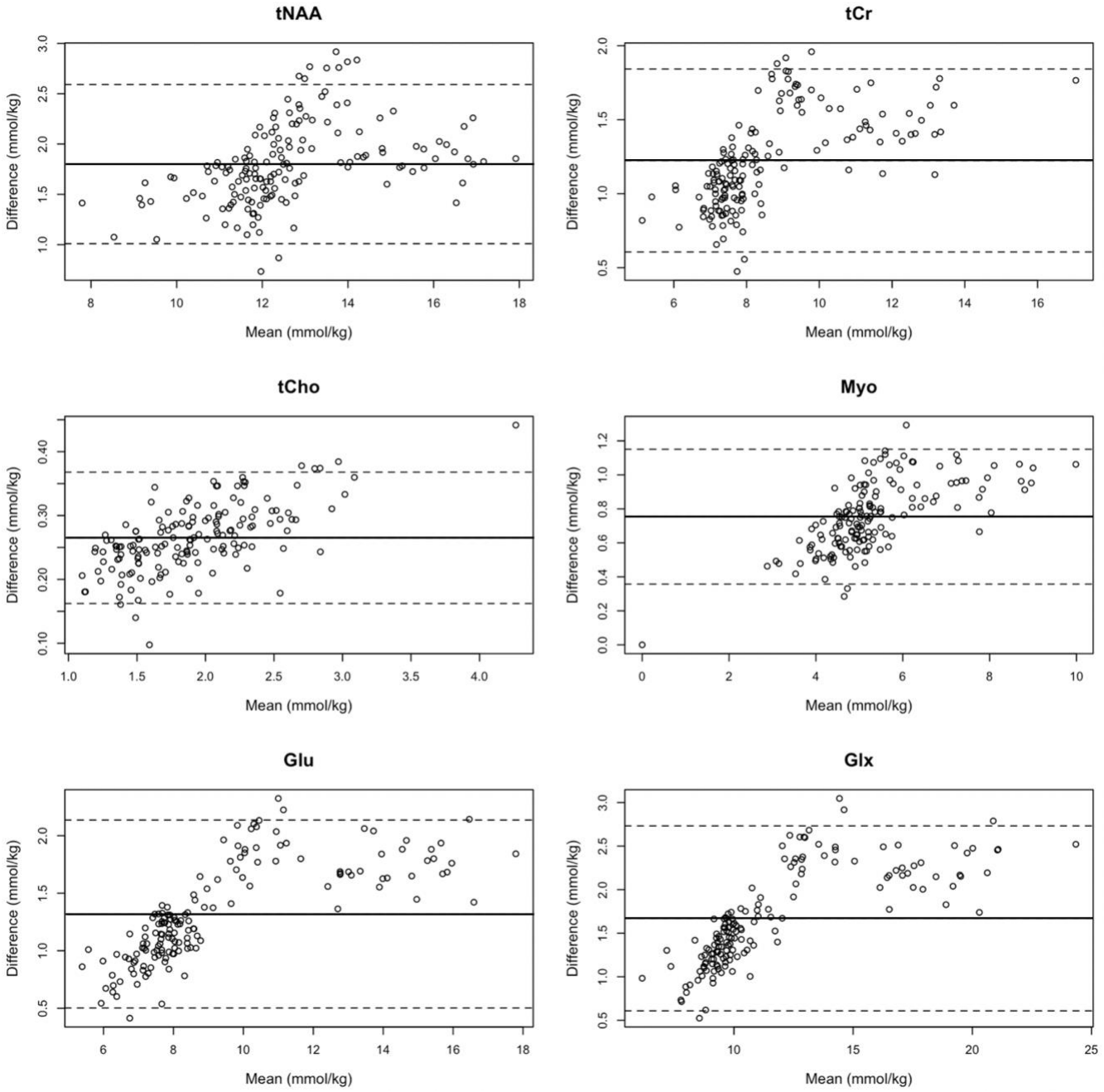

Figure 4.4. *Bland-Altman plots indicating the agreement between concentrations calculated using individually measured constants versus literature constants for A) tNAA, B) tCr, C) tCho, D) Myo, E) Glu, and F) Glx. The x-axis represents the average of the two methods, while the y-axis shows the difference between them (literature – measured). The solid middle line represents the mean difference, and the outer dashed lines indicate the limits of agreement (mean difference ± 1.96 standard deviations).*

4.7.3 Sensitivity Analyses

Results for all four sensitivity analyses are summarized in **Table 4.3** with their respective input ranges and are visualized in **Figure 4.5**. Among our metrics of interest (T1, T2, PD), T2 – particularly in GM and WM – was found to have the most significant contribution to the variance in tissue-corrected concentration measures (sensitivity indices > 0.05). In three of the four sensitivity analyses, $T2_{GM}$ and $T2_{WM}$ yield significant contributions to variance in neurochemical concentrations with their highest contribution being when the range of T2 values is exaggerated (**Figure 4.5**, blue).

Results from the sensitivity analyses with extended CSF metrics ranging to 0 were as expected (**Figure 4.5**, purple) where the variance contribution of PD_{CSF} and $T2_{CSF}$ are most prominent among our metrics of interest (T1, T2, PD). This is due the signal being derived solely from GM and WM in some cases rather than from GM, WM, and CSF, as usual (i.e., when f_{CSF} is 0, the mole fraction of water – which relies primarily on PD_{CSF} and f_{CSF} – is also 0).

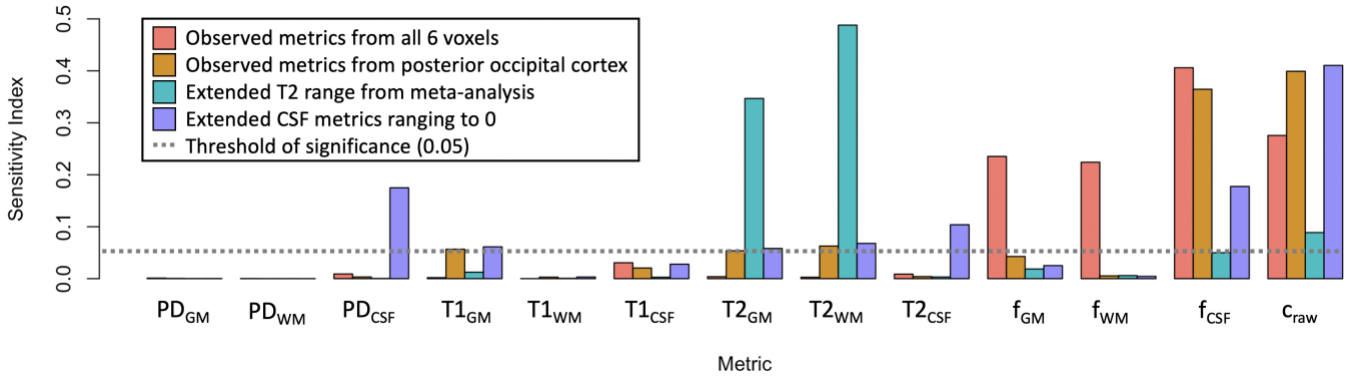

Figure 4.5. *Sensitivity indices indicating variance contributions to absolute neurochemical concentrations based on 4 sensitivity analyses using: 1) ranges within our observed metrics for all 6 voxels (red), 2) ranges within our observed metrics for a single voxel with consistent tissue fractions (posterior occipital cortex, orange), 3) a larger T2 range from a meta-analysis (blue), and 4) values ranging to 0 in the CSF compartment (i.e., f_{CSF}, PD_{CSF}, $T1_{CSF}$, $T2_{CSF}$ ranging to 0, purple).*

Table 4.3. *Results from all four sensitivity analyses. Sensitivity indices measure the contribution of each input metric (main effects and interactions with other metrics) to output variance, with higher values indicating greater influence and overall importance. Metrics are reported as sensitivity indices ± uncertainty (percent contribution to measured variance). Values with a sensitivity index of greater than 0.05 are in bold as this is the threshold for significant contribution to variance.*

	All Voxels		**Single Voxel**		**Larger T2 Range**		**CSF Ranging to 0**	
Metric	**Input Range**	**Sensitivity Index**	**Input Range**	**Sensitivity Index**	**Input Range**	**Sensitivity Index**	**Input Range**	**Sensitivity Index**
PD_{GM}	[0.78, 0.89]	<0.01 ± 0.00 (0%)	[0.80, 0.86]	<0.01 ± 0.00 (0%)	[0.80, 0.86]	<0.01 ± 0.00 (0%)	[0.80, 0.86]	<0.01 ± 0.00 (0%)
PD_{WM}	[0.67, 0.74]	<0.01± 0.00 (0%)	[0.67, 0.72]	<0.01± 0.00 (0%)	[0.67, 0.72]	<0.01 ± 0.00 (0%)	[0.67, 0.72]	<0.01 ± 0.00 (0%)
PD_{CSF}	[0.84, 1.00]	0.01± 0.00 (1%)	[0.91, 1.00]	<0.01± 0.00 (0%)	[0.91, 1.00]	<0.01 ± 0.00 (0%)	[0.00, 1.00]	**0.17 ± 0.01 (16%)**
$T1_{GM}$	[1.26, 1.76]	<0.01± 0.00 (0%)	[1.26, 1.64]	**0.06± 0.00 (6%)**	[1.26, 1.64]	0.01 ± 0.00 (1%)	[1.26, 1.64]	**0.06 ± 0.00 (5%)**
$T1_{WM}$	[0.77, 0.94]	<0.01 ± 0.00 (0%)	[0.78, 0.90]	<0.01 ± 0.00 (0%)	[0.78, 0.90]	<0.01 ± 0.00 (0%)	[0.78, 0.90]	<0.01 ± 0.00 (0%)
$T1_{CSF}$	[1.68, 4.08]	0.03± 0.00 (3%)	[1.99, 3.94]	0.02± 0.00 (2%)	[1.99, 3.94]	<0.01 ± 0.00 (0%)	[0.00, 3.94]	0.03 ± 0.00 (2%)
$T2_{GM}$	[0.07, 0.09]	<0.01 ± 0.00 (0%)	[0.07, 0.08]	**0.05± 0.00 (5%)**	[0.04, 0.72]	**0.35 ± 0.01 (34%)**	[0.07, 0.08]	**0.06 ± 0.00 (5%)**
$T2_{WM}$	[0.06, 0.07]	<0.01 ± 0.00 (0%)	[0.06, 0.07]	**0.06± 0.00 (6%)**	[0.04, 0.72]	**0.49 ± 0.02 (48%)**	[0.06, 0.07]	**0.07 ± 0.00 (6%)**
$T2_{CSF}$	[0.09, 0.40]	0.01± 0.00 (1%)	[0.10, 0.18]	<0.01 ± 0.00 (0%)	[0.04, 0.72]	<0.01 ± 0.00 (0%)	[0.00, 0.72]	**0.10 ± 0.01 (9%)**
f_{GM}	[0.10, 0.81]	**0.24± 0.02 (20%)**	[0.28, 0.58]	0.04± 0.00 (4%)	[0.28, 0.58]	0.02 ± 0.00 (2%)	[0.28, 0.58]	0.03 ± 0.00 (2%)
f_{WM}	[0.02, 0.90]	**0.22± 0.02 (19%)**	[0.39, 0.69]	0.01± 0.00 (1%)	[0.39, 0.69]	0.01 ± 0.00 (1%)	[0.39, 0.69]	<0.01 ± 0.00 (0%)
f_{CSF}	[0.001, 0.44]	**0.41± 0.03 (34%)**	[0.004, 0.08]	**0.36± 0.01 (36%)**	[0.004, 0.08]	**0.05 ± 0.00 (5%)**	[0.00, 0.08]	**0.18 ± 0.01 (16%)**
c_{raw}	[10.06, 16.73]	**0.28± 0.01 (23%)**	[11.04, 12.10]	**0.40± 0.01 (39%)**	[11.04, 12.10]	**0.09 ± 0.00 (9%)**	[11.04, 12.10]	**0.41 ± 0.01 (37%)**

4.8 Discussion

In this study, we quantified the effect of individually measured T1, T2, and proton density (PD) constants from quantitative synthetic images on determining neurochemical concentrations and compared this to the standard approach of using literature values. Our results show that in a young healthy population, interindividual differences in these parameters only contribute to subtle differences in calculated neurochemical concentrations. Although these differences are subtle, we found that when using standard literature values for T1, T2, and PD, the calculated neurochemical concentrations were statistically significantly higher compared to those calculated with individually measured values. The fact that concentrations were higher with literature values and their difference becomes more pronounced at higher concentrations suggests a proportional bias, rather than a simple systematic difference. Specifically, differences in T1 and T2 values could make it harder to detect small but meaningful changes in neurochemical concentrations, especially when those concentrations are low. This implies that for more accurate neurochemical measurements, it might be better to use individually measured T1, T2, and PD values rather than relying on standard literature values.

A limitation of measuring individual T1, T2, and PD values with the multi-contrast sequences it there is up to 7% variability on measured T1, T2, and PD has been reported depending on sequence selection, though most intersequence differences are less than 3% (Zheng et al., 2023). Despite this limitation, the use of a global, variance-based sensitivity analysis allowed for a representative analysis of varying T1, T2, and PD over observed ranges and attribute variances in neurochemical concentrations to main effect and interaction between input metrics. This was necessary to determine the impact of variations in T1, T2, and PD measures on neurochemical concentrations as the model for calculating absolute

neurochemical concentrations is complex and difficult to attribute sources of variation with a local sensitivity analysis (i.e., a sensitivity analysis where variables are altered one at a time).

Our sensitivity analyses suggest the wider ranges of T1, T2, and PD values seen with aging (Canales-Rodríguez et al., 2021; Hagiwara et al., 2021; Knight et al., 2016; Kumar et al., 2011, 2012; Nürnberger et al., 2017) and clinical disorders (Gracien et al., 2017; Wearn et al., 2020) may have a more substantial effect on neurochemical concentrations. Exploring the impact of a large range of T2 values acquired from a meta-analysis revealed that large ranges in T2 show significant contributions to variance in neurochemical concentrations. This effect is likely similar for large ranges of T1 values, although this was not explicitly tested due to the lack of readily available T1 ranges in the literature. This motivates a need to explore the impact of these parameters more explicitly across populations of different ages and pathologies.

4.9 Conclusion

In this study, we quantified the effect of individually measured T1, T2, and PD constants from quantitative synthetic images on determining neurochemical concentrations and compared this to the standard approach of using literature values. Our results show that in a young healthy population, interindividual differences in these parameters contribute to subtle, yet significant differences in calculated neurochemical concentrations. This indicates that using uniform literature values may not be accurate for every individual and these inaccuracies likely are greater in a wider age range or with clinical disorders.

CHAPTER FIVE

※

Neurochemical Alterations in Painful Knee Osteoarthritis

Chapter 5: Neurochemical Alterations in Painful Knee Osteoarthritis

This chapter is being presented as a journal submission:

Leech SA, DeMayo MM, Bell TK, Campbell CM, Lee CH, Batuyong E, Clark M, Schneider G, White N, Millar K, Hasselaar C, Ng R, Manske SL, Harris AD. *Relationships Between Centralized Pain and Cortical Neurochemical Concentrations in Painful Knee Osteoarthritis*. (In preparation for submission).

Conceptualization, study design, data analysis, and write-up of this chapter was completed by the lead author, with support from co-authors.

There may be some overlap with materials and methods presented in previous chapters.

5.1 Abstract

Understanding the neurobiological mechanisms, particularly centralized pain, in knee osteoarthritis (KOA), is essential for improving treatment outcomes, especially considering the persistent pain experienced by many patients post-total knee arthroplasty (TKA). This preliminary study enrolled twenty female KOA patients awaiting TKA and nineteen pain-free age-matched controls. Neurochemical levels were measured using proton magnetic resonance spectroscopy (^{1}H-MRS) and centralized pain evaluation via questionnaires and quantitative sensory testing (QST). Although knee pain showed improvement following total knee arthroplasty (TKA) ($p < 0.001$), measures of centralized pain did not significantly improve post-TKA ($p > 0.05$). This suggests that persistent post-surgical pain is related to central pain not the peripheral joint pain alone. Comparing neurochemical levels between patients and controls in four brain regions between groups, gamma-aminobutyric acid (GABA) levels were lower in the anterior cingulate cortex of KOA patients ($p = 0.012$). Significant associations were found between centralized pain measures and neurochemical levels, with differing trends in sensory and affective brain regions. Specifically, in comparing both pain-free controls and KOA patients and in changes pre- and post-surgery, elevated Glx, Myo, and tCho levels were associated with higher centralized pain in sensory brain regions. In contrast, affective regions had lower Myo and tCho levels associated with centralized pain. Our findings highlight regional neurochemical changes in KOA, emphasizing their role in pain processing and suggesting therapeutic targets for centralized pain management in KOA patients.

5.2 Introduction

Knee osteoarthritis (KOA) is a leading cause of chronic pain worldwide (Neogi, 2013) and presents challenges in pain management. Total knee arthroplasty (TKA) is the final treatment option for knee osteoarthritis after non-surgical interventions (i.e., when exercise (Roos & Juhl, 2012) and analgesics (Bjordal et al., 2006; Sharma, 2021; W. Zhang, 2004) prove ineffective). TKA is one of the most commonly performed surgical procedures (Canadian Institute for Health Information, 2019; Fingar et al., 2006). Unfortunately, following TKA, 15-40% of patients report unresolved pain (Beswick et al., 2012; Bourne et al., 2010; Werner & Kongsgaard, 2014). This inadequate pain relief is more prevalent among females, with 37% more women than men reporting moderate to severe pain 2-5 years after TKA (Singh et al., 2008). The relationship between pain and knee osteoarthritis is further complicated by a lack of consistency between joint damage as visualized on x-ray and pain levels quantified with either self-report or quantitative sensory testing (QST) (Cooper et al., 2000; Dieppe et al., 1997; Finan et al., 2013; Hannan et al., 2000). This dissociation suggests centrally (brain) driven pain amplifies pain beyond that driven by osteoarthritic tissue damage (Phillips & Clauw, 2011). Therefore, to effectively treat knee osteoarthritis pain, it is essential to consider and understand both the central and peripheral pain mechanisms.

Further evidence of centralized pain in KOA is that some patients exhibit increased pain sensitivity, characterized by heightened responses to painful stimuli, associated with dysfunction in central pain processing (Clauw & Hassett, 2017; Clauw & Witter, 2009; Imamura et al., 2008; Lee et al., 2011; Wessel, 1995). This phenomenon is present in other chronic pain conditions, such as fibromyalgia (Bradley et al., 2004; Clauw, 2014; Sluka & Clauw, 2016). Previous research has shown alterations in gamma-aminobutyric acid (GABA), glutamate, myoinositol, and choline in fibromyalgia patients (Fayed et al., 2010;

Jung et al., 2021; Pomares et al., 2020) as measured with single voxel proton magnetic resonance spectroscopy (^{1}H-MRS) (Z. Zhang et al., 2022). Thus, in this study, we investigated these neurochemicals to determine whether KOA pain results in similar brain alterations as fibromyalgia and whether these neurochemicals normalize following TKA to improve our understanding of the neurobiological underpinnings of pain in KOA.

Based on previous studies in chronic pain, we selected the anterior cingulate cortex and anterior insula (affective regions), as well as the posterior insula and somatosensory cortex (sensory regions), as regions of interest. Understanding the distinct roles of these sensory and affective brain regions in pain processing is crucial for elucidating the mechanisms underlying both acute and chronic pain, as these regions collectively contribute to the integration of sensory information and emotional-motivational responses.

This preliminary study investigated neurochemical changes in chronic pain associated with KOA in females. Using ^{1}H-MRS, we seek to elucidate the neurochemical basis of centralized pain in KOA, potentially informing targeted therapeutic interventions to alleviate chronic pain. Specifically, we aimed to 1) compare neurochemical levels between pain-free controls and KOA patients before TKA; 2) explore the association between neurochemical levels and centralized pain in KOA patients versus pain-free controls; and 3) determine whether post-TKA neurochemical changes correlate with improvements in centralized pain.

5.3 Methods

5.3.1 Participants

Twenty female participants (aged 40-75 years) with knee osteoarthritis awaiting TKA were recruited from the surgical waitlists. Fourteen patients were retained for a longitudinal study visit approximately three months after knee replacement surgery. Nineteen pain-free control participants were recruited from the community and were age-matched ± 2 years of

KOA participant age. Control participants had no known arthritis in any joint, no history of joint replacement or knee surgery, no chronic pain, and did not experience knee pain at rest or during walking.

Exclusion criteria for all participants included contraindications to MRI, inability to speak, understand, and read English, neurological disorders (e.g., multiple sclerosis and epilepsy), physical impairment hindering participants from remaining motionless during MRI, significant mental health disorders (e.g., psychosis or PTSD), GABA-targeting medications (e.g., gabapentin) or central sensitization-targeting drugs (e.g., duloxetine), and arthritis diagnosis in other joints. Other pain medications (such as ibuprofen and acetaminophen) were permitted.

All participants provided written informed consent before involvement in the study, and study approval was obtained from the Conjoint Health Research Ethics Board at the University of Calgary (REB20-0019).

5.3.2 Questionnaires

Self-reported pain was measured for descriptive purposes using the Western Ontario and McMaster Universities Osteoarthritis Index (WOMAC), painDETECT questionnaire, Central Sensitization Inventory (CSI), Pain Catastrophizing Scale (PCS), Beck Depression Inventory (BDI), Profile of Mood States (POMS), McGill Pain Questionnaire (MPQ), and 36-Item Short-Form Health Survey (SF-36) to capture participant-reported pain characteristics, including pain intensity, physical functioning, and emotional functioning as per recommended reporting standards for chronic pain research (Dworkin et al., 2008). Participants completed questionnaires via REDCap, a secure online database, one week before their visit. The painDETECT survey was completed during the visit.

While these multiple questionnaires were collected for descriptive purposes, the painDETECT questionnaire was used in subsequent analyses as an assessment of centralized pain. The painDETECT questionnaire assesses the likelihood of a patient having centralized pain (also referred to as neuropathic pain) based on different pain qualities (i.e., burning, tingling, numbness, etc.). The overall painDETECT score represents the likelihood of centralized pain being less than 15% (0 to 12), ambiguous/unclear (13 to 18), and high (90%) likelihood of centralized pain (19 to 38) (Freynhagen et al., 2006, 2016).

5.3.3 Quantitative Sensory Testing (QST)

Pain was also characterized with quantitative sensory testing (QST) using four standardized tests: pain pressure thresholds (PPT), conditioned pain modulation (CPM), mechanical temporal summation (MTS), and cold pressor tolerance (CPT) (Finan et al., 2013). PPT, CPM, and MTS tests target the threshold between discomfort and pain. As such, participants were instructed to end test trials when their discomfort levels became painful, exceeding discomfort. For CPT, participants were instructed to tolerate pain for as long as possible. Participants were familiarized with all equipment and procedures before each test.

5.3.3.1 Pain Pressure Threshold (PPT)

PPT measures the amount of pressure required for the pressure stimulus to elicit pain perception (i.e., pain thresholds). PPT was tested using an algometer (NorthStar Echo algometer with 1 cm^2 tip attachment, JTech Medical) to assess the pressure threshold between discomfort and pain. The applied pressure was increased at approximately 10 N/sec to a maximum of 111N. PPT (converted to kPa) was assessed at the trapezius contralateral to the affected knee (i.e., a distal site from the knee) for 3 trials, each with 30 seconds of rest in between.

5.3.3.2 Conditioned Pain Modulation (CPM)

CPM assesses descending pain inhibitory control by measuring the degree to which a secondary noxious stimulus (pressure using an algometer on the trapezius, as above) alters the perception of the first stimulus (hand submerged in a 4°C water bath, VWR International Refrigerated Open Bath, ANOVA Precision Cooker Pro), compared to the baseline PPT (Yarnitsky, 2010). CPM was calculated by subtracting the pressure required to elicit pain (PPT) from the pressure applied during the conditioned pain modulation test to, both measured in kPa.

5.3.3.3 Mechanical Temporal Summation (MTS)

MTS quantifies the increased perception of pain with repeated mechanical stimuli and is thought to reflect enhanced central sensitization and altered pain processing, characteristic of chronic pain (Woolf, 2011). MTS was quantified as the ratio of discomfort levels from a single weighted pinprick (256 mN on the index finger) to a train of 10. The train of 10 pin pricks was applied at a rate of 1 Hz, standardized using a metronome. The Wong-Baker FACES® Pain Rating Scale ranging from 0 (no hurt) to 100 (hurts worse) as a reference for pain levels. A small constant (+1) was added to avoid a loss of zero-rating values.

5.3.3.4 Cold Pressor Tolerance (CPT)

CPT was quantified as the maximum duration a participant can endure with their hand submerged in a 4°C water bath, up to a maximum of 5 minutes. Participants were instructed to keep their hands in the cold water until they could no longer tolerate the discomfort. The duration for which participants' hands remained submerged in water was considered their cold pain tolerance. If participants did not withdraw their hands after 5 minutes, the test ended.

5.3.4 ^{1}H-MRS Acquisition

Single voxel ^{1}H-MRS data were collected from four brain regions: the anterior cingulate cortex, the anterior insular cortex, the posterior insular cortex, and the somatosensory cortex (**Figure 5.1**). We categorized the selected brain regions into sensory components, including the primary somatosensory cortices and posterior insula, and affective components, including the anterior cingulate cortex and anterior insula, to systematically investigate their roles in pain perception and modulation.

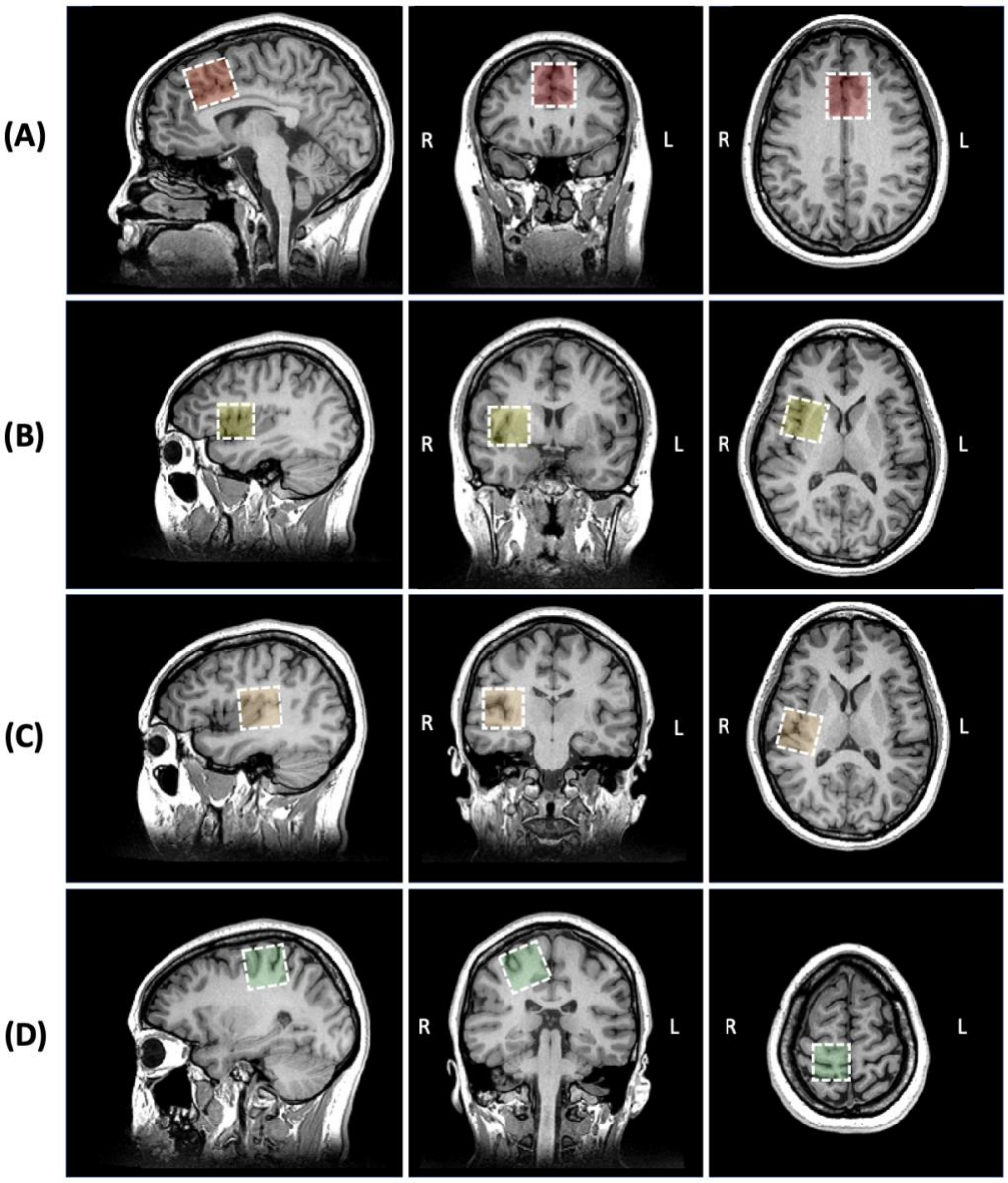

Figure 5.1. *Location of 3x3x3cm^{3} voxels in the (A) anterior cingulate cortex, (B) right anterior insula, (C) right posterior insula, and (D) somatosensory cortex, where the voxel was placed in the hemisphere contralateral to the knee affected with osteoarthritis.*

^{1}H-MRS data were collected on a 3T 750W GE (General Electric Healthcare) scanner using a 32-channel receiver head coil. Anatomical T1-weighted images were acquired to guide voxel placement and for subsequent tissue segmentation for neurochemical quantification. GABA data were collected using a macromolecule-suppressed GABA-edited ^{1}H-MRS acquisition (TR/TE=1800ms/80ms, 20ms editing pulses at 1.5ppm and 1.9ppm, 3x3x3cm^{3} voxels, 256 averages). total glutamate and glutamine (Glx), myoinositol (Myo), and total choline (tCho) were quantified from a short-echo Point RESolved Spectroscopy (PRESS) sequence (TR/TE= 1800ms/30ms, 3x3x3cm^{3} voxels, 64 averages) using the same voxel placement as the GABA-edited sequence.

5.3.5 ^{1}H-MRS Processing and Analysis

GABA-edited spectroscopy data were processed and analyzed using a MATLAB based open-source software package, *Gannet 3.3.1* (A. D. Harris et al., 2015) (MATLAB version 2022b). Preprocessing steps included coil combination, exponential line broadening, zero-filling, Fourier transformation, frequency and phase correction using spectral registration, outlier rejection (if frequency, phase, or full-width at half maximum (FWHM) of the creatine peak are greater than three standard deviations from the group mean), and subtraction to generate the edited difference spectrum. Visual inspection and consideration of FWHM and fit error values were used for quality assessment. Data were rejected if unresolvable subtraction artifacts were present. Tissue correction was done within Gannet by co-registering ^{1}H-MRS voxels to participant T1-weighted structural images and segmenting the voxels using Statistical Parametric Mapping (SPM12; The FIL Methods Group, London, UK) software to determine voxel fractions of gray matter (GM), white matter (WM), and cerebral spinal fluid (CSF). Quantification calculations accounted for tissue-specific density, T1 and T2 relaxation (Near et al., 2021). We report GABA including the "α-correction" (A.

D. Harris et al., 2015), which accounts for the higher concentration of GABA in grey matter (GM) compared to white matter (WM) ($\alpha = 0.5$, which assumes the concentration of GABA in GM is twice that of WM).

PRESS data was preprocessed using *FID-A*, a MATLAB based software (Simpson et al., 2017). The automated preprocessing pipeline includes coil combination, removal of bad averages, frequency drift correction, and zero-order phase correction. Outputs from *FID-A* were then analyzed with *LCModel* software (Version 6.3) (Provencher, 2001). The basis set was simulated using *FID-A* based on sequence timings and the shape of radiofrequency pulses used during our acquisition. Our basis set included alanine, aspartate, choline, glycerophosphocholine, phosphocholine, creatine, phosphocreatine, GABA, glutamate, glutamine, lactate, inositol, N-acetylaspartate, N-acetylaspartylglutamate, scyllo-inositol, glutathione, glucose, taurine, β-hydroxybutyrate, citrate, ethanol, glycine, phosphoethanolamine. *LCModel* default macromolecules were also included. Data were excluded if visual inspection indicated substantial artifacts, the signal-to-noise (SNR) ratio was less than 15 and/or the full width at half maximum (FWHM) of the NAA peak was greater than 0.07 ppm. Tissue correction (again including tissue-specific T1, T2, and density correction) was performed to report absolute neurochemical concentrations in molar units (moles per liter of tissue) (Near et al., 2021).

5.3.6 Statistical Analysis

Shapiro-Wilks tests were employed to check the normality of continuous data elements. Means and standard deviations (SD) are reported for normally distributed data, while medians and interquartile ranges [IQR] are reported for non-normally distributed data.

All statistical analyses were performed in R (version 4.2.3) and RStudio (version 2023.06.1+524) and used a significance level of $p < 0.05$.

5.3.6.1 Group Differences in Centralized Pain Measures and Neurochemical Levels

For normally distributed data, independent t-tests were used to test for differences between KOA and control groups, and paired t-tests were used to measure changes pre-post TKA. For non-normally distributed data, Mann-Whitney U tests were used for group differences (i.e., KOA patients and controls), and Wilcoxon signed-rank tests were used to test for changes pre-post TKA.

5.3.6.2 Association between Neurochemicals and Measures of Centralized Pain

Multiple linear regression analyses examined the relationships between centralized pain measures to test whether this relationship differed between groups. Centralized pain measures included PPT, CPM, MTS, CPT, and painDETECT. These measures were adjusted for improved interpretability so that higher values indicated higher pain sensitivity or more centralized pain likelihood. Measured neurochemicals included gamma-aminobutyric acid (GABA), total glutamate and glutamine (Glx), myoinositol (Myo), and total choline (tCho) within the Anterior Cingulate Cortex (AC), Anterior Insula (AI), Posterior Insula (PI), and Somatosensory Cortex (SS). Significant relationships were explored further using univariate regression plots.

5.3.6.3 Association between Post-TKA Neurochemical Changes and Centralized Pain Improvement

Pearson correlations were used to examine the relationships between longitudinal changes (post-TKA minus pre-TKA) in neurochemical levels (glutamate, GABA, myoinositol, and choline) and changes in centralized pain measures (PPT, CPM, MTS, CPT, and painDETECT).

5.4 Results

The mean age of the twenty KOA patients was 66±4.7 (57-75) years, and nineteen control participants was 65.5±4.7 (59-76) years. Data quality metrics and proportions of ^{1}H-MRS data included in the analysis following quality assessment are summarized in Error! Not a valid bookmark self-reference..

Table 5.1. *Number of MRS datasets collected and analyzed after quality assessment. Mean line width measurements (reported as the full width half maximum, FWHM, of the NAA peak for PRESS and of the Cr peak for GABA-edited, Hz) and the signal to noise ratio (SNR) for the 2 acquisitions of each of the 4 voxels. Quality metrics were extracted from FIDA for PRESS and Gannet for GABA-edited.*

	Anterior Cingulate		**Anterior Insula**		**Posterior Insula**		**Somatosensory Cortex**	
	PRESS	*GABA-edited*	*PRESS*	*GABA-edited*	*PRESS*	*GABA-edited*	*PRESS*	*GABA-edited*
Controls								
Acquired (n)	19	19	19	19	19	19	19	19
Analyzed (n)	18	17	15	18	17	19	19	19
Mean FWHM (Hz)	13.0 (2.3)	10.1 (2.3)	14.0 (1.9)	12.6 (1.1)	13.7 (2.2)	12.2 (1.4)	8.54 (0.9)	9.0 (0.5)
Mean SNR	129.6 (15.2)	127.9 (29.5)	116.2 (12.0)	111.4 (20.4)	129.5 (15.5)	128.8 (25.7)	152.4 (25.6)	145.9 (22.8)
Pre-TKA								
Acquired (n)	20	20	20	20	20	20	18	19
Analyzed (n)	18	15	17	18	20	19	18	18
Mean FWHM (Hz)	14.9 (3.0)	11.3 (2.1)	16.2 (3.2)	13.5 (2.2)	13.0 (2.3)	11.8 (1.5)	8.26 (1.00)	9.2 (0.8)
Mean SNR	122.5 (20.0)	111.9 (20.1)	108.5 (21.3)	99.6 (10.0)	130.7 (26.7)	119.8 (29.5)	160.2 (25.1)	148.3 (26.4)
Post-TKA								
Acquired (n)	14	14	14	14	14	14	14	14
Analyzed (n)	12	13	14	13	11	13	14	14
Mean FWHM (Hz)	14.2 (3.0)	10.5 (1.8)	14.5 (2.2)	12.6 (0.7)	13.9 (3.5)	11.8 (1.0)	8.6 (0.7)	9.0 (0.6)
Mean SNR	124.4 (10.6)	111.3 (22.0)	112.8 (15.1)	105.7 (10.6)	122.1 (14.5)	111.4 (13.3)	159.5 (29.9)	143.0 (29.6)

KOA had higher pain levels on all questionnaires compared to controls, indicating higher pain severity, as well as poorer functioning and stiffness. Additionally, KOA patients had higher levels of catastrophizing and depression, worse mood, and poorer overall mental and physical health (**Table 5.3A**). Pain and function improved significantly on all questionnaires following TKA, except painDETECT (p=0.177) (**Table 5.3B**). Other demographic characteristics of the participants are detailed in **Table 5.2**.

Table 5.2. *Participant demographic information. Data reported as mean (SD) or N (%), as applicable.*

Demographics	Controls (n=19)	KOA (n=20)
Age (years)		
Mean (SD)	65.5 (4.9)	66 (4.7)
Range	59 – 76	57 – 75
Body Mass Index		
Mean (SD)	23.7 (4.5)	27.7 (4.0)
Range	18.6 – 33.9	20.6 - 33.2
Ethnicity, n (%)		
Caucasian	17 (89%)	17 (85%)
South Asian	2 (11%)	0 (0%)
Indigenous	0 (0%)	1 (5%)
Other/mixed	0 (0%)	2 (10%)
Current Marital Status n (%)		
Married	9 (47%)	11 (55%)
Single	1 (5%)	1 (5%)
Common-law	1 (5%)	1 (5%)
Widow/widower	5 (26%)	2 (10%)
Separated or divorced	3 (16%)	5 (25%)
Prefer not to answer	0 (0%)	0 (0%)
Education, n (%)		
Professional school degree (e.g., PhD, law, medicine, ministry)	0 (0%)	3 (15%)
Master's Degree	5 (26%)	3 (15%)
Bachelor's Degree	8 (42%)	2 (10%)
Technical/Trades School	4 (21%)	5 (25%)
High school	2 (11%)	7 (35%)
Did no complete high school	0 (0%)	0 (0%)
Current Employment Status, n (%)		
Full-time	2 (11%)	5 (25%)
Part-time	3 (16%)	3 (15%)
Retired	14 (74%)	12 (60%)
Handedness, R/L	17 (89%) / 2 (11%)	19 (95%) / 1 (5%)
Affected Knee R/L	–	9 (45%) / 11 (55%)

Table 5.3. *Summary of participant questionnaire characteristics, with data reported as median [IQR]. Scoring ranges are reported. As all questionnaire measures were non-normally distributed, group differences were tested between control and KOA groups (Manning-U tests for unpaired samples) and between pre- vs. post-TKA groups (Wilcoxon tests for paired samples); p-values < 0.05 indicate statistical significance.*

A)

Pain Characteristics [Scoring Ranges]	Controls (n=19) Median [IQR]	KOA (n=20) Median [IQR]	p-value
WOMAC			
Pain [0 – 20]	0 [0 – 0.5]	9 [7.8 – 11]	<0.001*
Function [0 – 68]	0 [0 – 1]	31 [24.8 – 41.5]	<0.001*
Stiffness [0 – 8]	0 [0 – 1]	4 [3 – 5]	<0.001*
Overall [0 – 96]	1 [0 – 2.5]	42.5 [34.8 – 59]	<0.001*
CSI			
Total [0 – 100]	18 [15 – 24.5]	28.5 [26.5 – 40.2]	<0.001*
PCS			
Total [0 – 52]	8 [3.5 – 10.5]	11.5 [5.8 – 19.2]	<0.001*
BDI			
Total [0 – 40]	3 [1 – 5.5]	8 [5 – 15.5]	<0.001*
POMS			
Total Mood Disturbance [-24 – 94]	-27 [-31.5 – -15]	2 [-13 – 18.75]	<0.001*
MPQ			
Sensory Dimension [0 – 33]	0 [0 – 0]	15 [10.8 – 21]	<0.001*
Affective Dimension [0 – 12]	0 [0 – 0]	3.5 [2 – 5.2]	<0.001*
VAS general pain [0 – 100]	1 [0 – 10.2]	64 [53 – 70]	<0.001*
SF-36			
Mental Health [0 – 100]	84.1 [76.4 – 87.2]	59.2 [47.1 – 68.7]	<0.001*
Physical Functioning [0 – 100]	97.4 [93.4 – 98.0]	46.0 [28.6 – 52.6]	<0.001*

B)

Pain Characteristics	Pre-TKA (n=14)	Post-TKA (n=14)	p-value
WOMAC			
Pain [0 – 20]	8.5 [8 – 10.8]	4 [2 – 5.8]	0.002*
Function [0 – 68]	31 [25.5 – 40.2]	10 [7 – 19.8]	0.001*
Stiffness [0 – 8]	4 [3 – 5]	3 [2 – 3.8]	0.038*
Overall [0 – 96]	42.5 [36.2 – 57.2]	17.5 [11.2 – 29.5]	0.001*
CSI			
Total [0 – 100]	27.5 [25.5 – 36.5]	21.5 [19 – 25.5]	0.008*
PCS			
Total [0 – 52]	13.5 [7.2 – 24.2]	4 [2 – 6]	0.002*
BDI			
Total [0 – 40]	7 [5 – 11.8]	3.5 [2 – 5.8]	0.013*
POMS			
Total Mood Disturbance [-24 – 94]	-2 [-16.5 – 7]	-15 [-20.5 – -7.8]	0.002*
MPQ			
Sensory Dimension [0 – 33]	15 [10.2 – 21]	4.5 [2.2 – 6]	0.001*
Affective Dimension [0 – 12]	3.5 [2 – 8]	1 [0 – 1.8]	0.003*
VAS general pain [0 – 100]	64 [55 – 69]	21 [8.5 – 26.5]	0.002*
SF-36			
Mental Health [0 – 100]	60.5 [55.1 - 67.7]	74.1 [64.1 – 78.0]	0.002*
Physical Functioning [0 – 100]	48.7 [34.5 - 52.6]	60.5 [55 - 64.1]	0.028*

WOMAC: Western Ontario and McMaster Universities Osteoarthritis Index; PD-Q: painDETECT; CSI: Central Sensitization Inventory; PCS: Pain Catastrophizing Scale; BDI: Beck Depression Inventory; POMS: Profile of Mood States; MPQ: McGill Pain Questionnaire; SF-36: 36-Item Short-Form Health Survey; VAS: visual analog scale.

5.4.1 Group Differences in Centralized Pain Measures and Neurochemical Levels

Overall, KOA patients had more centralized pain (i.e., widespread pain sensitivity) than controls (**Table 5.4A**). Centralized pain metrics did not significantly improve 3-months following TKA (p>0.05), though self-reported knee pain did improve (**Table 5.4B**).

Table 5.4. *Summary of centralized pain measures (untransformed), with data presented as median [IQR]. Group differences were tested between A) control and KOA groups (Manning-U tests for unpaired samples) and B) pre- and post-TKA groups (Wilcoxon tests for paired samples); p-values < 0.05 indicate statistical significance.*

A)

Pain Characteristics [Scoring Range]	Controls (n=19) Median [IQR]	KOA (Pre-TKA, n=20) Median [IQR]	p-value
Pain Pressure Threshold (PPT)			
Trapezius (kPa) [0 – 1110]	776.67 [651.7 – 1012.7]	576.7 [422.5 – 721.7]	0.012*
Conditioned Pain Modulation (CPM)			
Conditioned-baseline (kPa) [-1110 – 1110]	100 [3.33 – 158.5]	28.33 [-52.17 – 230]	0.305
Mechanical Temporal Summation (MTS)			
Finger WUR 256 mN [1 – 101]	1.1 [1 – 3.2]	3.3 [1.6 – 9.1]	0.042*
Cold Pressor Tolerance (CPT)			
Time (seconds) [0 – 300]	69 [31 – 300]	35 [20 – 52.2]	0.036*
painDETECT			
VAS current pain [0 – 10]	0 [0 – 0]	4 [2.8 – 5.5]	<0.001*
VAS strongest pain [0 – 10]	1 [0.5 –2]	8 [7.8 – 9]	<0.001*
VAS average pain [0 – 10]	0 [0 – 1]	6 [5 – 7]	<0.001*
Neuropathic pain score [0 – 38]	1 [0 – 2]	12.5 [8.5 – 15.5]	<0.001*

B)

Pain Characteristics	Pre-TKA (n=14)	Post-TKA (n=14)	p-value
Pain Pressure Threshold (PPT)			
Trapezius (kPa) [0 – 1110]	571.7 [407.5 – 771.7]	544 [496.6 – 689.9]	0.890
Conditioned Pain Modulation (CPM)			
Conditioned-baseline (kPa) [-1110 – 1110]	20 [-45 – 230]	76.3 [30.4 – 122.8]	0.597
Mechanical Temporal Summation (MTS)			
Finger WUR 256 mN [1-101]	3.1 [1.7 – 7.9]	2 [1.5 – 5.5]	0.462
Cold Pressor Tolerance (CPT)			
Time (seconds) [0 – 300]	27.5 [19.2 – 35.5]	40.5 [25.8 – 60]	0.069
painDETECT			
VAS current pain [0 – 10]	5 [3.2 – 6.5]	1 [0.2 – 2]	<0.001*
VAS strongest pain [0 – 10]	8 [8 – 9]	5.5 [2.2 – 6]	<0.001*
VAS average pain [0 – 10]	6 [5 – 7]	2.5 [1 – 3.8]	<0.001*
Neuropathic pain score [0 – 38]	13 [9.2 – 15]	9 [7.2 – 12.2]	0.214

Significantly lower GABA levels were observed within the anterior cingulate cortex in KOA patients compared to controls (p=0.012) (**Table 5.5A**). These lower GABA levels did not significantly change 3-months following TKA (**Figure 5.2**). There were no statistically significant differences in other neurochemicals or other brain regions (**Table 5.5B**).

Table 5.5. *Summary of neurochemical concentrations with testing for group differences between A) osteoarthritis patients to healthy controls (unpaired t-tests) and B) pre- and post-TKA patients (paired t-tests).*

A)

Neurochemical Concentration (mmol/L)	Controls (n=19) mean (SD)	KOA (pre-TKA, n=20) mean (SD)	p-values
Anterior Cingulate Cortex			
GABA	1.01 (0.32)	0.75 (0.23)	**0.012***
Glx	11.86 (2.39)	11.85 (2.12)	0.988
Myo	4.64 (1.34)	5.54 (1.69)	0.082
tCho	2.23 (0.25)	2.14 (0.45)	0.469
Anterior Insular Cortex			
GABA	1.19 (0.38)	1.07 (0.39)	0.392
Glx	13.18 (2.47)	14.17 (2.06)	0.205
Myo	4.59 (1.22)	4.96 (1.06)	0.348
tCho	2.14 (0.39)	2.19 (0.26)	0.658
Posterior Insular Cortex			
GABA	1.07 (0.42)	1.11 (0.44)	0.769
Glx	12.46 (2.1)	11.39 (1.72)	0.108
Myo	4.5 (1.7)	5.53 (1.44)	0.062
tCho	1.86 (0.26)	1.83 (0.29)	0.710
Somatosensory Cortex			
GABA	1.68 (0.25)	1.75 (0.43)	0.553
Glx	9.33 (1.13)	9.46 (0.81)	0.702
Myo	4.26 (1.01)	4.32 (0.68)	0.844
tCho	1.78 (0.11)	1.75 (0.15)	0.420

B)

Neurochemical Concentration	Pre-TKA (n=14)	Post-TKA (n=14)	p-values
Anterior Cingulate Cortex			
GABA	0.75 (0.27)	0.9 (0.3)	0.206
Glx	12.22 (2.04)	12.19 (3.15)	0.705
Myo	5.6 (1.52)	5.54 (0.94)	0.919
tCho	2.01 (0.28)	2.25 (0.34)	0.105
Anterior Insular Cortex			
GABA	1.04 (0.33)	1.16 (0.29)	0.262
Glx	14.13 (2.22)	13.11 (2.61)	0.133
Myo	4.89 (1.06)	5.65 (1.27)	0.178
tCho	2.18 (0.22)	2.19 (0.46)	0.731
Posterior Insular Cortex			
GABA	1.14 (0.52)	1.13 (0.34)	0.913
Glx	11.09 (1.67)	11.81 (2.14)	0.631
Myo	5.69 (1.5)	5.24 (1.21)	0.667
tCho	1.81 (0.28)	1.88 (0.31)	0.635
Somatosensory Cortex			
GABA	1.65 (0.34)	1.5 (0.35)	0.288
Glx	9.53 (0.72)	9.4 (0.61)	0.671
Myo	4.33 (0.77)	4.42 (0.67)	0.776
tCho	1.74 (0.17)	1.91 (0.23)	0.059

GABA: gamma-aminobutyric acid; Glx: total glutamate and glutamine; Myo: myoinositol; tCho: total choline

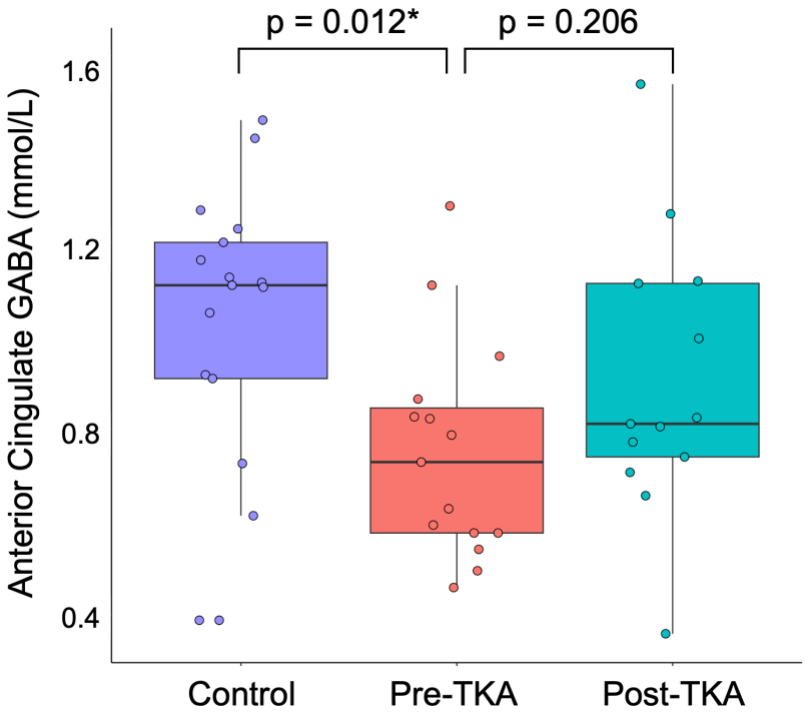

Figure 5.2. *GABA levels (mmol/L) in the anterior cingulate cortex in healthy controls (left), knee osteoarthritis patients before TKA (middle), and after TKA (right). P-values from unpaired t-tests comparing controls and pre-TKA groups and paired t-tests comparing pre-TKA and post-TKA longitudinally.*

5.4.2 Association between Neurochemicals and Measures of Centralized Pain

The coefficients for the multiple linear regression model are detailed in **Table 5.6**.

Table 5.6. *Summary of multiple linear regression coefficients for the model Pain ~ β0 + β1*Neurochemical + β2*Group + β3*Neurochemical*Group, the data were transformed to represent higher sensitivity with higher numbers and lower sensitivity with lower numbers. Statistically significant coefficients (p < 0.05) are denoted with an asterisk (*).*

Neurochemical	**PPT**			**CPM**			**MTS**			**CPT**			**painDETECT**		
	β1	β2	β3	β1	β2	β3	β1	β2	β3	β1	β2	β3	β1	β2	β3
Anterior Cingulate															
GABA	-64.7	296.0	-169.7	56.9	250.8	-246.2	0.7	14.3	-13.9	**154.6***	**258.8***	-159.7	0.9	**11.8***	-2.1
Glx	12.7	**845.7***	-55.2	-5.4	-213.5	22.1	1.4	25.9	-1.9	2.2	124.1	-2.3	0.5	13.2	-0.3
Myo	-2.6	68.9	26.8	39.5	**719.8***	**-125.1***	1.9	14.7	-1.7	-25.7	-5.3	16.3	0.5	**20.0***	-1.7
tCho	205.6	362.2	-81.9	-138.4	5.8	24.8	11.6	15.8	-5.8	-15.1	89.7	3.3	0.9	-3.2	6.3
Anterior Insula															
GABA	-34.9	112.1	60.5	114.9	228.6	-167.7	-0.2	-4.4	8.5	-27.6	53.7	20.1	0.4	4.7	5.5
Glx	-5.1	-332.0	38.8	17.8	487.9	-33.3	-0.5	-8.0	0.8	7.2	214.1	-9.7	-0.1	10.4	0.0
Myo	-20.0	-124.6	62.3	76.6	**652.5***	**-121.7***	0.0	10.3	-1.8	-21.9	21.4	12.6	-0.9	12.8	-0.4
tCho	329.9	377.2	-94.1	173.8	632.1	-274.1	6.6	23.9	-10.6	20.9	172.0	-42.1	-1.7	13.9	-1.4
Posterior Insula															
GABA	22.4	372.5	-149.4	88.0	234.0	-183.1	1.3	5.2	-1.6	-52.4	34.0	51.6	-1.7	7.3	2.6
Glx	-25.4	154.9	3.3	7.1	136.3	-8.0	**-2.8***	**-46.2***	**4.3***	-14.9	-113.0	18.0	-0.4	-12.1	**1.9***
Myo	16.6	238.6	-9.7	2.2	165.9	-24.5	0.1	-5.9	2.0	8.1	166.9	-13.9	-0.6	4.4	1.2
tCho	-7.4	141.9	21.6	57.7	583.6	-293.2	-5.0	-30.4	18.7	-9.6	75.0	10.4	-2.1	-1.9	6.8
Somatosensory															
GABA	-55.2	296.1	-49.7	161.8	267.0	-139.7	-1.7	-7.2	6.8	15.1	130.0	-24.6	4.0	12.0	-0.8
Glx	26.8	1352.0	-119.1	-17.7	76.1	-5.6	-1.3	-5.8	1.0	20.2	233.2	-15.6	-0.3	-15.3	2.7
Myo	2.0	131.7	19.2	9.1	406.4	-85.0	-0.4	-6.6	2.2	-5.0	103.3	-3.3	-1.0	0.2	2.2
tCho	327.5	328.0	-77.6	-42.0	128.5	-56.0	6.1	16.6	-7.5	164.9	461.0	-211.1	5.0	1.4	4.4

PPT: Pain Pressure Thresholds; CPM: Conditioned Pain Modulation; MTS: Mechanical Temporal Summation; CPT: Cold Pressor Tolerance; AC: Anterior Cingulate Cortex; AI: Anterior Insula; PI: Posterior Insula; SS: Somatosensory Cortex; GABA: gamma-aminobutyric acid; Glx: total glutamate and glutamine; Myo: myoinositol; tCho: total choline.

Significant group interactions were further explored using univariate regressions. Significant group interactions were identified between MTS and posterior insula Glx concentrations (univariate relationships shown in **Figure 5.3A**) and painDETECT and posterior insula Glx concentrations (**Figure 5.3B**) as well as between CPM and myoinositol concentration in the anterior cingulate cortex (**Figure 5.3C**) and the anterior insular cortex (**Figure 5.3D**).

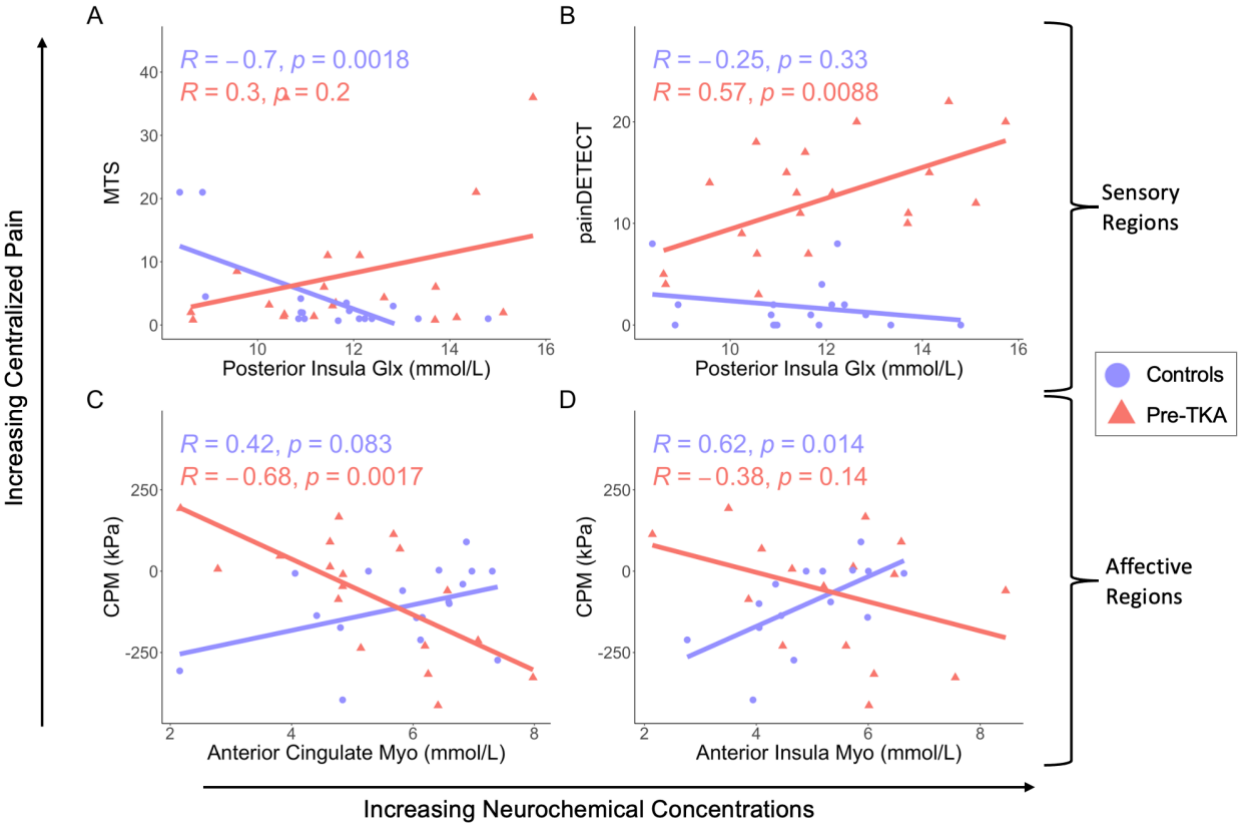

Figure 5.3. *Univariate analyses of the statistically significant multivariate regression group interactions (from Table 5.5) between A) MTS and Glx levels (mmol/L) in the posterior insular cortex, B) painDETECT and Glx levels (mmol/L) in the posterior insular cortex, C) CPM and myoinositol levels (mmol/L) in the anterior cingulate cortex, as well as D) CPM and myoinositol levels (mmol/L) in the anterior insular cortex for controls (circles, purple) and KOA patients (triangles, red). All values were adjusted so that higher values indicated higher pain sensitivity or more centralized pain likelihood. P-values indicate significance for group level univariate relationships between centralized pain and neurochemical concentrations.*

Univariate analyses showed negative relationships (higher centralized pain associated with lower neurochemical levels) in the KOA group between CPM and myoinositol concentration in anterior insular cortex (r = -0.68, p = 0.0017, **Figure 5.3D**), and a trend towards an association in the anterior cingulate (r = -0.38, p = 0.14, **Figure 5.3C**).

Positive relationships (higher centralized pain associated with higher neurochemical levels) were observed in the control group (r = 0.62, p = 0.014, **Figure 5.3D**; r=0.42, p = 0.083, **Figure 5.3C**, respectively). In the posterior insular cortex, a trend-level positive relationship in the KOA group (r = 0.3, p = 0.2) and a significant negative relationship in the control group (r = -0.7, p = 0.0018, **Figure 5.3A**) was observed between MTS and Glx concentrations. In the posterior insula, there was a positive relationship between painDETECT scores and Glx concentrations in the KOA group (r = 0.57, p = 0.0088) and a trend-level negative relationship in the control group (r = -0.25, p = 0.33, **Figure 5.3B**).

5.4.3 Association between Post-TKA Neurochemical Changes and Centralized Pain Improvement

Figure 5.4 details the coefficients for the correlations between changes in neurochemical levels and centralized pain improvement post-TKA.

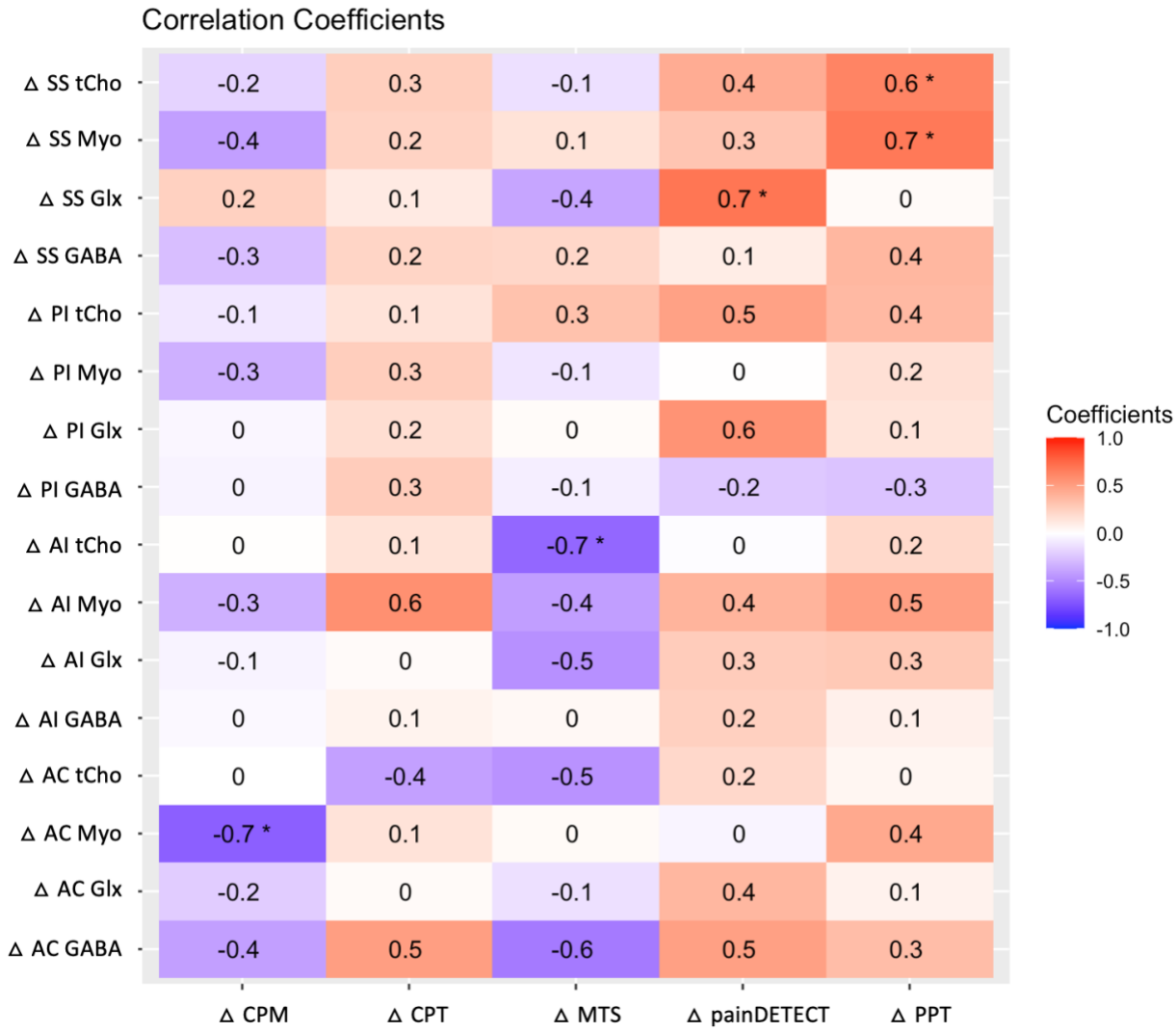

Figure 5.4. *Correlation coefficients between changes in neurochemical levels (mmol/L) and changes in centralized pain metrics post-TKA. (Change calculated as post – pre for both). Red coefficients indicate a positive relationship (i.e., greater pain improvements associated with decreases in neurochemical levels post-TKA compared to pre-TKA). Blue coefficients indicate a negative relationship (i.e., greater pain improvements associated with higher neurochemical levels post-TKA). PPT: Pain Pressure Thresholds; CPM: Conditioned Pain Modulation; MTS: Mechanical Temporal Summation; CPT: Cold Pressor Tolerance; AC: Anterior Cingulate Cortex; AI: Anterior Insula; PI: Posterior Insula; SS: Somatosensory Cortex; GABA: gamma-aminobutyric acid; Glx: total glutamate and glutamine; Myo: myoinositol; tCho: total choline.*

Significant positive relationships (lower neurochemical levels post-TKA associated with greater improvement in centralized pain measures post-TKA) were identified between changes in painDETECT questionnaire scores and changes in Glx levels in the somatosensory cortex before and after TKA surgery (r = 0.69, p = 0.013, **Figure 5.5A**), as well as between changes in PPT and changes in myoinositol levels (r = 0.68, p = 0.016, **Figure 5.5B**) and total choline levels (r = 0.62, p = 0.031, **Figure 5.5C**) in the somatosensory cortex. Significant negative relationships (higher neurochemical levels post-TKA associated with greater improvement in centralized pain measures post-TKA) were found between changes in CPM and changes in myoinositol levels in the anterior cingulate cortex (r = -0.69, p = 0.018, **Figure 5.5D**) and between changes in MTS and changes in total choline levels in the anterior insula (r = -0.66, p = 0.027, **Figure 5.5E**).

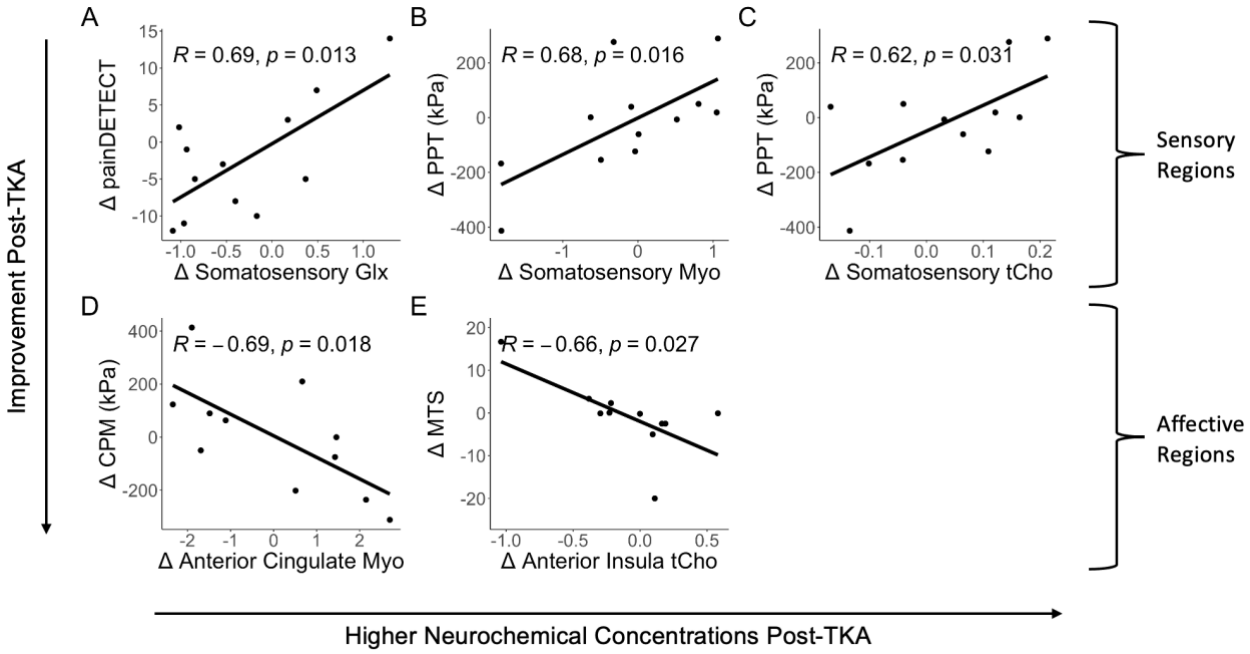

Figure 5.5. *Significant Pearson correlations coefficients between changes in neurochemical levels (mmol/L) and changes in centralized pain measures before and after TKA. (Change calculated as post – pre). All pain measures were adjusted so that lower values indicated improvement in centralized pain measures post-TKA.*

5.5 Discussion

Knee pain improved overall in female patients who underwent total knee arthroplasty (TKA). However, measures of centralized (widespread) pain did not significantly improve at the group level following TKA, indicating that these measures capture a distinct mechanism of pain (central pain as opposed to peripheral). In comparing neurochemical levels between pain-free controls and KOA patients, we discovered lower GABA levels in the anterior cingulate cortex in KOA patients. When investigating the relationship between neurochemical levels and centralized pain (both between pain-free controls and KOA patients and in changes pre- and post-surgery), we found that, broadly, centralized pain in sensory brain regions was associated with higher levels of Glx, Myo, and tCho, while in affective regions, centralized pain was associated with lower levels of Myo and tCho.

In contrast to our finding of lower levels of GABA compared to controls in the anterior cingulate cortex, previous studies examining neurochemistry in the anterior cingulate cortex in KOA patients did not report significant differences compared to controls (El-Najjar et al., 2020; Reckziegel et al., 2016). However, it's worth noting that previous studies utilized a long echo time (TE = 105 ms) PRESS sequence optimized for GABA detection, rather than employing editing techniques designed explicitly for GABA detection. It's been demonstrated that selecting an optimal TE holds little value when the overlapping neurochemical (in this instance, creatine overlaps GABA at 3ppm) necessitates removal via editing (Choi et al., 2021). Interestingly, significantly lower levels of GABA compared to controls were observed in the insula of fibromyalgia patients (Foerster et al., 2012). Notably, this GABA measure was obtained using a GABA-edited sequence (MEGA-PRESS), albeit from a smaller voxel size of 18 mL (3 x 2 x 3 cm^3) as opposed to the recommended 27 mL (3 x 3 x 3 cm^3) voxel size when using edited sequences. While we did not find differences in Myo levels in any

brain regions examined, elevated Myo levels compared to controls were detected in the thalamus of KOA patients (Weerasekera et al., 2021). This discrepancy from our findings could be attributed to the thalamus being a subcortical structure, whereas our study focused on cortical regions.

We found intriguing associations between these neurochemicals and centralized pain-related measures across different brain regions. In case-control comparisons, higher pain sensitivity (higher MTS values) as well as a higher likelihood of having centralized pain (higher painDETECT scores) were associated with higher Glx concentrations in the posterior insula of KOA patients while the opposite relationship was true for controls. When analyzing longitudinal changes, worsening of centralized pain (higher painDETECT scores post-TKA) was associated with increased Glx levels in the somatosensory cortex after TKA. These elevated levels of Glx associated with centralized pain may explain why randomized controlled trials have shown that duloxetine, a compound that decreases glutamatergic receptor expression (Calabrese et al., 2012), is efficacious in improving pain for some KOA patients (Chappell et al., 2009).

Additionally, worsening in pain thresholds (higher adjusted PPT values post-TKA) were associated with increases in Myo and tCho in the somatosensory cortex following TKA. This increase in Myo levels post-TKA may explain why some anticonvulsant drugs, shown to deplete myoinositol levels (Lepore et al., 2021), are efficacious in improving pain for some patients. The discovery of associations between increased Glx, Myo, and tCho levels in specific sensory brain areas of KOA patients and worsening centralized pain post-TKA supports the understanding of why central pain conditions respond best to medications that

modulate the central nervous system, such as serotonin-norepinephrine reuptake inhibitors (e.g. duloxetine) and anticonvulsants (Clauw & Hassett, 2017).

In case-control comparisons, worse pain inhibition (lower adjusted MTS values) was associated with lower Myo concentrations in both the anterior cingulate cortex and the anterior insula of KOA patients while the opposite relationship was true for controls. When analyzing longitudinal changes, improvement in pain inhibition (higher adjusted CPM values post-TKA) was associated with increased Myo levels in the anterior cingulate after TKA while improved pain sensitivity (higher adjusted MTS values post-TKA) was associated with increased tCho in the anterior insula after TKA. Broadly, Myo and tCho are indicative of neuroinflammation and are markers of activated glial cells (increased glial cell volume) and membrane turnover, respectively (Chang et al., 2013; de Graaf, 2019). These findings partly support the idea of neuroinflammation having a dual role in KOA pain, whereby, surgery-induced neuroinflammation might aid in short-term recovery by promoting neuronal health, but it could be harmful if it becomes uncontrolled or prolonged (Weerasekera et al., 2021). Building on this, it is possible that sensory regions of the brain (which play a crucial role in integrating sensory information from various body regions (Brooks et al., 2005; Frot et al., 2013)) are involved in restoring neuronal health by increasing neuroinflammatory neurochemicals for healing purposes, while affective brain regions (second order brain regions that integrate emotional and motivational information following sensory processing (Bushnell et al., 2013; Wiech & Tracey, 2009)) may be attempting to compensate for this rise in neuroinflammation. Given this hypothesis, a promising avenue for further exploration is the implementation of brain stimulation techniques to target sensory brain regions, such as the somatosensory cortex. Transcranial magnetic stimulation (TMS) or transcranial direct current stimulation (tDCS) provide a means to modulate activity in the sensory regions which

may have downstream effects in the second order affective brain regions, effectively normalizing neurochemistry throughout the brain.

This study distinguishes itself by employing a macromolecule-suppressed GABA-edited sequence, which provides a purer measure of GABA compared to previous studies that report GABA+ (the combination of the GABA signal, ~55%, and the macromolecule signal, ~45%). Notably, it is the first investigation in KOA to simultaneously examine four brain regions using magnetic resonance spectroscopy ^{1}H-MRS. This multi-region investigation proved insightful as it revealed opposing associated between neurochemistry and centralized pain measures in affective and sensory regions.

Despite these observed trends in this exploratory study, our small sample size may have limited our ability to draw broad conclusions about centralized pain in females with KOA given the variability and complex nature of pain processing. Thus, future studies with larger sample sizes could likely provide deeper insights into the role of neurochemicals in modulating centralized pain perception in KOA. Additionally, despite the suggestion that some reversals in pain-related brain alterations can be seen after only 1 month following peripheral surgical treatment (Weerasekera et al., 2021), our findings suggest that 3-months post-TKA may be too early to see signs of reversals in neurochemical levels.

5.6 Conclusion

Overall, our results highlight the complexity of neurochemical alterations in different brain regions in individuals with KOA and their associations with centralized pain-related measures. These findings underscore the importance of considering the regional specificity of neurochemical changes and their implications for pain processing mechanisms in KOA as

lower neurochemical levels in affective brain regions (anterior cingulate cortex and anterior insular cortex) and higher neurochemical levels in sensory brain regions (posterior insular cortex and somatosensory cortex) were associated with altered sensory processing in KOA patients. Future research focusing on elucidating the underlying mechanisms of these neurochemical alterations and their contributions to centralized pain perception in a larger cohort of KOA patients is warranted. Additionally, further investigation into potential therapeutic interventions targeting these neurochemical pathways may hold promise for the management of centralized pain in individuals with KOA.

CHAPTER SIX

※

Discussion

Chapter 6: Discussion

The overarching goal of this thesis was to examine neurochemical alterations in KOA and changes following TKA with the motivation that understanding the central (brain) changes will support the development of new therapies. Over the course of performing this study, two possible shortcomings of ^{1}H-MRS neurochemical quantification were identified and studied. This chapter will discuss the specific contributions of this thesis in the areas of ^{1}H-MRS methods development and neurochemical alterations in painful knee osteoarthritis within the context of the broader literature. Further, the limitations and challenges encountered in this thesis work will be discussed, as well as recommendations for future work.

6.1 ^{1}H-MRS Methods Development

The current recommended quantification model for ^{1}H-MRS is hindered by unknown variables. One of these variables is the correction factor for differences in neurochemical concentrations between WM and GM (α). As such, I determined α for six commonly measured neurochemicals (tNAA, tCr, tCho, Myo, Glu and Glx). Additionally, I propose a tissue correction model than not only implements our calculated correction but also uses the correction factor to normalize measures to a pure GM voxel, as per Harris, et al (2015), to enhance comparability between studies. Secondly, it is customary to use literature values for T1, T2 and proton density within the tissue correction model. However, it was unknown how inter-individual differences in relaxation rates constants may affect concentration measures. Using individually measures T1, T2 and PD, I determined that interindividual differences in these parameters contribute to subtle, yet significant differences in calculated neurochemical concentrations. For both of these analyses, I performed sensitivity analyses to demonstrates the efficacy and reliability of these methods. Establishing tissue correction factors and

determining the impact of inter-individual differences in constants were necessary steps for improving the accuracy and consistency of absolute ^{1}H-MRS neurochemical measurements.

Due to previously undetermined correction factors (α), existing ^{1}H-MRS quantification software packages that implement tissue correction, including Osprey (Oeltzschner et al., 2020), Gannet (Edden et al., 2014), and FSL-MRS (Clarke et al., 2021), only utilize an old tissue correction model (Charles Gasparovic et al., 2006). With the determination and implementation of these correction factors, the consensus recommended tissue correction model will be able to be implemented as prescribed (Charles Gasparovic et al., 2018; Near et al., 2021). While the consensus recommended tissue correction model exists in the form of a published equation, there was previously no standardized way to implement this equation when using quantification software that do not implement tissue correction (e.g., jMRUI (Jabłoński et al., 2017), TARQUIN (Wilson et al., 2011), and LCModel (Provencher, 2001)). To address these challenges, I developed a tool designed to standardize the implementation of tissue correction procedures in ^{1}H-MRS analyses, which includes tissue correction factors calculated in **Chapter 3** and constants compiled in **Chapter 4**. This tool facilitates automated calculation of corrected neurochemical concentrations, thereby streamlining data processing and enhancing methodological consistency across studies.

Challenges and future directions

A limitation of absolute quantification is its dependence on several assumptions, such as the ratio of neurochemical concentrations within gray matter (GM) and white matter (WM) (α), the relaxation times of water and neurochemicals within GM, WM, and CSF (T1 and T2), and the relative water density within GM, WM, and CSF. Chapters 3 and 4 aimed to evaluate the assumed α and properties of water, respectively, while maintaining all other

standard assumptions. Although these assumptions are likely accurate for our young, healthy adult cohort, they may not apply universally to all populations. It is crucial to test and refine each assumption individually to enhance absolute quantification methods. Therefore, each assumption needs to be independently tested across different populations (e.g., various ages and pathologies) to determine the reliability of these methods.

The determination of the correction factors (α) was an important initial step towards understanding the nuances of neurochemical distributions within the WM and GM of a young healthy population. However, future research should aim to expand upon this foundation by exploring potential variations of α across different age groups and in various pathological conditions. Furthermore, building upon the identified regional disparities within the anterior and posterior brain regions, future investigations should delve into elucidating potential distinctions within the superior and inferior brain regions. This holistic approach will ensure a more comprehensive understanding of neurochemical distributions in the brain. Such investigations are important to determine whether α effectively captures the full spectrum of neurochemical distributions across diverse populations, thus ensuring the generalizability and applicability of our findings.

When exploring the effects of inter-individual differences in T1, T2, and PD, a preliminary sensitivity analysis was performed using an extended range of T2 values from a meta-analysis to determine the potential effects T2 across a wider age range and in clinical disorders. This analysis provided further evidence that using uniform literature values may not be accurate, motivating the explicit exploration of 1, T2, and PD across different age groups and clinical disorders in future studies.

6.2 Neurochemical Alterations in Painful Knee Osteoarthritis

As the only study to date that has investigated neurochemistry in multiple brain regions in KOA, this study highlights the importance of considering regional differences in

neurochemical profiles and suggests further investigation of potential therapeutic interventions targeting these neurochemical pathways for the management of centralized pain in KOA. Briefly, centralized pain in KOA patients was associated with higher inflammatory neurochemicals levels in sensory brain regions and lower inflammatory neurochemical levels in affective brain regions. These findings of regional disparities suggest that neuroinflammation in sensory brain regions may attempt to promote healing with increased inflammatory neurochemicals, while affective brain regions may try to compensate for this by decreasing inflammatory neurochemicals. One promising avenue for further exploration is the implementation of brain stimulation techniques for targeted treatment of centralized pain. Considering sensory regions as first order regions (receiving pain signals from the body) and affective regions as second order regions (receiving pain signals from sensory regions), brain stimulation techniques like transcranial magnetic stimulation (TMS) or transcranial direct current stimulation (tDCS) applied to sensory regions may be used to modulate excitatory/inhibitory activity, potentially normalizing neurochemistry across the brain. By targeting specific brain regions implicated in pain processing, these interventions have the potential to offer personalized and effective pain relief for individuals living with KOA.

This study distinguishes itself from other studies in KOA (El-Najjar et al., 2020; Reckziegel et al., 2016; Weerasekera et al., 2021) as it measures GABA levels using the macromolecule-suppressed GABA-editing technique. This acquisition is specifically designed to suppress the macromolecule signal, to provide a more specific measure of GABA compared to previous studies that report GABA+ (the combination of the GABA signal, ~55%, and the macromolecule signal, ~45%). Previous research from our lab has highlighted the importance of this approach, as it prevents inaccuracies in reported GABA levels that could arise from including macromolecule signals. For example, while past studies have suggested that GABA+ levels increase with age, macromolecule suppression shows no such

correlation between age and GABA levels (T. Bell, Stokoe, & Harris, 2021). This suggests that age-related changes previously attributed to GABA may actually be due to changes in macromolecule levels. This could similarly explain why two studies found negative correlations between pain and GABA+ levels but no GABA+ differences between KOA patients and controls (El-Najjar et al., 2020; Reckziegel et al., 2016). It is possible that macromolecules negatively correlate with pain, but not GABA, and that macromolecules prevent the detection of differences between KOA patients and controls.

Challenges and future directions

In an effort to have a homogeneous KOA sample that were expected to have pain resolution following TKA (i.e., no OA in the contralateral knee), we decided to study unilateral KOA and pain. This decision was supported by population data that suggests the majority of patients with KOA have a single knee replacement (Leech et al., 2024). Despite efforts to recruit exclusively unilateral KOA participants, the prevalence of widespread pain and likely multi-joint OA involvement as well as the tendency for those undergoing TKA often progress to develop OA in the contralateral knee resulted in the inclusion of both unilateral and bilateral cases. While this may enhance the generalizability of our study to the broader OA population, it raises questions about the impact of sample characteristics on study outcomes.

Extensive literature underscores the presence of sex differences in pain perception, with women often exhibiting increased pain sensitivity and a higher risk for pain compared to men. Even among cohorts of men and women with similar pain severity, women consistently report higher pain sensitivity and ratings on psychosocial modulators of pain (Y. Zhu et al., 2023). Our study, conducted exclusively on a female sample, provides valuable insights into pain mechanisms in female KOA patients. However, given the documented sex differences in

pain responses, it is imperative to explore whether similar findings would be observed in a larger cohort including both males and females. By incorporating males into future studies, we can evaluate the generalizability of our findings and elucidate potential sex-specific differences in neurochemistry profiles and pain processing mechanisms. This comparative approach will enhance our understanding of sex-related disparities in pain perception and inform tailored treatment strategies for knee OA patients of both sexes.

6.3 Testing the Effect of Tissue Correction Factors (α) on Application Results

While this thesis developed correction factors for differences in neurochemical concentration between WM and GM, I did not implement these correction factors (in **Chapter 3**) to the study of KOA pain (**Chapter 5**)'s quantification of neurochemical concentrations, as this correction method has not yet been accepted in the field. For interest, I have re-performed all the statistical analyses using the correction factors, with results shown in **Appendix C**. Implementing our correction factors resulted in larger effects but generally does not affect the interpretations. Specifically, while using our correction factors (determined in **Chapter 3**) affects neurochemical concentration, it is not a meaningful effect for tCho and Myo. It is, however, meaningful for Glx as there is approximately 2 times more Glx in GM than WM. As shown in the sensitivity analysis in **Chapter 3**, this difference becomes even more pronounced in voxels with higher WM content (~90%) when normalizing to a pure GM voxel.

The only case where the results were different was in the longitudinal change analyses, where a change in painDETECT scores was no longer significantly positively associated with a change in somatosensory Glx ($p = 0.17$). Additionally, a change in somatosensory Glx was negatively associated with a change in MTS ($p = 0.029$). The cause of these differences could be threefold: the subtraction of 2 neurochemical concentrations with implicit error/noise exacerbates the error/noise in our neurochemical concentrations, the

somatosensory is the voxel with the highest WM content introducing errors in normalization, and/or Glx has the correction factor with the most prominent effect. Our sensitivity analysis in **Chapter 3** shows that voxels with higher WM content normalized to a purely GM voxel are associated with more error. The somatosensory voxels in this dataset have ~60% WM compared to ~30% WM in other voxels, potentially indicating that it would be better to normalize to 50% GM / 50% WM voxel, as discussed in **Appendix C**. While these concentrations are technically more accurate with the implementation of correction factors, the only detectable change is in the Glx concentrations, where 2x more Glx in GM than WM has a meaningful effect (compared to other neurochemicals that range from equal distributions in GM than WM to 1.4x more neurochemicals in GM than WM).

In **Chapter 3**, I show that tissue correction is essential for more accurate neurochemical concentration measures. However, when I apply this method to my own data, it does not provide a meaningful change in concentrations. Although these measures can be up to 55% more accurate for voxels with high WM content (~90% WM), the voxels in this study where more equally distributed (~40% GM, 40% WM, and 10% CSF) and thus, the application of the correction factor had little effect, despite being more accurate in theory. Furthermore, I have shown in **Chapter 4** that inter-individual differences in T1, T2, and PD do not provide a meaningful change in concentrations. Thus, while it may be desired to use the most accurate measures possible by acquiring individual measures using quantitative synthetic imaging, it was not necessary to apply individually measured constants to my pain in KOA data in **Chapter 5**.

6.4 Conclusions

In conclusion, this dissertation has significantly advanced the field through three key contributions. Firstly, I developed tissue correction factors and created an open-source tool,

enabling researchers to implement these factors for accurate and standardized quantification of neurochemical concentrations. Secondly, I used quantitative synthetic imaging to acquire individualized constants required to use the consensus recommended quantification method, to determine the impact of inter-individual differences on measurement accuracy. Finally, the application of ^{1}H-MRS to KOA revealed diverse relationships within brain regions associated with the sensory and affective dimensions of pain, providing valuable insights into the complex mechanisms underlying pain in KOA. Together, these contributions advance our understanding of neurochemical quantification techniques and their application in studying pain mechanisms, laying the groundwork for future ^{1}H-MRS and chronic pain research.

References

An, L., Li, S., & Shen, J. (2017). Simultaneous determination of metabolite concentrations, T 1 and T 2 relaxation times. *Magnetic Resonance in Medicine*, *78*(6), 2072–2081. https://doi.org/10.1002/mrm.26612

Barker, P. B., Soher, B. J., Blackband, S. J., Chatham, J. C., Mathews, V. P., & Bryan, R. N. (1993). Quantitation of proton NMR spectra of the human brain using tissue water as an internal concentration reference. *NMR in Biomedicine*, *6*(1), 89–94. https://doi.org/10.1002/nbm.1940060114

Bell, T., Stokoe, M., & Harris, A. D. (2021). Macromolecule suppressed GABA levels show no relationship with age in a pediatric sample. *Scientific Reports*, *11*(1), 6–12. https://doi.org/10.1038/s41598-020-80530-8

Bell, T., Stokoe, M., Khaira, A., Webb, M., Noel, M., Amoozegar, F., & Harris, A. D. (2021). GABA and glutamate in pediatric migraine. *Pain*, *162*(1), 300–308. https://doi.org/10.1097/J.PAIN.0000000000002022

Bell, Tiffany K., Godfrey, K. J., Ware, A. L., Yeates, K. O., & Harris, A. D. (2022). Harmonization of multi-site MRS data with ComBat. *NeuroImage*, *257*, 119330. https://doi.org/10.1016/j.neuroimage.2022.119330

Bell, Tiffany Kay, Boudes, E. S., Loo, R. S., Barker, G. J., Lythgoe, D. J., Edden, R. A., Lebel, R. M., Wilson, M. P., & Harris, and A. D. (2019). Reliability of in vivo Glx measurements from GABA-edited MRS at 3T. *Proc. Intl. Soc. Mag. Reson. Med.*

Beswick, A. D., Wylde, V., Gooberman-Hill, R., Blom, A., & Dieppe, P. (2012). What proportion of patients report long-term pain after total hip or knee replacement for osteoarthritis? A systematic review of Prospective studies in unselected patients. *BMJ Open*, *2*(1), 1–12. https://doi.org/10.1136/bmjopen-2011-000435

Bjordal, J. M., Klovning, A., Ljunggren, A. E., & Slørdal, L. (2006). *Short-term efficacy of*

pharmacotherapeutic interventions in osteoarthritic knee pain: A meta-analysis of randomised placebo-controlled trials. https://doi.org/10.1016/j.ejpain.2006.02.013

Bourne, R. B., Chesworth, B. M., Davis, A. M., Mahomed, N. N., & Charron, K. D. J. (2010). Patient Satisfaction after Total Knee Arthroplasty: Who is Satisfied and Who is Not? *Clinical Orthopaedics and Related Research®*, *468*(1), 57–63. https://doi.org/10.1007/s11999-009-1119-9

Bradley, L. A., Kersh, B. C., DeBerry, J. J., Deutsch, G., Alarcón, G. A., & McLain, D. A. (2004). Lessons from fibromyalgia: abnormal pain sensitivity in knee osteoarthritis. *Novartis Foundation Symposium*, *260*, 258–270; discussion 270-9. http://www.ncbi.nlm.nih.gov/pubmed/15283455

Brandão, L. A., & Castillo, M. (2016). Adult Brain Tumors: Clinical Applications of Magnetic Resonance Spectroscopy. *Magnetic Resonance Imaging Clinics of North America*, *24*(4), 781–809. https://doi.org/10.1016/J.MRIC.2016.07.005

Brandt, A. S., Unschuld, P. G., Pradhan, S., Lim, I. A. L., Churchill, G., Harris, A. D., Hua, J., Barker, P. B., Ross, C. A., van Zijl, P. C. M., Edden, R. A. E., & Margolis, R. L. (2016). Age-related changes in anterior cingulate cortex glutamate in schizophrenia: A (1)H MRS Study at 7 Tesla. *Schizophrenia Research*, *172*(1–3), 101–105. https://doi.org/10.1016/J.SCHRES.2016.02.017

Brooks, J. C. W., Roberts, N., Kemp, G. J., Gosney, M. A., Lye, M., & Whitehouse, G. H. (2001). A Proton Magnetic Resonance Spectroscopy Study of Age-related Changes in Frontal Lobe Metabolite Concentrations. *Cerebral Cortex*, *11*(7), 598–605. https://doi.org/10.1093/cercor/11.7.598

Brooks, J. C. W., Zambreanu, L., Godinez, A., Craig, A. D. (Bud), & Tracey, I. (2005). Somatotopic organisation of the human insula to painful heat studied with high resolution functional imaging. *NeuroImage*, *27*(1), 201–209.

https://doi.org/10.1016/j.neuroimage.2005.03.041

Bushnell, M. C., Čeko, M., & Low, L. A. (2013). Cognitive and emotional control of pain and its disruption in chronic pain. *Nature Reviews Neuroscience*, *14*(7), 502–511. https://doi.org/10.1038/nrn3516

Calabrese, F., Guidotti, G., Molteni, R., Racagni, G., Mancini, M., & Riva, M. A. (2012). Stress-Induced Changes of Hippocampal NMDA Receptors: Modulation by Duloxetine Treatment. *PLoS ONE*, *7*(5), e37916. https://doi.org/10.1371/journal.pone.0037916

Canadian Institute for Health Information. (2019). *Canadian Joint Replacement Registry: 2019–2020 Full Annual Report.*

Canales-Rodríguez, E. J., Alonso-Lana, S., Verdolini, N., Sarró, S., Feria, I., Montoro, I., Garcia-Ruiz, B., Jimenez, E., Varo, C., Albacete, A., Argila-Plaza, I., Lluch, A., Bonnin, C. M., Vilella, E., Vieta, E., Pomarol-Clotet, E., & Salvador, R. (2021). Age- and gender-related differences in brain tissue microstructure revealed by multi-component T2 relaxometry. *Neurobiology of Aging*, *106*, 68–79. https://doi.org/10.1016/j.neurobiolaging.2021.06.002

Chang, L., Munsaka, S. M., Kraft-Terry, S., & Ernst, T. (2013). Magnetic Resonance Spectroscopy to Assess NeuroInflammation and Neuropathic Pain. *Journal of Neuroimmune Pharmacology*, *8*(3), 576–593. https://doi.org/10.1007/s11481-013-9460-x

Chappell, A. S., Ossanna, M. J., Liu-Seifert, H., Iyengar, S., Skljarevski, V., Li, L. C., Bennett, R. M., & Collins, H. (2009). Duloxetine, a centrally acting analgesic, in the treatment of patients with osteoarthritis knee pain: A 13-week, randomized, placebo-controlled trial. *Pain*, *146*(3), 253–260. https://doi.org/10.1016/j.pain.2009.06.024

Choi, I., Andronesi, O. C., Barker, P., Bogner, W., Edden, R. A. E., Kaiser, L. G., Lee, P., Marjańska, M., Terpstra, M., & Graaf, R. A. (2021). Spectral editing in 1 H magnetic

resonance spectroscopy: Experts' consensus recommendations. *NMR in Biomedicine*, *34*(5), 1–18. https://doi.org/10.1002/nbm.4411

Cirstea, C. M. (2011). Primary somatosensory cortex in chronic low back pain - a 1H-MRS study. *Journal of Pain Research*, *4*, 143. https://doi.org/10.2147/JPR.S19297

Clarke, W. T., Stagg, C. J., & Jbabdi, S. (2021). FSL-MRS: An end-to-end spectroscopy analysis package. *Magnetic Resonance in Medicine*, *85*(6), 2950–2964. https://doi.org/10.1002/mrm.28630

Clauw, D. J. (2014). Fibromyalgia: a clinical review. *JAMA*, *311*(15), 1547. https://doi.org/10.1001/jama.2014.3266

Clauw, D. J., & Hassett, A. L. (2017). The role of centralised pain in osteoarthritis. *Clinical and Experimental Rheumatology*, *35*(5), S79–S84. https://www.clinexprheumatol.org/abstract.asp?a=12198

Clauw, D. J., & Witter, J. (2009). Pain and rheumatology: Thinking outside the joint. *Arthritis & Rheumatism*, *60*(2), 321–324. https://doi.org/10.1002/art.24326

Cooper, C., Snow, S., McAlindon, T. E., Kellingray, S., Stuart, B., Coggon, D., & Dieppe, P. A. (2000). Risk factors for the incidence and progression of radiographic knee osteoarthritis. *Arthritism & Rhreumatism*, *43*(5), 995–1000.

Davis, K. D., Flor, H., Greely, H. T., Iannetti, G. D., Mackey, S., Ploner, M., Pustilnik, A., Tracey, I., Treede, R.-D., & Wager, T. D. (2017). Brain imaging tests for chronic pain: medical, legal and ethical issues and recommendations. *Nature Reviews Neurology*, *13*(10), 624–638. https://doi.org/10.1038/nrneurol.2017.122

de Graaf, R. A. (2019). In vivo NMR spectroscopy. In *Basic life sciences* (Vol. 55). John Wiley & Sons Ltd. https://doi.org/10.1007/978-1-4613-1473-8_59

DeMayo, M. M., Harris, A. D., Song, Y. J. C., Pokorski, I., Thapa, R., Patel, S., Ambarchi, Z., Thomas, E. E., Hickie, I. B., & Guastella, A. J. (2021). Age-related parietal GABA

alterations in children with autism spectrum disorder. *Autism Research : Official Journal of the International Society for Autism Research*, *14*(5), 859–872. https://doi.org/10.1002/AUR.2487

Diederichs, C., DeMayo, M. M., Cole, J., Yatham, L. N., Harris, A. D., & McGirr, A. (2021). Intermittent Theta-Burst Stimulation Transcranial Magnetic Stimulation Increases GABA in the Medial Prefrontal Cortex: A Preliminary Sham-Controlled Magnetic Resonance Spectroscopy Study in Acute Bipolar Depression. *Frontiers in Psychiatry*, *12*. https://doi.org/10.3389/FPSYT.2021.665402

Dieppe, P. A., Cushnaghan, J., & Shepstone, L. (1997). Progression of osteoarthritis (OA) over 3 years and the relationship between clinical and radiographic changes at the knee joint. *Osteoarthritis and Cartilage*, *5*(2), 87–97. https://doi.org/10.1016/S1063-4584(97)80002-7

Dieringer, M. A., Deimling, M., Santoro, D., Wuerfel, J., Madai, V. I., Sobesky, J., von Knobelsdorff-Brenkenhoff, F., Schulz-Menger, J., & Niendorf, T. (2014). Rapid Parametric Mapping of the Longitudinal Relaxation Time T1 Using Two-Dimensional Variable Flip Angle Magnetic Resonance Imaging at 1.5 Tesla, 3 Tesla, and 7 Tesla. *PLoS ONE*, *9*(3), e91318. https://doi.org/10.1371/journal.pone.0091318

Dworkin, R. H., Turk, D. C., Wyrwich, K. W., Beaton, D., Cleeland, C. S., Farrar, J. T., Haythornthwaite, J. A., Jensen, M. P., Kerns, R. D., Ader, D. N., Brandenburg, N., Burke, L. B., Cella, D., Chandler, J., Cowan, P., Dimitrova, R., Dionne, R., Hertz, S., Jadad, A. R., … Zavisic, S. (2008). Interpreting the Clinical Importance of Treatment Outcomes in Chronic Pain Clinical Trials: IMMPACT Recommendations. *The Journal of Pain*, *9*(2), 105–121. https://doi.org/10.1016/j.jpain.2007.09.005

Edden, R. A. E., Puts, N. A. J., Harris, A. D., Barker, P. B., & Evans, C. J. (2014). Gannet: A batch-processing tool for the quantitative analysis of gamma-aminobutyric acid-edited

MR spectroscopy spectra. *Journal of Magnetic Resonance Imaging*, *40*(6), 1445–1452. https://doi.org/10.1002/jmri.24478

El-Najjar, A. R., Abdelwhab, S. M., & Elsammak, ahmad A. (2020). Potential role of brain biomarkers in primary knee osteoarthritis patients using magnetic resonance spectroscopy. *The Egyptian Rheumatologist*, *42*(2), 101–106. https://doi.org/10.1016/j.ejr.2019.11.002

Ernst, T., Kreis, R., & Ross, B. D. (1993). Absolute Quantitation of Water and Metabolites in the Human Brain. I. Compartments and Water. *Journal of Magnetic Resonance, Series B*, *102*(1), 1–8. https://doi.org/10.1006/jmrb.1993.1055

Ethofer, T., Mader, I., Seeger, U., Helms, G., Erb, M., Grodd, W., Ludolph, A., & Klose, U. (2003). Comparison of longitudinal metabolite relaxation times in different regions of the human brain at 1.5 and 3 Tesla. *Magnetic Resonance in Medicine*, *50*(6), 1296–1301. https://doi.org/10.1002/mrm.10640

Fayed, N., Garcia-Campayo, J., Magallón, R., Andrés-Bergareche, H., Luciano, J. V, Andres, E., & Beltrán, J. (2010). Localized 1H-NMR spectroscopy in patients with fibromyalgia: a controlled study of changes in cerebral glutamate/glutamine, inositol, choline, and N-acetylaspartate. *Arthritis Research & Therapy*, *12*(4), R134. https://doi.org/10.1186/ar3072

Fillingim, R. B., Loeser, J. D., Baron, R., & Edwards, R. R. (2016). Assessment of Chronic Pain: Domains, Methods, and Mechanisms. *The Journal of Pain*, *17*(9 Suppl), T10–T20. https://doi.org/10.1016/J.JPAIN.2015.08.010

Finan, P. H., Buenaver, L. F., Bounds, S. C., Hussain, S., Park, R. J., Haque, U. J., Campbell, C. M., Haythornthwaite, J. A., Edwards, R. R., & Smith, M. T. (2013). Discordance between pain and radiographic severity in knee osteoarthritis: Findings from quantitative sensory testing of central sensitization. *Arthritis and Rheumatism*, *65*(2), 363–372.

https://doi.org/10.1002/art.34646

Fingar, K. R., Stocks, C., Weiss, A. J., & Steiner, C. A. (2006). Most Frequent Operating Room Procedures Performed in U.S. Hospitals, 2003–2012. In *Healthcare Cost and Utilization Project (HCUP) Statistical Briefs*. http://www.ncbi.nlm.nih.gov/pubmed/25695123

Foerster, B. R., Petrou, M., Edden, R. A. E., Sundgren, P. C., Schmidt-Wilcke, T., Lowe, S. E., Harte, S. E., Clauw, D. J., & Harris, R. E. (2012). Reduced insular γ-aminobutyric acid in fibromyalgia. *Arthritis and Rheumatism*, *64*(2), 579–583. https://doi.org/10.1002/art.33339

Freynhagen, R., Baron, R., Gockel, U., & Tölle, T. R. (2006). pain DETECT : a new screening questionnaire to identify neuropathic components in patients with back pain. *Current Medical Research and Opinion*, *22*(10), 1911–1920. https://doi.org/10.1185/030079906X132488

Freynhagen, R., Tölle, T. R., Gockel, U., & Baron, R. (2016). The painDETECT project - Far more than a screening tool on neuropathic pain. *Current Medical Research and Opinion*, *32*(6), 1033–1057. https://doi.org/10.1185/03007995.2016.1157460

Frot, M., Magnin, M., Mauguière, F., & Garcia-Larrea, L. (2013). Cortical representation of pain in primary sensory-motor areas (S1/M1)-a study using intracortical recordings in humans. *Human Brain Mapping*, *34*(10), 2655–2668. https://doi.org/10.1002/hbm.22097

Gasparovic, C., Neeb, H., Feis, D. L., Damaraju, E., Chen, H., Doty, M. J., South, D. M., Mullins, P. G., Bockholt, H. J., & Shah, N. J. (2009). Quantitative spectroscopic imaging with in situ measurements of tissue water T1 , T2 , and density. *Magnetic Resonance in Medicine*, *62*(3), 583–590. https://doi.org/10.1002/mrm.22060

Gasparovic, Charles, Chen, H., & Mullins, P. G. (2018). Errors in 1H-MRS estimates of brain metabolite concentrations caused by failing to take into account tissue-specific signal

relaxation. *NMR in Biomedicine*, *31*(6). https://doi.org/10.1002/NBM.3914

Gasparovic, Charles, Song, T., Devier, D., Bockholt, H. J., Caprihan, A., Mullins, P. G., Posse, S., Jung, R. E., & Morrison, L. A. (2006). Use of tissue water as a concentration reference for proton spectroscopic imaging. *Magnetic Resonance in Medicine*, *55*(6), 1219–1226. https://doi.org/10.1002/MRM.20901

Gasparovic, Charles, Yeo, R., Mannell, M., Ling, J., Elgie, R., Phillips, J., Doezema, D., & Mayer, A. R. (2009). Neurometabolite Concentrations in Gray and White Matter in Mild Traumatic Brain Injury: An 1 H–Magnetic Resonance Spectroscopy Study. *Journal of Neurotrauma*, *26*(10), 1635–1643. https://doi.org/10.1089/neu.2009.0896

Gelman, N., Gorell, J. M., Barker, P. B., Savage, R. M., Spickler, E. M., Windham, J. P., & Knight, R. A. (1999). MR Imaging of Human Brain at 3.0 T: Preliminary Report on Transverse Relaxation Rates and Relation to Estimated Iron Content. *Radiology*, *210*(3), 759–767. https://doi.org/10.1148/radiology.210.3.r99fe41759

Gogishvili, A., Farrher, E., Doppler, C. E. J., Seger, A., Sommerauer, M., & Shah, N. J. (2023). Quantification of the neurochemical profile of the human putamen using STEAM MRS in a cohort of elderly subjects at 3 T and 7 T: Ruminations on the correction strategy for the tissue voxel composition. *PloS One*, *18*(6), e0286633. https://doi.org/10.1371/journal.pone.0286633

Gracien, R.-M., Nürnberger, L., Hok, P., Hof, S.-M., Reitz, S. C., Rüb, U., Steinmetz, H., Hilker-Roggendorf, R., Klein, J. C., Deichmann, R., & Baudrexel, S. (2017). Evaluation of brain ageing: a quantitative longitudinal MRI study over 7 years. *European Radiology*, *27*(4), 1568–1576. https://doi.org/10.1007/s00330-016-4485-1

Gudmundson, A. T., Koo, A., Virovka, A., Amirault, A. L., Soo, M., Cho, J. H., Oeltzschner, G., Edden, R. A. E., & Stark, C. (2023). Meta-analysis and Open-source Database for In Vivo Brain Magnetic Resonance Spectroscopy in Health and Disease. *BioRxiv : The*

Preprint Server for Biology. https://doi.org/10.1101/2023.02.10.528046

Gussew, A., Erdtel, M., Hiepe, P., Rzanny, R., & Reichenbach, J. R. (2012). Absolute quantitation of brain metabolites with respect to heterogeneous tissue compositions in 1H-MR spectroscopic volumes. *Magnetic Resonance Materials in Physics, Biology and Medicine*, *25*(5), 321–333. https://doi.org/10.1007/s10334-012-0305-z

Hagiwara, A., Fujimoto, K., Kamagata, K., Murata, S., Irie, R., Kaga, H., Someya, Y., Andica, C., Fujita, S., Kato, S., Fukunaga, I., Wada, A., Hori, M., Tamura, Y., Kawamori, R., Watada, H., & Aoki, S. (2021). Age-Related Changes in Relaxation Times, Proton Density, Myelin, and Tissue Volumes in Adult Brain Analyzed by 2-Dimensional Quantitative Synthetic Magnetic Resonance Imaging. *Investigative Radiology*, *56*(3), 163–172. https://doi.org/10.1097/RLI.0000000000000720

Hagiwara, A., Warntjes, M., Hori, M., Andica, C., Nakazawa, M., Kumamaru, K. K., Abe, O., & Aoki, S. (2017). SyMRI of the Brain. *Investigative Radiology*, *52*(10), 647–657. https://doi.org/10.1097/RLI.0000000000000365

Hannan, M. T., Felson, D. T., & Pincus, T. (2000). Analysis of the discordance between radiographic changes and knee pain in osteoarthritis of the knee. *The Journal of Rheumatology*, *27*(6), 1513–1517. http://www.ncbi.nlm.nih.gov/pubmed/10852280

Hansson, P. (2002). Neuropathic pain: clinical characteristics and diagnostic workup. *European Journal of Pain*, *6*(SUPPL. 1), 47–50. https://doi.org/10.1053/EUJP.2001.0322

Harris, A. D., Gilbert, D. L., Horn, P. S., Crocetti, D., Cecil, K. M., Edden, R. A. E., Huddleston, D. A., Mostofsky, S. H., & Puts, N. A. J. (2021). Relationship between GABA levels and task-dependent cortical excitability in children with attention-deficit/hyperactivity disorder. *Clinical Neurophysiology : Official Journal of the International Federation of Clinical Neurophysiology*, *132*(5), 1163–1172.

https://doi.org/10.1016/J.CLINPH.2021.01.023

Harris, A. D., Puts, N. A. J., & Edden, R. A. E. (2015). Tissue correction for GABA-edited MRS: Considerations of voxel composition, tissue segmentation, and tissue relaxations. *Journal of Magnetic Resonance Imaging*, *42*(5), 1431–1440. https://doi.org/10.1002/jmri.24903

Harris, R. E., Sundgren, P. C., Craig, A. D., Kirshenbaum, E., Sen, A., Napadow, V., & Clauw, D. J. (2009). Elevated insular glutamate in fibromyalgia is associated with experimental pain. *Arthritis and Rheumatism*, *60*(10), 3146–3152. https://doi.org/10.1002/art.24849

Harris, R. E., Sundgren, P. C., Pang, Y., Hsu, M., Petrou, M., Kim, S. H., McLean, S. A., Gracely, R. H., & Clauw, D. J. (2008). Dynamic levels of glutamate within the insula are associated with improvements in multiple pain domains in fibromyalgia. *Arthritis and Rheumatism*, *58*(3), 903–907. https://doi.org/10.1002/art.23223

He, J. L., Oeltzschner, G., Mikkelsen, M., Deronda, A., Harris, A. D., Crocetti, D., Wodka, E. L., Mostofsky, S. H., Edden, R. A. E., & Puts, N. A. J. (2021). Region-specific elevations of glutamate + glutamine correlate with the sensory symptoms of autism spectrum disorders. *Translational Psychiatry*, *11*(1). https://doi.org/10.1038/S41398-021-01525-1

Henn, A. T., Larsen, B., Frahm, L., Xu, A., Adebimpe, A., Scott, J. C., Linguiti, S., Sharma, V., Basbaum, A. I., Corder, G., Dworkin, R. H., Edwards, R. R., Woolf, C. J., Habel, U., Eickhoff, S. B., Eickhoff, C. R., Wagels, L., & Satterthwaite, T. D. (2023). Structural imaging studies of patients with chronic pain: an anatomical likelihood estimate meta-analysis. *Pain*, *164*(1), e10–e24. https://doi.org/10.1097/j.pain.0000000000002681

Imamura, M., Imamura, S. T., Kaziyama, H. H. S., Targino, R. A., Hsing, W. T., De Souza, L. P. M., Cutait, Ma. M., Fregni, F., & Camanho, G. L. (2008). Impact of nervous

system hyperalgesia on pain, disability, and quality of life in patients with knee osteoarthritis: A controlled analysis. *Arthritis Care & Research*, *59*(10), 1424–1431. https://doi.org/10.1002/art.24120

International Association for the Study of Pain. (1994). *Classification of Chronic Pain, Descriptions of Chronic Pain Syndromes and Definitions of Pain Terms. 2nd Edition*.

Jabłoński, M., Starčuková, J., & Starčuk, Z. (2017). Processing tracking in jMRUI software for magnetic resonance spectra quantitation reproducibility assurance. *BMC Bioinformatics*, *18*(1), 56. https://doi.org/10.1186/s12859-017-1459-5

Jenkinson, M., Beckmann, C. F., Behrens, T. E. J., Woolrich, M. W., & Smith, S. M. (2012). FSL. *NeuroImage*, *62*(2), 782–790. https://doi.org/10.1016/j.neuroimage.2011.09.015

Joyce, J. M., La, P. L., Walker, R., & Harris, A. D. (2022). Magnetic Resonance Spectroscopy of Traumatic Brain Injury and Subconcussive Hits: A Systematic Review and Meta-Analysis. *Journal of Neurotrauma*, *39*(21–22), 1455–1476. https://doi.org/10.1089/NEU.2022.0125

Jung, Y.-H., Kim, H., Lee, D., Lee, J.-Y., Lee, W. J., Moon, J. Y., Choi, S.-H., & Kang, D.-H. (2021). Abnormal neurometabolites in fibromyalgia patients: Magnetic resonance spectroscopy study. *Molecular Pain*, *17*, 174480692199094. https://doi.org/10.1177/1744806921990946

Kim, D., Chae, Y., Park, H.-J., & Lee, I.-S. (2021). Effects of Chronic Pain Treatment on Altered Functional and Metabolic Activities in the Brain: A Systematic Review and Meta-Analysis of Functional Neuroimaging Studies. *Frontiers in Neuroscience*, *15*. https://doi.org/10.3389/fnins.2021.684926

Knight, M. J., McCann, B., Tsivos, D., Dillon, S., Coulthard, E., & Kauppinen, R. A. (2016). Quantitative T2 mapping of white matter: applications for ageing and cognitive decline. *Physics in Medicine and Biology*, *61*(15), 5587–5605. https://doi.org/10.1088/0031-

9155/61/15/5587

Kreis, R., Ernst, T., & Ross, B. D. (1993). Absolute Quantitation of Water and Metabolites in the Human Brain. II. Metabolite Concentrations. *Journal of Magnetic Resonance, Series B, 102*(1), 9–19. https://doi.org/10.1006/jmrb.1993.1056

Kumar, R., Delshad, S., Macey, P. M., Woo, M. A., & Harper, R. M. (2011). Development of T2-relaxation values in regional brain sites during adolescence. *Magnetic Resonance Imaging*, *29*(2), 185–193. https://doi.org/10.1016/j.mri.2010.08.006

Kumar, R., Delshad, S., Woo, M. A., Macey, P. M., & Harper, R. M. (2012). Age-related regional brain T2-relaxation changes in healthy adults. *Journal of Magnetic Resonance Imaging*, *35*(2), 300–308. https://doi.org/10.1002/jmri.22831

Lee, Y. C., Lu, B., Bathon, J. M., Haythornthwaite, J. A., Smith, M. T., Page, G. G., & Edwards, R. R. (2011). Pain sensitivity and pain reactivity in osteoarthritis. *Arthritis Care & Research*, *63*(3), 320–327. https://doi.org/10.1002/acr.20373

Leech, S. A., Khaira, A., Epp, S., Schneider, G., Werle, J., Ng, R., Harris, A. D., & Manske, S. L. (2024). Demographic, pain, and quality of life factors in unilateral and bilateral total knee arthroplasty. *The Journal of Science and Medicine*, *5*(1). https://doi.org/10.37714/josam.v4i1.114

Lepore, E., Lauretta, R., Bianchini, M., Mormando, M., Di Lorenzo, C., & Unfer, V. (2021). Inositols Depletion and Resistance: Principal Mechanisms and Therapeutic Strategies. *International Journal of Molecular Sciences*, *22*(13). https://doi.org/10.3390/ijms22136796

Lewis, G. N., Rice, D. A., McNair, P. J., & Kluger, M. (2015). Predictors of persistent pain after total knee arthroplasty: a systematic review and meta-analysis. *British Journal of Anaesthesia*, *114*(4), 551–561. https://doi.org/10.1093/BJA/AEU441

Li, Y. (2013). T1 and T2 Metabolite Relaxation Times in Normal Brain at 3T and 7T.

Journal of Molecular Imaging & Dynamics, *02*(02). https://doi.org/10.4172/2155-9937.S1-002

Lu, H., Nagae-Poetscher, L. M., Golay, X., Lin, D., Pomper, M., & van Zijl, P. C. M. (2005). Routine clinical brain MRI sequences for use at 3.0 Tesla. *Journal of Magnetic Resonance Imaging*, *22*(1), 13–22. https://doi.org/10.1002/jmri.20356

Mao, J. (2009). Translational Pain Research: Achievements and Challenges. *The Journal of Pain*, *10*(10), 1001–1011. https://doi.org/10.1016/j.jpain.2009.06.002

Mlynárik, V., Gruber, S., & Moser, E. (2001). Proton T 1 and T 2 relaxation times of human brain metabolites at 3 Tesla. *NMR in Biomedicine*, *14*(5), 325–331. https://doi.org/10.1002/nbm.713

Morgan, M., Nazemian, V., Harrington, K., & Ivanusic, J. J. (2022). Mini review: The role of sensory innervation to subchondral bone in osteoarthritis pain. *Frontiers in Endocrinology*, *13*. https://doi.org/10.3389/fendo.2022.1047943

Near, J., Harris, A. D., Juchem, C., Kreis, R., Marjańska, M., Öz, G., Slotboom, J., Wilson, M., & Gasparovic, C. (2021). Preprocessing, analysis and quantification in single-voxel magnetic resonance spectroscopy: experts' consensus recommendations. *NMR in Biomedicine*, *34*(5), 1–23. https://doi.org/10.1002/nbm.4257

Neogi, T. (2013). The epidemiology and impact of pain in osteoarthritis. *Osteoarthritis and Cartilage*, *21*(9), 1145–1153. https://doi.org/10.1016/j.joca.2013.03.018

Nunez-Gonzalez, L., van Garderen, K. A., Smits, M., Jaspers, J., Romero, A. M., Poot, D. H. J., & Hernandez-Tamames, J. A. (2022). Pre-contrast MAGiC in treated gliomas: a pilot study of quantitative MRI. *Scientific Reports*, *12*(1), 21820. https://doi.org/10.1038/s41598-022-24276-5

Nürnberger, L., Gracien, R.-M., Hok, P., Hof, S.-M., Rüb, U., Steinmetz, H., Hilker, R., Klein, J. C., Deichmann, R., & Baudrexel, S. (2017). Longitudinal changes of cortical

microstructure in Parkinson's disease assessed with T1 relaxometry. *NeuroImage: Clinical*, *13*, 405–414. https://doi.org/10.1016/j.nicl.2016.12.025

Oeltzschner, G., Zöllner, H. J., Hui, S. C. N., Mikkelsen, M., Saleh, M. G., Tapper, S., & Edden, R. A. E. (2020). Osprey: Open-source processing, reconstruction & estimation of magnetic resonance spectroscopy data. *Journal of Neuroscience Methods*, *343*, 108827. https://doi.org/10.1016/j.jneumeth.2020.108827

Öz, G., Deelchand, D. K., Wijnen, J. P., Mlynárik, V., Xin, L., Mekle, R., Noeske, R., Scheenen, T. W. J., Tkáč, I., Andronesi, O., Barker, P. B., Bartha, R., Berrington, A., Boer, V., Cudalbu, C., Emir, U. E., Ernst, T., Fillmer, A., Heerschap, A., … Wilson, M. (2021). Advanced single voxel 1H magnetic resonance spectroscopy techniques in humans: Experts' consensus recommendations. *NMR in Biomedicine*, *34*(5), 1–18. https://doi.org/10.1002/nbm.4236

Peek, A. L., Rebbeck, T., Puts, N. A., Watson, J., Aguila, M. E. R., & Leaver, A. M. (2020). Brain GABA and glutamate levels across pain conditions: A systematic literature review and meta-analysis of 1H-MRS studies using the MRS-Q quality assessment tool. *NeuroImage*, *210*(December 2019), 116532. https://doi.org/10.1016/j.neuroimage.2020.116532

Petrou, M., Pop-Busui, R., Foerster, B. R., Edden, R. A., Callaghan, B. C., Harte, S. E., Harris, R. E., Clauw, D. J., & Feldman, E. L. (2012). Altered Excitation-inhibition Balance in the Brain of Patients with Diabetic Neuropathy. *Academic Radiology*, *19*(5), 607–612. https://doi.org/10.1016/j.acra.2012.02.004

Phillips, K., & Clauw, D. J. (2011). Central pain mechanisms in chronic pain states – Maybe it is all in their head. *Best Practice & Research Clinical Rheumatology*, *25*(2), 141–154. https://doi.org/10.1016/j.berh.2011.02.005

Piechnik, S. K., Evans, J., Bary, L. H., Wise, R. G., & Jezzard, P. (2009). Functional changes

in CSF volume estimated using measurement of water T 2 relaxation. *Magnetic Resonance in Medicine*, *61*(3), 579–586. https://doi.org/10.1002/mrm.21897

Pigott, T., McPeak, A., de Chastelain, A., DeMayo, M. M., Rasic, N., Rayner, L., Noel, M., Miller, J. V., & Harris, A. D. (2023). Changes in Brain GABA and Glutamate and Improvements in Physical Functioning Following Intensive Pain Rehabilitation in Youth With Chronic Pain. *The Journal of Pain*, *24*(7). https://doi.org/10.1016/J.JPAIN.2023.02.027

Pomares, F. B., Roy, S., Funck, T., Feier, N. A., Thiel, A., Fitzcharles, M. A., & Schweinhardt, P. (2020). Upregulation of cortical GABAA receptor concentration in fibromyalgia. *Pain*, *161*(1), 74. https://doi.org/10.1097/J.PAIN.0000000000001707

Porges, E. C., Woods, A. J., Lamb, D. G., Williamson, J. B., Cohen, R. A., Edden, R. A. E., & Harris, A. D. (2017). Impact of tissue correction strategy on GABA-edited MRS findings. *NeuroImage*, *162*, 249–256. https://doi.org/10.1016/J.NEUROIMAGE.2017.08.073

Posse, S., Otazo, R., Caprihan, A., Bustillo, J., Chen, H., Henry, P., Marjanska, M., Gasparovic, C., Zuo, C., Magnotta, V., Mueller, B., Mullins, P., Renshaw, P., Ugurbil, K., Lim, K. O., & Alger, J. R. (2007). Proton echo-planar spectroscopic imaging of J - coupled resonances in human brain at 3 and 4 Tesla. *Magnetic Resonance in Medicine*, *58*(2), 236–244. https://doi.org/10.1002/mrm.21287

Považan, M., Mikkelsen, M., Berrington, A., Bhattacharyya, P. K., Brix, M. K., Buur, P. F., Cecil, K. M., Chan, K. L., Chen, D. Y. T., Craven, A. R., Cuypers, K., Dacko, M., Duncan, N. W., Dydak, U., Edmondson, D. A., Ende, G., Ersland, L., Forbes, M. A., Gao, F., … Barker, P. B. (2020). Comparison of Multivendor Single-Voxel MR Spectroscopy Data Acquired in Healthy Brain at 26 Sites. *Radiology*, *295*(1), 171–180. https://doi.org/10.1148/radiol.2020191037

Provencher, S. W. (2001). Automatic quantitation of localized in vivo 1H spectra with LCModel. *NMR in Biomedicine*, *14*(4), 260–264. https://doi.org/10.1002/nbm.698

Puts, N. A. J., Wodka, E. L., Harris, A. D., Crocetti, D., Tommerdahl, M., Mostofsky, S. H., & Edden, R. A. E. (2017). Reduced GABA and altered somatosensory function in children with autism spectrum disorder. *Autism Research : Official Journal of the International Society for Autism Research*, *10*(4), 608–619. https://doi.org/10.1002/AUR.1691

Reckziegel, D., Raschke, F., Cottam, W. J., & Auer, D. P. (2016). Cingulate GABA levels inversely correlate with the intensity of ongoing chronic knee osteoarthritis pain. *Molecular Pain*, *12*, 1–9. https://doi.org/10.1177/1744806916650690

Rooney, W. D., Johnson, G., Li, X., Cohen, E. R., Kim, S., Ugurbil, K., & Springer, C. S. (2007). Magnetic field and tissue dependencies of human brain longitudinal 1 H 2 O relaxation in vivo. *Magnetic Resonance in Medicine*, *57*(2), 308–318. https://doi.org/10.1002/mrm.21122

Roos, E. M., & Juhl, C. B. (2012). Osteoarthritis 2012 year in review: rehabilitation and outcomes. *Osteoarthritis and Cartilage*, *20*(12), 1477–1483. https://doi.org/10.1016/j.joca.2012.08.028

Sharma, L. (2021). Osteoarthritis of the Knee. *New England Journal of Medicine*, *384*(1), 51–59. https://doi.org/10.1056/NEJMcp1903768

Siao, P., & Cros, D. P. (2003). Quantitative sensory testing. *Physical Medicine and Rehabilitation Clinics of North America*, *14*(2), 261–286. https://doi.org/10.1016/S1047-9651(02)00122-5

Simpson, R., Devenyi, G. A., Jezzard, P., Hennessy, T. J., & Near, J. (2017). Advanced processing and simulation of MRS data using the FID appliance (FID-A)—An open source, MATLAB-based toolkit. *Magnetic Resonance in Medicine*, *77*(1), 23–33.

https://doi.org/10.1002/mrm.26091

Singh, J. A., Gabriel, S., & Lewallen, D. (2008). The Impact of Gender, Age, and Preoperative Pain Severity on Pain After TKA. *Clinical Orthopaedics & Related Research*, *466*(11), 2717–2723. https://doi.org/10.1007/s11999-008-0399-9

Sluka, K. A., & Clauw, D. J. (2016). Neurobiology of fibromyalgia and chronic widespread pain. *Neuroscience*, *338*, 114–129. https://doi.org/10.1016/j.neuroscience.2016.06.006

Spijkerman, J. M., Petersen, E. T., Hendrikse, J., Luijten, P., & Zwanenburg, J. J. M. (2018). T 2 mapping of cerebrospinal fluid: 3 T versus 7 T. *Magnetic Resonance Materials in Physics, Biology and Medicine*, *31*(3), 415–424. https://doi.org/10.1007/s10334-017-0659-3

Srinivasan, R., Cunningham, C., Chen, A., Vigneron, D., Hurd, R., Nelson, S., & Pelletier, D. (2006). TE-Averaged two-dimensional proton spectroscopic imaging of glutamate at 3 T. *NeuroImage*, *30*(4), 1171–1178. https://doi.org/10.1016/j.neuroimage.2005.10.048

Stanisz, G. J., Odrobina, E. E., Pun, J., Escaravage, M., Graham, S. J., Bronskill, M. J., & Henkelman, R. M. (2005). T 1 , T 2 relaxation and magnetization transfer in tissue at 3T. *Magnetic Resonance in Medicine*, *54*(3), 507–512. https://doi.org/10.1002/mrm.20605

SyntheticMR AB. (2021). *SyMRI ® SyntheticMR AB User Manual*. https://www.syntheticmr.com/legal

Tanenbaum, L. N., Tsiouris, A. J., Johnson, A. N., Naidich, T. P., DeLano, M. C., Melhem, E. R., Quarterman, P., Parameswaran, S. X., Shankaranarayanan, A., Goyen, M., & Field, A. S. (2017). Synthetic MRI for Clinical Neuroimaging: Results of the Magnetic Resonance Image Compilation (MAGiC) Prospective, Multicenter, Multireader Trial. *American Journal of Neuroradiology*, *38*(6), 1103–1110. https://doi.org/10.3174/ajnr.A5227

Träber, F., Block, W., Lamerichs, R., Gieseke, J., & Schild, H. H. (2004). 1 H metabolite

relaxation times at 3.0 tesla: Measurements of T1 and T2 values in normal brain and determination of regional differences in transverse relaxation. *Journal of Magnetic Resonance Imaging*, *19*(5), 537–545. https://doi.org/10.1002/jmri.20053

Tracey, I., & Mantyh, P. W. (2007). The Cerebral Signature for Pain Perception and Its Modulation. *Neuron*, *55*(3), 377–391. https://doi.org/10.1016/j.neuron.2007.07.012

Varacallo, M., Luo, T. D., & Johanson, N. A. (2022). Total Knee Arthroplasty Techniques. In *StatPearls*. http://www.ncbi.nlm.nih.gov/pubmed/29939641

Vymazal, J., Righini, A., Brooks, R. A., Canesi, M., Mariani, C., Leonardi, M., & Pezzoli, G. (1999). T1 and T2 in the Brain of Healthy Subjects, Patients with Parkinson Disease, and Patients with Multiple System Atrophy: Relation to Iron Content. *Radiology*, *211*(2), 489–495. https://doi.org/10.1148/radiology.211.2.r99ma53489

Wansapura, J. P., Holland, S. K., Dunn, R. S., & Ball, W. S. (1999). NMR relaxation times in the human brain at 3.0 Tesla. *Journal of Magnetic Resonance Imaging*, *9*(4), 531–538. https://doi.org/10.1002/(SICI)1522-2586(199904)9:4<531::AID-JMRI4>3.0.CO;2-L

Warntjes, J. B. M., Dahlqvist, O., & Lundberg, P. (2007). Novel method for rapid, simultaneous T 1 , T * 2 , and proton density quantification. *Magnetic Resonance in Medicine*, *57*(3), 528–537. https://doi.org/10.1002/mrm.21165

Warntjes, J. B. M., Leinhard, O. D., West, J., & Lundberg, P. (2008). Rapid magnetic resonance quantification on the brain: Optimization for clinical usage. *Magnetic Resonance in Medicine*, *60*(2), 320–329. https://doi.org/10.1002/mrm.21635

Wearn, A. R., Nurdal, V., Saunders-Jennings, E., Knight, M. J., Isotalus, H. K., Dillon, S., Tsivos, D., Kauppinen, R. A., & Coulthard, E. J. (2020). T2 heterogeneity: a novel marker of microstructural integrity associated with cognitive decline in people with mild cognitive impairment. *Alzheimer's Research & Therapy*, *12*(1), 105. https://doi.org/10.1186/s13195-020-00672-9

Weerasekera, A., Morrissey, E., Kim, M., Saha, A., Lin, Y., Alshelh, Z., Torrado-Carvajal, A., Albrecht, D., Akeju, O., Kwon, Y.-M., Bedair, H., Chen, A. F., Napadow, V., Schreiber, K., Ratai, E.-M., Edwards, R. R., & Loggia, M. L. (2021). Thalamic neurometabolite alterations in patients with knee osteoarthritis before and after total knee replacement. *Pain*, *162*(7), 2014–2023. https://doi.org/10.1097/j.pain.0000000000002198

Werner, M. U., & Kongsgaard, U. E. (2014). Defining persistent post-surgical pain: Is an update required? *British Journal of Anaesthesia*, *113*(1), 1–4. https://doi.org/10.1093/bja/aeu012

Wessel, J. (1995). The Reliability and Vatidity of Pain Threshold Measurements in Osteoarthritis of the Knee. *Scandinavian Journal of Rheumatology*, *24*(4), 238–242. https://doi.org/10.3109/03009749509100881

Wiech, K., & Tracey, I. (2009). The influence of negative emotions on pain: Behavioral effects and neural mechanisms. *NeuroImage*, *47*(3), 987–994. https://doi.org/10.1016/j.neuroimage.2009.05.059

Wilson, M., Reynolds, G., Kauppinen, R. A., Arvanitis, T. N., & Peet, A. C. (2011). A constrained least-squares approach to the automated quantitation of in vivo 1H magnetic resonance spectroscopy data. *Magnetic Resonance in Medicine : Official Journal of the Society of Magnetic Resonance in Medicine / Society of Magnetic Resonance in Medicine*, *65*(1), 1–12. https://doi.org/10.1002/mrm.22579

Woolf, C. J. (2011). Central sensitization: Implications for the diagnosis and treatment of pain. *Pain*, *152*(3 Suppl), S2. https://doi.org/10.1016/J.PAIN.2010.09.030

Wright, P. J., Mougin, O. E., Totman, J. J., Peters, A. M., Brookes, M. J., Coxon, R., Morris, P. E., Clemence, M., Francis, S. T., Bowtell, R. W., & Gowland, P. A. (2008). Water proton T 1 measurements in brain tissue at 7, 3, and 1.5T using IR-EPI, IR-TSE, and

MPRAGE: results and optimization. *Magnetic Resonance Materials in Physics, Biology and Medicine*, *21*(1–2), 121–130. https://doi.org/10.1007/s10334-008-0104-8

Wyss, P. O., Bianchini, C., Scheidegger, M., Giapitzakis, I. A., Hock, A., Fuchs, A., & Henning, A. (2018). In vivo estimation of transverse relaxation time constant (T 2) of 17 human brain metabolites at 3T. *Magnetic Resonance in Medicine*, *80*(2), 452–461. https://doi.org/10.1002/mrm.27067

Yarnitsky, D. (2010). Conditioned pain modulation (the diffuse noxious inhibitory control-like effect): its relevance for acute and chronic pain states. *Current Opinion in Anaesthesiology*, *23*(5), 611–615. https://doi.org/10.1097/ACO.0b013e32833c348b

Zachlod, D., Bludau, S., Cichon, S., Palomero-Gallagher, N., & Amunts, K. (2022). Combined analysis of cytoarchitectonic, molecular and transcriptomic patterns reveal differences in brain organization across human functional brain systems. *NeuroImage*, *257*(May), 119286. https://doi.org/10.1016/j.neuroimage.2022.119286

Zhang, W. (2004). Does paracetamol (acetaminophen) reduce the pain of osteoarthritis?: a meta-analysis of randomised controlled trials. *Annals of the Rheumatic Diseases*, *63*(8), 901–907. https://doi.org/10.1136/ard.2003.018531

Zhang, X., Trame, M., Lesko, L., & Schmidt, S. (2015). Sobol Sensitivity Analysis: A Tool to Guide the Development and Evaluation of Systems Pharmacology Models. *CPT: Pharmacometrics & Systems Pharmacology*, *4*(2), 69–79. https://doi.org/10.1002/psp4.6

Zhang, Z., Gewandter, J. S., & Geha, P. (2022). Brain Imaging Biomarkers for Chronic Pain. *Frontiers in Neurology*, *12*(January), 1–15. https://doi.org/10.3389/fneur.2021.734821

Zheng, Z., Liu, Y., Yin, H., Ren, P., Zhang, T., Yang, J., & Wang, Z. (2023). Evaluating T1, T2 Relaxation, and Proton Density in Normal Brain Using Synthetic MRI with Fast Imaging Protocol. *Magnetic Resonance in Medical Sciences*, tn.2022-0161. https://doi.org/10.2463/mrms.tn.2022-0161

Zhu, H., & Barker, P. B. (2011). *MR Spectroscopy and Spectroscopic Imaging of the Brain* (pp. 203–226). https://doi.org/10.1007/978-1-61737-992-5_9

Zhu, Y., Schreiber, K., Loggia, M., Haythornthwaite, J., Campbell, C., Smith, M., & Edwards, R. (2023). Sex Differences In Pain, Sensory Function And Psychosocial Factors Among Knee Osteoarthritis Patients. *The Journal of Pain*, *24*(4), 106. https://doi.org/10.1016/j.jpain.2023.02.301

Appendix A: Absolute Neurochemical Concentration Quantification Equations (Chapter 3)

Table A1. Tissue correction variables and their definitions. "*i*" indicates the tissue compartment (GM, WM, or CSF) in all cases

Variable	Definition
c_{raw}	$\frac{S_{M_{obs}}}{S_{H2O_{obs}}} \times \frac{2}{\#H_M} \times [H_2O]$ LCModel already does this for us so we can just call this c_{raw} to indicate the raw LCModel output but this may differ for different quantification software. $S_{M_{obs}}$= metabolite signal intensity $S_{H2O_{obs}}$= water signal intensity $\#H_M$= number of protons in the metabolite of interest $[H_2O]_{molal}$=55510 mmol/kg $[H_2O]_{molar}$=55510 mmol/L *e.g., For molar calculations, Gannet uses the Harris, 2015 equation where $c_{w,i} = [H_2O]_{molar} \times d_i$ but because $[H_2O]_{molar}$ is already included in the LCModel output, we only include d_i
MM	Correction factor for co-edited macromolecular signal (used in the Harris 2015 equation only)
k	Editing efficiency of GABA, assumed to be 0.5 (used in the Harris 2015 equation only)
I_G	Signal integral for GABA, modeled as a five-parameter Gaussian (used in the Harris 2015 equation only)
I_W	Signal integral for water, modeled as a Gaussian-Lorentzian (used in the Harris 2015 equation only)
d_i	Relative water densities: the ratio of signals from tissue water / total water
R_{H2O_i}	Signal attenuation factor that accounts/corrects for the longitudinal (T1) and transverse (T2) relaxation of water to correct/recover signal that was lost from not acquiring the signal under ideal/fully relaxed conditions. $e^{\left(-\frac{TE}{T_{2H2O_i}}\right)}\left(1 - e^{\left(-\frac{TR}{T_{1H2O_i}}\right)}\right)$
$R_{M_{avg}}$	Signal attenuation factor that accounts/corrects for the longitudinal (T1) and transverse (T2) relaxation of the neurochemical of interest to correct/recover signal that was lost from not acquiring the signal under ideal/fully relaxed conditions. Requires known T1 and T2 for the neurochemical of interest **<u>averaged</u>** in GM and WM. (This is a combined measure.) $e^{\left(-\frac{TE}{T_{2M}}\right)}\left(1 - e^{\left(-\frac{TR}{T_{1M}}\right)}\right)$
R_{M_i}	Signal attenuation factor that accounts/corrects for the longitudinal (T1) and transverse (T2) relaxation of the neurochemical of interest to correct/recover signal that was lost from not acquiring the signal under ideal/fully relaxed conditions. Requires known T1 and T2 for the neurochemical of interest **<u>in both</u>** GM and WM. (These are separate measure for GM and WM.) $e^{\left(-\frac{TE}{T_{2M,i}}\right)}\left(1 - e^{\left(-\frac{TR}{T_{1M,i}}\right)}\right)$
f_i	Fraction of water in the tissue compartment of interest relative to total water in the voxel $\frac{f_{i_{vol}} \times d_i}{f_{GM_{vol}} \times d_{GM} + f_{WM_{vol}} \times d_{WM} + f_{CSF_{vol}} \times d_{CSF}}$
$f_{i_{vol}}$	Volume fractions estimated from image segmentation
α	Ratio of the concentration of metabolite in WM over the concentration of metabolite in GM (used in Harris 2015 equation) $\frac{cWM}{cGM}$
β	Ratio of the concentration of metabolite in GM over the concentration of metabolite in WM $\frac{cGM}{cWM}$
$\mu_{i_{vol}}$	Average of volume fraction for all files supplied in the batch analysis *We use $\mu_{GM_{vol}}$=0.5 and $\mu_{WM_{vol}}$=0.5 to simulate a voxel with 50% GM and 50% WM rather than a group normalized representative voxel
$R_{M_{GM\_WM}}$	$\frac{\beta f_{GM_{vol}} \times d_{GM} \times R_{M_{GM}} + f_{WM_{vol}} \times d_{WM} \times R_{M_{WM}}}{\beta f_{GM_{vol}} \times d_{GM} + f_{WM_{vol}} \times d_{WM}} = \frac{\beta f_{GM} \times R_{M_{GM}} + f_{WM} \times R_{M_{WM}}}{\beta f_{GM} + f_{WM}}$ *molar (left) and molal (right) versions yield the same result
$R_{M_{WM\_GM}}$	$\frac{f_{GM_{vol}} \times d_{GM} \times R_{M_{GM}} + \alpha f_{WM_{vol}} \times d_{WM} \times R_{M_{WM}}}{f_{GM_{vol}} \times d_{GM} + \alpha f_{WM_{vol}} \times d_{WM}} = \frac{f_{GM} \times R_{M_{GM}} + \alpha f_{WM} \times R_{M_{WM}}}{f_{GM} + \alpha f_{WM}}$ *molar (left) and molal (right) versions yield the same result

Table A2. Tissue correction constants from literature, values used, and references where values were found.

Variable	*Value*	*Reference*
d_{CSF}	0.97	Ernst et al. 1993 (JMR)
d_{GM}	0.78	Ernst et al. 1993 (JMR)
d_{WM}	0.65	Ernst et al. 1993 (JMR)
$T_{1_{W_{CSF}}}$	3.817	Piechnik 2009 (MRM)
$T_{1_{W_{GM}}}$	1.331	Wansapura et al. 1999 (JMRI)
$T_{1_{W_{WM}}}$	0.832	Wansapura et al. 1999 (JMRI)
$T_{2_{W_{CSF}}}$	0.503	Lu et al. 2005 (JMRI)
$T_{2_{W_{GM}}}$	0.110	Wansapura et al. 1999 (JMRI)
$T_{2_{W_{WM}}}$	0.0792	Wansapura et al. 1999 (JMRI)
$T_{1_{NAA_{GM}}}$	1.47	Average from Mlynarik et al. 2001 (NMRBiomed) & Posse et al. 2007 (MRM)
$T_{1_{NAA_{WM}}}$	1.46	Average from Mlynarik et al. 2001 (NMRBiomed) & Posse et al. 2007 (MRM)
$T_{2_{NAA_{GM}}}$	0.25	Average from Mlynarik et al. 2001 (NMRBiomed) & Posse et al. 2007 (MRM)
$T_{2_{NAA_{WM}}}$	0.30	Average from Mlynarik et al. 2001 (NMRBiomed) & Posse et al. 2007 (MRM)
$T_{1_{Cr_{GM}}}$	1.40	Average from Mlynarik et al. 2001 (NMRBiomed) & Posse et al. 2007 (MRM)
$T_{1_{Cr_{WM}}}$	1.32	Average from Mlynarik et al. 2001 (NMRBiomed) & Posse et al. 2007 (MRM)
$T_{2_{Cr_{GM}}}$	0.16	Average from Mlynarik et al. 2001 (NMRBiomed) & Posse et al. 2007 (MRM)
$T_{2_{Cr_{WM}}}$	0.17	Average from Mlynarik et al. 2001 (NMRBiomed) & Posse et al. 2007 (MRM)
$T_{1_{Cho_{GM}}}$	1.28	Average from Mlynarik et al. 2001 (NMRBiomed) & Posse et al. 2007 (MRM)
$T_{1_{Cho_{WM}}}$	1.15	Average from Mlynarik et al. 2001 (NMRBiomed) & Posse et al. 2007 (MRM)
$T_{2_{Cho_{GM}}}$	0.21	Average from Mlynarik et al. 2001 (NMRBiomed) & Posse et al. 2007 (MRM)
$T_{2_{Cho_{WM}}}$	0.20	Average from Mlynarik et al. 2001 (NMRBiomed) & Posse et al. 2007 (MRM)
$T_{1_{Glu_{GM}}}$	1.27	Mlynarik et al. 2001 (NMRBiomed)
$T_{1_{Glu_{WM}}}$	1.17	Mlynarik et al. 2001 (NMRBiomed)
$T_{2_{Glu_{GM}}}$	0.14	Wyss et al. 2018 (MRM)
$T_{2_{Glu_{WM}}}$	0.14	Wyss et al. 2018 (MRM)
$T_{1_{Glx_{GM}}}$	1.25	Posse et al. 2007 (MRM)
$T_{1_{Glx_{WM}}}$	1.21	Posse et al. 2007 (MRM)
$T_{2_{Glx_{GM}}}$	0.20	Posse et al. 2007 (MRM)
$T_{2_{Glx_{WM}}}$	0.20	Posse et al. 2007 (MRM)
$T_{1_{Myo_{GM}}}$	1.18	Average from Mlynarik et al. 2001 (NMRBiomed) & Posse et al. 2007 (MRM)
$T_{1_{Myo_{WM}}}$	0.99	Average from Mlynarik et al. 2001 (NMRBiomed) & Posse et al. 2007 (MRM)
$T_{2_{Myo_{GM}}}$	0.22	Average from Wyss et al. 2018 (MRM) & Posse et al. 2007 (MRM)
$T_{2_{Myo_{WM}}}$	0.22	Average from Wyss et al. 2018 (MRM) & Posse et al. 2007 (MRM)

Exploration of Correction Methods

Gasparovic et al. (2006) Equation (MOLAL)

Several correction methods have previously been proposed to account for the tissue composition within the voxel. The conventional approach, expressed in units of molality (moles of neurochemical per kg of water) proposed by Gasparovic et al in 2006, corrects for differences in tissue relaxation but assumes equal metabolite concentrations in GM and WM.

Derivation:

Since neurochemicals are only found in the parenchyma (GM/WM) of the voxel (i.e., CSF contains negligible metabolites) the internal water reference is also only water from the parenchyma.

$$\frac{S_{M_R}}{S_{H_2O_{GM/WM_R}}} = \frac{moles_M}{moles_{H_2O_{GM/WM}}} \times \frac{\#H_M}{2}$$

Key assumption: the fully relaxed signals of the neurochemical (S_{M_R}) and water ($S_{H_2O_{GM/WM_R}}$) are directly proportional to their respective concentrations in the voxel. Therefore, the ratio of their signals is proportional to the ratio of their moles and multiplying both sides by the concentration of water leaves us with the concentration of the metabolite, where $[M] = \frac{moles_M}{moles_{H_2O_{GM/WM}}} \times [H2O]$ and $[H2O] = \frac{moles_{H_2O_{GM/WM}}}{kg\ of\ solvent(i.e.\ water)}$.

$$[M] = \frac{S_{M_R}}{S_{H_2O_{GM/WM_R}}} \times \frac{2}{\#H_M} \times [H_2O]$$

The observed water signal ($S_{H_2O_{obs}}$) is the sum of the weighted contributions of the total fully relaxed water signal ($S_{H_2O_R}$) from each tissue compartment, taking into account their respective water fractions and relaxation factors. $\left[\left(f_{GM} \cdot R_{H_2O_{GM}}\right) + \left(f_{WM} \cdot R_{H_2O_{WM}}\right) + \left(f_{CSF} \cdot R_{H_2O_{CSF}}\right)\right]$ is the effective signal remaining after considering signal loss due to relaxation in each

compartment. (This accounts for the impact of different relaxation rates of water in different tissues within the voxel).

$$S_{H_2O_{obs}} = S_{H_2O_R}\left[\left(f_{GM} \cdot R_{H_2O_{GM}}\right) + \left(f_{WM} \cdot R_{H_2O_{WM}}\right) + \left(f_{CSF} \cdot R_{H_2O_{CSF}}\right)\right]$$

Same thing for the metabolites if we assume $R_{M_{GM}} \cong R_{M_{WM}}$:

$$S_{M_{obs}} \approx S_{M_R} \times R_{M_{avg}} \text{ therefore } S_{M_R} \approx \frac{S_{M_{obs}}}{R_{M_{avg}}}$$

Where $R_{x_y} = (e^{-TE/T2_{x_y}})(1 - e^{-TR/T1_{x_y}})$ and x=metabolite or water and y=GM, WM, CSF or GM/WM avg

The fully relaxed signal in the parenchyma (GM/WM) ($S_{H_2O_{GM/WM_R}}$) is the is the weighted average of the parenchymal tissue water over total amount of relaxed water in the voxel:

$$S_{H_2O_{GM/WM_R}} = \frac{S_{H_2O_{obs}}(1 - f_{CSF})}{\left(f_{GM} \cdot R_{H_2O_{GM}}\right) + \left(f_{WM} \cdot R_{H_2O_{WM}}\right) + \left(f_{CSF} \cdot R_{H_2O_{CSF}}\right)}$$

Mole fraction of water in each compartment of the voxel:

$$f_{GM} = \frac{f_{GM_{vol}} \cdot 0.78}{\left(f_{GM_{vol}} \cdot 0.78\right) + \left(f_{WM_{vol}} \cdot 0.65\right) + \left(f_{CSF_{vol}} \cdot 0.97\right)}$$

$$f_{WM} = \frac{f_{WM_{vol}} \cdot 0.65}{\left(f_{GM_{vol}} \cdot 0.78\right) + \left(f_{WM_{vol}} \cdot 0.65\right) + \left(f_{CSF_{vol}} \cdot 0.97\right)}$$

$$f_{CSF} = \frac{f_{CSF_{vol}} \cdot 0.97}{\left(f_{GM_{vol}} \cdot 0.78\right) + \left(f_{WM_{vol}} \cdot 0.65\right) + \left(f_{CSF_{vol}} \cdot 0.97\right)}$$

Final equation:

$$[M] = \frac{S_{M_{obs}}}{S_{H_2O_{obs}}} \times \frac{\left(f_{GM} \cdot R_{H_2O_{GM}}\right) + \left(f_{WM} \cdot R_{H_2O_{WM}}\right) + \left(f_{CSF} \cdot R_{H_2O_{CSF}}\right)}{(1 - f_{CSF})R_{M_{avg}}} \times \frac{2}{\#H_M} \times [H_2O]_{molal}$$

Rearranged:

$$[M]_{molal} = \frac{S_{M_{obs}}}{S_{H2O_{obs}}} \times \frac{2}{\#H_M} \times [H_2O]_{molal} \times \left(\frac{\sum_i^{GM,WM,CSF} R_{H2O_i} f_i}{R_{M_{avg}}}\right)\left(\frac{1}{1 - f_{CSF}}\right)$$

$$[M]_{molal} = c_{raw}\left(\frac{\sum_i^{GM,WM,CSF} R_{H2O_i} f_i}{R_{M_{avg}}}\right)\left(\frac{1}{1 - f_{CSF}}\right)$$

Harris et al. (2015) Equation (MOLAR)

This method was improved upon by Harris et al in 2015, specifically for the neurochemical gamma-aminobutyric acid (GABA), to differentiate GM and WM but in units of molarity (moles of neurochemical and water per volume of tissue). This approach takes into account the known ratio of metabolite concentration between GM and WM, which can differ for different neurochemicals.

$$[M]_{molar} = \frac{MM\ I_G}{k\ I_W}\left(\frac{\sum_i^{GM,WM,CSF} c_{w,i}\ R_{H2O_i} f_{i_{vol}}}{R_{M_{avg}}}\right)\left(\frac{1}{f_{GM_{vol}} + \alpha f_{WM_{vol}}}\right)$$

While the above equation now scales neurochemical contributions to the overall signal, $[M]_{molar}$ represents what the measured concentration would be if the voxel were entirely GM. Harris et al 2015 proposed the following equation to scale $[M]_{molar}$ to any representative voxel (e.g. a voxel with 50% GM and 50% WM or the mean tissue fractions from the sample, "group normal").

$$[M]_{molar} = \frac{MM\ I_G}{k\ I_W}\left(\frac{\sum_i^{GM,WM,CSF} c_{w,i}\ R_{H2O_i} f_{i_{vol}}}{R_{M_{avg}}}\right)\left(\frac{1}{f_{GM_{vol}} + \alpha f_{WM_{vol}}}\right)\left(\frac{\mu_{GM_{vol}} + \alpha\mu_{WM_{vol}}}{\mu_{GM_{vol}} + \mu_{WM_{vol}}}\right)$$

However, both of the equations above use a combined measure for the attenuation of the neurochemical of interest ($R_{M_{avg}}$).

Gasparovic et al. (2018) Equation (MOLAR & MOLAL)

In 2018, Gasparovic et al. made improvements that employ separate attenuation factors ($R_{M_{GM}}$ and $R_{M_{WM}}$) for GM and WM to account for different relaxation rates (i.e., T1 and T2) for specific metabolites in GM and WM. While this technique corrects for differences in tissue water

concentration, the normalization to a standardized voxel established by Harris et al was not applied (i.e., a pure GM voxel).

Derivation:

As before, since neurochemicals are only found in the parenchyma (GM/WM) of the voxel (i.e., CSF contains negligible metabolites) the internal water reference is also only water from the parenchyma.

$$\frac{S_{M_R}}{S_{H_2O_{GM/WM_R}}} = \frac{moles_M}{moles_{H_2O_{GM/WM}}} \times \frac{\#H_M}{2}$$

Key assumption: the fully relaxed signals of the neurochemical (S_{M_R}) and water ($S_{H_2O_{GM/WM_R}}$) are directly proportional to their respective concentrations in the voxel. Therefore, the ratio of their signals is proportional to the ratio of their moles and multiplying both sides by the concentration of water leaves us with the concentration of the metabolite, where $[M] = \frac{moles_M}{moles_{H_2O_{GM/WM}}} \times [H2O]$ and $[H2O] = \frac{moles_{H_2O_{GM/WM}}}{kg\ of\ solvent(i.e.\ water)}$.

$$[M] = \frac{S_{M_R}}{S_{H_2O_{GM/WM_R}}} \times \frac{2}{\#H_M} \times [H_2O]$$

The observed water signal ($S_{H_2O_{obs}}$) is the sum of the weighted contributions of the total fully relaxed water signal ($S_{H_2O_R}$) from each tissue compartment, taking into account their respective water fractions and relaxation factors. $\left[\left(f_{GM} \cdot R_{H_2O_{GM}}\right) + \left(f_{WM} \cdot R_{H_2O_{WM}}\right) + \left(f_{CSF} \cdot R_{H_2O_{CSF}}\right)\right]$ is the effective signal remaining after considering signal loss due to relaxation in each compartment. (This accounts for the impact of different relaxation rates of water in different tissues within the voxel).

$$S_{H_2O_{obs}} = S_{H_2O_R}\left[\left(f_{GM} \cdot R_{H_2O_{GM}}\right) + \left(f_{WM} \cdot R_{H_2O_{WM}}\right) + \left(f_{CSF} \cdot R_{H_2O_{CSF}}\right)\right]$$

At this point, the derivation changes from Gasparovic et al (2006) and we assume $R_{M_{GM}} \neq R_{M_{WM}}$. The observed metabolite signal is equal to the sum of the mole fractions of the fully relaxed signal S_{M_R}, with each fractional signal weighted by its compartment-specific relaxation factor:

$$S_{M_{obs}} = S_{M_R}\left[\left(f_{M_{GM}} \cdot R_{M_{GM}}\right) + \left(f_{M_{WM}} \cdot R_{M_{WM}}\right)\right]$$

Solve for S_{M_R}:

$$S_{M_R} = \frac{S_{M_{obs}}}{\left[\left(f_{M_{GM}} \cdot R_{M_{GM}}\right) + \left(f_{M_{WM}} \cdot R_{M_{WM}}\right)\right]}$$

Because metabolite concentrations are not the same in all compartments, the metabolite mole fractions ($f_{M_{GM}}$ and $f_{M_{WM}}$) are not simply determined by the volume fractions and water tissue densities, but also by the different neurochemical concentrations in the GM and WM water fractions (where $[M]_{GM}$ is the neurochemical concentration in GM and $[M]_{WM}$ is the neurochemical concentration in WM):

$$f_{M_{GM}} = \frac{f_{GM} \cdot [M]_{GM}}{f_{GM} \cdot [M]_{GM} + f_{WM} \cdot [M]_{WM}}$$

$$f_{M_{WM}} = \frac{f_{WM} \cdot [M]_{WM}}{f_{GM} \cdot [M]_{GM} + f_{WM} \cdot [M]_{WM}}$$

Observing the parallels from the Gasparovic et al 2006 equation, we are essentially replacing $R_{M_{avg}}$ with $R_{M_{GM\_WM}}$:

$$S_{M_{obs}} \approx S_{M_R} \times R_{M_{GM\_WM}} \text{ therefore } S_{M_R} \approx \frac{S_{M_{obs}}}{R_{M_{GM\_WM}}}$$

Where:

$$R_{M_{GM\_WM}} = \left(f_{M_{GM}} \cdot R_{M_{GM}}\right) + \left(f_{M_{WM}} \cdot R_{M_{WM}}\right)$$

Expanded and rearranged:

$$R_{M_{GM\_WM}} = \left(\frac{f_{GM}\cdot\left({}^{M_{GM}}/_{M_{WM}}\right)\cdot R_{M_{GM}} + f_{WM}\cdot R_{M_{WM}}}{f_{GM}\cdot\left({}^{M_{GM}}/_{M_{WM}}\right) + f_{WM}}\right)_{molal} =$$

$$\left(\frac{f_{GM_{vol}}\cdot d_{GM}\cdot\left({}^{M_{GM}}/_{M_{WM}}\right)\cdot R_{M_{GM}} + f_{WM_{vol}}\cdot d_{WM}\cdot R_{M_{WM}}}{f_{GM_{vol}}\cdot d_{GM}\cdot\left({}^{M_{GM}}/_{M_{WM}}\right) + f_{WM_{vol}}\cdot d_{WM}}\right)_{molar}$$

We can then put this into the baseline equation that assumes the fully relaxed signals of the neurochemical (S_{M_R}) and water ($S_{H_2O_{GM/WM_R}}$) are directly proportional to their respective concentrations in the voxel:

$$[M] = \frac{S_{M_R}}{S_{H_2O_{GM/WM_R}}} \times \frac{2}{\#H_M} \times [H_2O]$$

$$[M]_{molar} = \frac{S_{M_{obs}} \times \left(f_{GM_{vol}} \times d_{GM} \times R_{H2O_{GM}} + f_{WM_{vol}} \times d_{WM} \times R_{H2O_{WM}} + f_{CSF_{vol}} \times d_{CSF} \times R_{H2O_{CSF}}\right)}{S_{H2O_{obs}} \times (1 - f_{CSF_{vol}}) \times R_{M_{GM\_WM}}} \times \frac{2}{\#H_M} \times [H_2O]_{molar}$$

$$[M]_{molal} = \frac{S_{M_{obsv}} \times \left(f_{GM} \times R_{H2O_{GM}} + f_{WM} \times R_{H2O_{WM}} + f_{CSF} \times R_{H2O_{CSF}}\right)}{S_{H2O_{obs}} \times (1 - f_{CSF}) \times R_{M_{GM\_WM}}} \times \frac{2}{\#H_M} \times [H_2O]_{molal}$$

Rearranging and expanding into same format as the Harris et al (2015) Equation:

Note: Gasparovic uses β, the GM to WM concentration ratio, rather than α, the WM to GM concentration ratio

$$[M]_{molar} = \left(\frac{S_{M_{obs}}}{S_{H2O_{obs}}} \times \frac{2}{\#H_M} \times [H_2O]_{molar}\right)\left(\frac{\sum_i^{GM,WM,CSF} d_i\, R_{H2O_i} f_{i_{vol}}}{\left(\frac{f_{GM_{vol}} \times d_{GM} \times \beta \times R_{M_{GM}} + f_{WM_{vol}} \times d_{WM} \times R_{M_{WM}}}{f_{GM_{vol}} \times d_{GM} \times \beta + f_{WM_{vol}} \times d_{WM}}\right)}\right)\left(\frac{1}{1 - f_{CSF_{vol}}}\right)$$

NOTE: In the Harris et al (2015) equation, we have $c_{w,i} = [H_2O]_{molar} \times d_i$ but because $[H_2O]_{molar}$ is already included in c_{raw} from analysis outputs such as LCModel, we only include

d_i (relative water densities – the ratio of signals from tissue water / total water) in the relaxation correction

Similarly, this can be expressed in units of molality:

$$[M]_{molal} = \left(\frac{S_{M_{obs}}}{S_{H2O_{obs}}} \times \frac{2}{\#H_M} \times [H_2O]_{molal}\right)\left(\frac{\sum_i^{GM,WM,CSF} R_{H2O_i} f_i}{\left(\frac{f_{GM} \times \beta \times R_{M_{GM}} + f_{WM} \times R_{M_{WM}}}{f_{GM} \times \beta + f_{WM}}\right)}\right)\left(\frac{1}{1 - f_{CSF_{vol}}}\right)$$

NOTE: The denominator in the second bracket (summarized as $R_{M\_GM\_WM}$ in the Gasparovic et al 2018 paper) is a scaling factor that affects the molarity and molality expressions similarly, therefore, these can be used interchangeably between the two expressions.

$$\left(\frac{f_{GM_{vol}} \times d_{GM} \times \beta \times R_{M_{GM}} + f_{WM_{vol}} \times d_{WM} \times R_{M_{WM}}}{f_{GM_{vol}} \times d_{GM} \times \beta + f_{WM_{vol}} \times d_{WM}}\right)_{molar} = \left(\frac{f_{GM} \times \beta \times R_{M_{GM}} + f_{WM} \times R_{M_{WM}}}{f_{GM} \times \beta + f_{WM}}\right)_{molal}$$

PROPOSED EQUATIONS

A combination of the Harris et al (2015) equation (tissue correction) and the Gasparovic et al. (2018) equation (advanced tissue relaxation) has been proposed in this paper. c_{raw} is the raw signal that is reported from LCModel analysis software, the contents of the first large bracket perform tissue relaxation correction, and the contents of the second large bracket performs tissue correction.

$$[M]_{molal} = c_{raw}\left(\frac{\sum_i^{GM,WM,CSF} f_i \times R_{H2O_i}}{R_{M_{WM\_GM}}}\right)\left(\frac{1}{(f_{GM} + \alpha f_{WM})}\right)$$

$$[M]_{molar} = c_{raw}\left(\frac{\sum_i^{GM,WM,CSF} f_{i_{vol}} \times d_i \times R_{H2O_i}}{R_{M_{WM\_GM}}}\right)\left(\frac{1}{(f_{GM_{vol}} + \alpha f_{WM_{vol}})}\right)$$

This combination of the two equations is important as the Gasparovic 2018 equation only uses α (or β the GM-to-WM concentration ratio) to account for differing relaxation rates of the metabolite in GM and WM but does NOT account for the actual proportion of tissue in the voxel (as shown in **Figure A1**, sub-figure B below). To use α to its fullest potential, applying

$(f_{GM} + \alpha f_{WM})$ in the denominator in place of $(1 - f_{CSF})$ corrects for tissue composition in the voxel (as shown in **Figure A1**, sub-figure A below). Note: while this α does not contribute much to relaxation correction with our short-TE data, Gasparovic shows it makes a difference for longer TE acquisitions and therefore, for the most accurate concentration estimates, it is best to use α for both relaxation correction (as per Gasparovic et al 2018) and composition correction (as per Harris et al 2015).

Figure A1. *Example plot of corrected tNAA concentrations vs β values, the GM-to-WM concentration ratio. Corrected tNAA concentrations were calculated 1) using our proposed equation which incorporates the Harris et al 2015 tissue composition correction and 2) using Gasparovic et al's 2018 equation that used CSF correction with no modification.*

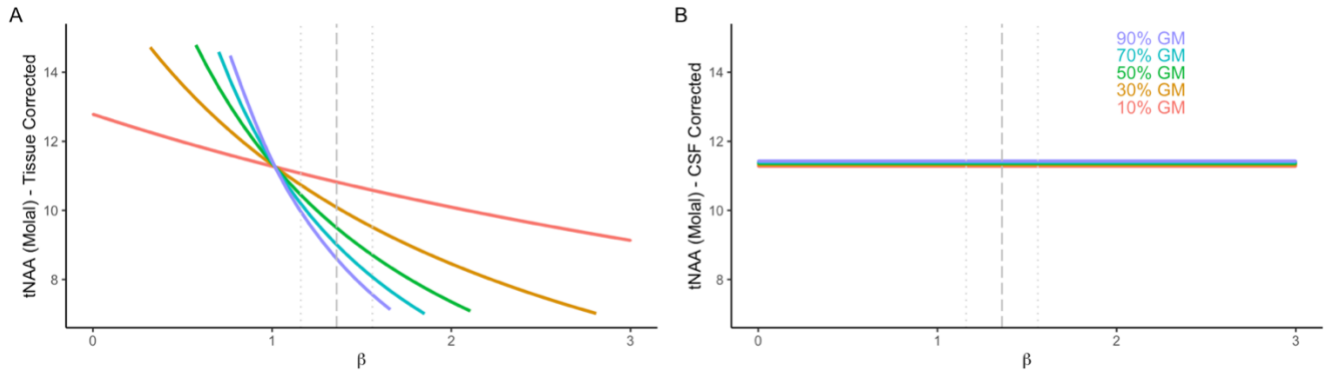

NORMALIZATION CONSIDERATIONS

Akin to how structural imaging studies register individual brain images to a common template or standard space for accurate volume comparisons, neurochemical measurements can be normalized to a standardized voxel to ensure that individual neurochemical measurements are comparable by bringing them to a consistent baseline. Thus, normalizing individual voxel fractions to a standard voxel enables direct comparison neurochemical measures between individuals and between studies if the same standardized voxel is chosen. Proposed standardized voxels include; 1) a voxel consisting solely of GM or WM, which often results in an over or underestimation of observed neurochemical concentrations respectively (shown below for a purely GM voxel),

$$[M]_{molal_{norm}} = c_{raw}\left(\frac{\sum_i^{GM,WM,CSF} f_i \times R_{H2O_i}}{R_{M_{WM\_GM}}}\right)\left(\frac{1}{(f_{GM} + \alpha f_{WM})}\right)$$

$$[M]_{molar_{norm}} = c_{raw}\left(\frac{\sum_i^{GM,WM,CSF} f_{i_{vol}} \times d_i \times R_{H2O_i}}{R_{M_{WM\_GM}}}\right)\left(\frac{1}{(f_{GM_{vol}} + \alpha f_{WM_{vol}})}\right)$$

and 2) a group-average voxel that amalgamates the average fractions of GM and WM from the collected data [15].

$$[M]_{molal_{norm}} = c_{raw}\left(\frac{\sum_i^{GM,WM,CSF} f_i \times R_{H2O_i}}{R_{M_{WM\_GM}}}\right)\left(\frac{1}{(f_{GM} + \alpha f_{WM})}\right)\left(\frac{\mu_{GM_{vol}} + \alpha\mu_{WM_{vol}}}{\mu_{GM_{vol}} + \mu_{WM_{vol}}}\right)$$

$$[M]_{molar_{norm}} = c_{raw}\left(\frac{\sum_i^{GM,WM,CSF} f_{i_{vol}} \times d_i \times R_{H2O_i}}{R_{M_{WM\_GM}}}\right)\left(\frac{1}{(f_{GM_{vol}} + \alpha f_{WM_{vol}})}\right)\left(\frac{\mu_{GM_{vol}} + \alpha\mu_{WM_{vol}}}{\mu_{GM_{vol}} + \mu_{WM_{vol}}}\right)$$

The selection of standardized voxel composition for normalization may vary depending on the study; for example, if two groups with different structural changes are being compared. However, it may be appropriate to also report results standardized to a balanced voxel composition of 50% GM and 50% WM, representing a typical composition encountered in many brain regions, offering valuable insights into concentrations commonly encountered in clinical and research settings where voxels often encompass mixed tissue types.

$$[M]_{molal_{norm}} = c_{raw}\left(\frac{\sum_i^{GM,WM,CSF} f_i \times R_{H2O_i}}{R_{M_{WM\_GM}}}\right)\left(\frac{1}{(f_{GM} + \alpha f_{WM})}\right)\left(\frac{0.5 + \alpha 0.5}{0.5 + 0.5}\right)$$

$$[M]_{molar_{norm}} = c_{raw}\left(\frac{\sum_i^{GM,WM,CSF} f_{i_{vol}} \times d_i \times R_{H2O_i}}{R_{M_{WM\_GM}}}\right)\left(\frac{1}{(f_{GM_{vol}} + \alpha f_{WM_{vol}})}\right)\left(\frac{0.5 + \alpha 0.5}{0.5 + 0.5}\right)$$

Appendix B: Compilation of Commonly Used T1, T2, and PD Constants (Chapter 4)

Standard errors are reported where available.

Table B.1 *Relative tissue water densities.*

Variable	*Value*	*Reference*	*Used in*
d_{CSF}	0.97	*Ernst et al. 1993 (*J. Magn. Reson.*) (Ernst et al., 1993) Kreis et al., 1993 (*J. Magn. Reson.)* (Kreis et al., 1993)	Gannet, Osprey, FLS-MRS
d_{GM}	0.78	*Ernst et al. 1993 (*J. Magn. Reson.)* (Ernst et al., 1993) Kreis et al., 1993 (*J. Magn. Reson.)* (Kreis et al., 1993)	Gannet, Osprey, FLS-MRS
d_{WM}	0.65	*Ernst et al. 1993 (*J. Magn. Reson.*) (Ernst et al., 1993) Kreis et al., 1993 (*J. Magn. Reson.)* (Kreis et al., 1993)	Gannet, Osprey, FLS-MRS

***** Gasparovic et al. 2006 (MRM) (Charles Gasparovic et al., 2006), references to Ernst et al. 1993 (JMR) (Ernst et al., 1993) but Gasparovic et al. 2009 (J.Neurotrauma) (Charles Gasparovic et al., 2009), reference to Kreis et al., 1993 (Kreis et al., 1993) *for the same values*

Table B.2 *Water relaxation constants (sec).*

Variable	*Value*	*Reference*	*Used in*
$T_{1_{W_{CSF}}}$	3.817 ± 0.424	Lu et al. 2005 (JMRI) (Lu et al., 2005)	Gannet
	4.472 ± 0.085	Rooney et al. 2007 (MRM) (Rooney et al., 2007)	FSL-MRS
$T_{1_{W_{GM}}}$	1.331 ± 0.013	Wansapura et al. 1999 (JMRI) (Wansapura et al., 1999)	Gannet
	1.304	Gasparovic et al. 2009 (J.Neurotrauma) (Charles Gasparovic et al., 2009) Vymazal et al., 1999 (Radiology) (Vymazal et al., 1999)	
	1.820 ± 0.114	Stanisz et al. 2005 (MRM) (Stanisz et al., 2005)	FSL-MRS
	1.47 ± 0.05	Posse et al. 2007 (MRM) (Posse et al., 2007) Ethofer et al. 2003 (MRM) (Ethofer et al., 2003)	
$T_{1_{W_{WM}}}$	0.832 ± 0.010	Wansapura et al. 1999 (JMRI) (Wansapura et al., 1999)	Gannet
	0.660	Gasparovic et al. 2009 (J.Neurotrauma) (Charles Gasparovic et al., 2009)	

		Vymazal et al., 1999 (Radiology) (Vymazal et al., 1999)	
	1.084 ± 0.045	Stanisz et al. 2005 (MRM) (Stanisz et al., 2005)	
	1.11 ± 0.04	Ethofer et al. 2003 (MRM) (Ethofer et al., 2003)	
	1.06 ± 0.06	Ethofer et al. 2003 (MRM) (Ethofer et al., 2003)	
$T_{2_{W_{CSF}}}$	0.503 ± 0.0643	Piechnik 2009 (MRM) (Piechnik et al., 2009)	Gannet
	2.03 ± 0.215	Spijkerman 2018 (MAGMA) (Spijkerman et al., 2018)	FSL-MRS
	2.47	Gasparovic et al. 2009 (J.Neurotrauma) (Charles Gasparovic et al., 2009)	
$T_{2_{W_{GM}}}$	0.110 ± 0.02	Posse et al. 2007 (MRM) (Posse et al., 2007) Wansapura et al. 1999 (JMRI) (Wansapura et al., 1999)	Gannet
	0.093	Gasparovic et al. 2009 (J.Neurotrauma) (Charles Gasparovic et al., 2009) Vymazal et al., 1999 (Radiology) (Vymazal et al., 1999)	
	0.099 ± 0.007	Stanisz et al. 2005 (MRM) (Stanisz et al., 2005)	
$T_{2_{W_{WM}}}$	0.0796 ± 0.006	Wansapura et al. 1999 (JMRI) (Wansapura et al., 1999)	Gannet
	0.073	Gasparovic et al. 2009 (J.Neurotrauma) (Charles Gasparovic et al., 2009) Vymazal et al., 1999 (Radiology) (Vymazal et al., 1999)	
	0.069 ± 0.003	Stanisz et al. 2005 (MRM) (Stanisz et al., 2005)	

* Rooney et al. 2007 lists value for 4T but states that T1of CSF H_2O is not field-dependent (Gasparovic et al. 2009 (J.Neurotrauma) (Charles Gasparovic et al., 2009) uses this value)
* Vymazal et al., 1999 (Vymazal et al., 1999) (Radiology) determined values at 1.5T (Gasparovic et al. 2009 (J.Neurotrauma) (Charles Gasparovic et al., 2009) uses these values)
*Osprey uses averages relaxations for GM and WM, T1w = 1100 ms and T2w =95 ms, but cites Wansapura et al., 1999 [7]

Table B.3. *Neurochemical relaxation constants (in seconds). Many spectroscopists cite the secondary source, Posse et al. 2007 (MRM) (Posse et al., 2007), who summarized many of these constants. Therefore, both primary and secondary sources are included where possible.*

Variable	***Value***	***Reference***
$T_{1_{NAA_{GM}}}$	1.47 ± 0.06	Mlynarik et al. 2001 (NMRBiomed) (Mlynárik et al., 2001)
	1.47 ± 0.08	Posse et al. 2007 (MRM) (Posse et al., 2007) Ethofer et al. 2003 (MRM) (Ethofer et al., 2003)
	1.21 ± 0.01	Srinivasan et al. 2006 (NeuroImage) (Srinivasan et al., 2006)
$T_{1_{NAA_{WM}}}$	1.35 ± 0.12	Mlynarik et al. 2001 (NMRBiomed) (Mlynárik et al., 2001)
	1.40 ± 0.15	Ethofer et al. 2003 (MRM) (Ethofer et al., 2003)
	1.56	Posse et al. 2007 (MRM) (Posse et al., 2007)
	1.03 ± 0.1	Srinivasan et al. 2006 (NeuroImage) (Srinivasan et al., 2006)
$T_{2_{NAA_{GM}}}$	0.247 ± 0.019	Mlynarik et al. 2001 (NMRBiomed) (Mlynárik et al., 2001)
	0.247 ± 0.013	Posse et al. 2007 (MRM) (Posse et al., 2007) Träber et al. 2004 (JMRI) (Träber et al., 2004)
	0.1717 ± 0.015	Srinivasan et al. 2006 (NeuroImage) (Srinivasan et al., 2006)
$T_{2_{NAA_{WM}}}$	0.295 ± 0.029	Mlynarik et al. 2001 (NMRBiomed) (Mlynárik et al., 2001)
	0.301 ± 0.018	Posse et al. 2007 (MRM) (Posse et al., 2007) Träber et al. 2004 (JMRI) (Träber et al., 2004)
	0.2063 ± 0.0087	Srinivasan et al. 2006 (NeuroImage) (Srinivasan et al., 2006)
$T_{1_{Cr_{GM}}}$	1.46 ± 0.07	Mlynarik et al. 2001 (NMRBiomed) (Mlynárik et al., 2001)
	1.33 ± 0.13	Posse et al. 2007 (MRM) (Posse et al., 2007) Ethofer et al. 2003 (MRM) (Ethofer et al., 2003)
	1.07 ± 0.4	Srinivasan et al. 2006 (NeuroImage) (Srinivasan et al., 2006)
$T_{1_{Cr_{WM}}}$	1.24 ± 0.10	Mlynarik et al. 2001 (NMRBiomed) (Mlynárik et al., 2001)
	1.31 ± 0.13	Ethofer et al. 2003 (MRM) (Ethofer et al., 2003)
	1.40	Posse et al. 2007 (MRM) (Posse et al., 2007)
	0.96 ± 0.13	Srinivasan et al. 2006 (NeuroImage) (Srinivasan et al., 2006)
$T_{2_{Cr_{GM}}}$	0.152 ± 0.007	Mlynarik et al. 2001 (NMRBiomed) (Mlynárik et al., 2001)
	0.162 ± 0.016	Posse et al. 2007 (MRM) (Posse et al., 2007) Träber et al. 2004 (JMRI) (Träber et al., 2004)
	0.1101 ± 0.0036	Srinivasan et al. 2006 (NeuroImage) (Srinivasan et al., 2006)
$T_{2_{Cr_{WM}}}$	0.156 ± 0.020	Mlynarik et al. 2001 (NMRBiomed) (Mlynárik et al., 2001)
	0.178 ± 0.009	Posse et al. 2007 (MRM) (Posse et al., 2007) Träber et al. 2004 (JMRI) (Träber et al., 2004)
	0.108 ± 0.006	Srinivasan et al. 2006 (NeuroImage) (Srinivasan et al., 2006)
$T_{1_{Cho_{GM}}}$	1.30 ± 0.06	Mlynarik et al. 2001 (NMRBiomed) (Mlynárik et al., 2001)
	1.25 ± 0.22	Posse et al. 2007 (MRM) (Posse et al., 2007) Ethofer et al. 2003 (MRM) (Ethofer et al., 2003)
	0.84 ± 0.14	Srinivasan et al. 2006 (NeuroImage) (Srinivasan et al., 2006)
$T_{1_{Cho_{WM}}}$	1.08 ± 0.06	Mlynarik et al. 2001 (NMRBiomed) (Mlynárik et al., 2001)
	1.17 ± 0.15	Ethofer et al. 2003 (MRM) (Ethofer et al., 2003)
	1.21	Posse et al. 2007 (MRM) (Posse et al., 2007)
	0.78 ± 0.08	Srinivasan et al. 2006 (NeuroImage) (Srinivasan et al., 2006)

$T_{2_{Cho_{GM}}}$	0.207 ± 0.016	Mlynarik et al. 2001 (NMRBiomed) (Mlynárik et al., 2001)
	0.222 ± 0.015	Posse et al. 2007 (MRM) (Posse et al., 2007) Träber et al. 2004 (JMRI) (Träber et al., 2004)
	0.1255 ± 0.0038	Srinivasan et al. 2006 (NeuroImage) (Srinivasan et al., 2006)
$T_{2_{Cho_{WM}}}$	0.187 ± 0.020	Mlynarik et al. 2001 (NMRBiomed) (Mlynárik et al., 2001)
	0.222 ± 0.017	Posse et al. 2007 (MRM) (Posse et al., 2007) Träber et al. 2004 (JMRI) (Träber et al., 2004)
	0.1359 ± 0.0085	Srinivasan et al. 2006 (NeuroImage) (Srinivasan et al., 2006)
$T_{1_{Glu_{GM}}}$	1.27 ± 0.10	Mlynarik et al. 2001 (NMRBiomed) (Mlynárik et al., 2001)
	0.88 ± 0.03	Srinivasan et al. 2006 (NeuroImage) (Srinivasan et al., 2006)
$T_{1_{Glu_{WM}}}$	1.17 ± 0.08	Mlynarik et al. 2001 (NMRBiomed) (Mlynárik et al., 2001)
	0.67 ± 0.2	Srinivasan et al. 2006 (NeuroImage) (Srinivasan et al., 2006)
$T_{2_{Glu_{GM}}}$	0.122±0.032	Wyss et al. 2018 (MRM) (Wyss et al., 2018)
$T_{2_{Glu_{WM}}}$	0.124±0.037	Wyss et al. 2018 (MRM) (Wyss et al., 2018)
$T_{1_{Glx_{GM}}}$	1.25	Posse et al. 2007 (MRM) (Posse et al., 2007)
	1.20 ± 0.10	Mlynarik et al. 2001 (NMRBiomed) (Mlynárik et al., 2001)
$T_{1_{Glx_{WM}}}$	1.21	Posse et al. 2007 (MRM) (Posse et al., 2007)
	0.96 ± 0.20	Mlynarik et al. 2001 (NMRBiomed) (Mlynárik et al., 2001)
$T_{2_{Glx_{GM}}}$	0.20	Posse et al. 2007 (MRM) (Posse et al., 2007)
$T_{2_{Glx_{WM}}}$	0.20	Posse et al. 2007 (MRM) (Posse et al., 2007)
$T_{1_{Myo_{GM}}}$	1.23 ± 0.09	Mlynarik et al. 2001 (NMRBiomed) (Mlynárik et al., 2001)
	1.12 ± 0.25	Ethofer et al. 2003 (MRM) (Ethofer et al., 2003)
	1.00 ± 0.2	Srinivasan et al. 2006 (NeuroImage) (Srinivasan et al., 2006)
$T_{1_{Myo_{WM}}}$	1.01 ± 0.09	Mlynarik et al. 2001 (NMRBiomed) (Mlynárik et al., 2001)
	0.91 ± 0.13	Ethofer et al. 2003 (MRM) (Ethofer et al., 2003)
	0.54 ± 0.08	Srinivasan et al. 2006 (NeuroImage) (Srinivasan et al., 2006)
$T_{2_{Myo_{GM}}}$	0.229 ±105	Wyss et al. 2018 (MRM) (Wyss et al., 2018)
	0.110	Posse et al. 2007 (MRM) (Posse et al., 2007)
$T_{2_{Myo_{WM}}}$	0.161±0.037	Wyss et al. 2018 (MRM) (Wyss et al., 2018)
	0.200	Posse et al. 2007 (MRM) (Posse et al., 2007)

FSL-MRS used averaged values $T_{1_{W_{WM}}} = 0.97$ (Dieringer et al., 2014; Ethofer et al., 2003; Rooney et al., 2007; Stanisz et al., 2005; Wansapura et al., 1999; Wright et al., 2008), $T_{1_{W_{GM}}} = 1.50$ (Dieringer et al., 2014; Ethofer et al., 2003; Rooney et al., 2007; Stanisz et al., 2005; Wansapura et al., 1999; Wright et al., 2008), $T_{1_{W_{CSF}}} = 4.47$ (Rooney et al., 2007), $T_{1_{Metab}} = 1.29$ (An et al., 2017; Ethofer et al., 2003; Li, 2013; Mlynárik et al., 2001), $T_{2_{W_{WM}}} = 0.003$ (Gelman et al., 1999; Stanisz et al., 2005; Wansapura et al., 1999), $T_{2_{W_{GM}}} = 0.073$(Gelman et al., 1999; Stanisz et al., 2005; Wansapura et al., 1999), $T_{2_{W_{CSF}}} = 2.030$ (Spijkerman et al., 2018), $T_{2_{Metab}} = 0.194$ (An et al., 2017; Li, 2013; Mlynárik et al., 2001; Träber et al., 2004; Wyss et al., 2018).

Appendix C: Tissue Correction Factors Applied to KOA Data (Chapter 5)

Same analysis as **Table 5.5,** but with α corrected concentrations:

Table C.1 *Summary of neurochemical concentrations with testing for group differences between A) osteoarthritis patients to healthy controls (unpaired t-tests) and B) pre- and post-TKA patients (paired t-tests).*

Neurochemical Concentration (mmol/L)	Controls (n=19) mean (SD)	KOA (n=20) mean (SD)	p-values
Anterior Cingulate Cortex			
Glx	16.64 (2.69)	15.33 (3.43)	0.205
Myo	7.25 (1.73)	6.44 (1.7)	0.159
tCho	2.17 (0.3)	2.31 (0.38)	0.221
Anterior Insular Cortex			
Glx	18.85 (2.56)	17.72 (3.32)	0.296
Myo	6 (1.22)	6.44 (1.81)	0.433
tCho	2.22 (0.21)	2.36 (0.52)	0.332
Posterior Insular Cortex			
Glx	16.37 (2.2)	16.72 (2.66)	0.665
Myo	6.94 (1.84)	6.15 (1.74)	0.190
tCho	1.85 (0.29)	1.89 (0.31)	0.676
Somatosensory Cortex			
Glx	14.72 (1.2)	14.74 (1.19)	0.949
Myo	5.86 (1)	5.98 (1.33)	0.748
tCho	1.78 (0.16)	1.89 (0.2)	0.071

Neurochemical Concentration	Pre-TKA (n=14)	Post-TKA (n=14)	p-values
Anterior Cingulate Cortex			
Glx	14.51 (2.97)	17.32 (3.87)	0.080
Myo	5.94 (1.6)	5.97 (1.56)	0.863
tCho	2.27 (0.3)	2.44 (0.23)	0.075
Anterior Insular Cortex			
Glx	17.24 (3.15)	16.86 (2.65)	0.742
Myo	5.78 (1.48)	5.62 (1.25)	0.563
tCho	2.27 (0.43)	2.14 (0.29)	0.416
Posterior Insular Cortex			
Glx	16.66 (2.43)	18 (3.07)	0.356
Myo	5.73 (1.7)	5.72 (2.31)	0.784
tCho	1.89 (0.29)	1.95 (0.27)	0.919
Somatosensory Cortex			
Glx	14.79 (1.27)	14.17 (1.41)	0.350
Myo	5.78 (1.36)	5.43 (0.84)	0.623
tCho	1.86 (0.11)	1.85 (0.16)	0.668

Glx: total glutamate and glutamine; Myo: myoinositol; tCho: total choline; tCr: total creatine; tNAA: N-acetylaspartate

Same analysis as **Table 5.6** but with α corrected concentrations:

Table C.2 *Summary of multiple linear regression coefficients for the model Pain ~ β0 + β1*Neurochemical + β2*Group + β3*Neurochemical*Group, the data were transformed to represent higher sensitivity with higher numbers and lower sensitivity with lower numbers. Statistically significant coefficients (p < 0.05) are denoted with an asterisk (*).*

Neurochemical	**PPT**			**CPM**			**MTS**			**CPT**			**painDETECT**		
	β1	β2	β3	β1	β2	β3	β1	β2	β3	β1	β2	β3	β1	β2	β3
Anterior Cingulate															
Glx	-97.6	**-845.7***	55.2	38.7	213.5	-22.1	-2.5	-25.9	1.9	-2.4	-124.1	2.3	0.0	-13.2	0.3
Myo	50.9	-68.9	-26.8	**-210.7***	**-719.8***	**125.1***	-1.6	-14.7	1.7	6.9	5.3	-16.3	-3.0	**-20.0***	1.7
tCho	41.8	-362.2	81.9	-88.7	-5.8	-24.8	0.0	-15.8	5.8	-8.5	-89.7	-3.3	13.5	3.2	-6.3
Anterior Insula															
Glx	72.4	332.0	-38.8	-48.9	-487.9	33.3	1.0	8.0	-0.8	-12.2	-214.1	9.7	0.0	-10.4	0.0
Myo	104.5	124.6	-62.3	**-166.7***	**-652.5***	**121.7***	-3.6	-10.3	1.8	3.3	-21.4	-12.6	-1.6	-12.8	0.4
tCho	141.8	-377.2	94.1	-374.3	-632.1	274.1	-14.6	-23.9	10.6	-63.3	-172.0	42.1	-4.6	-13.9	1.5
Posterior Insula															
Glx	-18.8	-154.9	-3.3	-9.0	-136.3	8.0	**5.9***	**46.3***	**-4.3***	21.1	113.0	-18.0	**3.4***	12.1	**-1.9***
Myo	-2.8	-238.6	9.7	-46.7	-165.9	24.5	4.0	5.9	-2.0	-19.7	-166.9	13.9	1.7	-4.4	-1.2
tCho	35.7	-141.9	-21.6	-528.6	-583.6	293.2	**32.3***	30.4	-18.7	11.1	-75.0	-10.4	11.5	1.9	-6.8
Somatosensory															
Glx	-211.5	-1352.0	119.1	-28.9	-76.1	5.6	0.7	5.8	-1.0	-11.0	-233.2	15.6	**5.0***	15.3	-2.7
Myo	40.5	-131.7	-19.2	-160.9	-406.4	85.0	4.0	6.7	-2.2	-11.6	-103.3	3.3	3.3	-0.2	-2.2
tCho	172.4	-328.0	77.5	-154.1	-128.5	56.0	-8.8	-16.6	7.5	-257.3	-461.0	211.1	13.7	-1.4	-4.3

PPT: Pain Pressure Thresholds; CPM: Conditioned Pain Modulation; MTS: Mechanical Temporal Summation; CPT: Cold Pressor Tolerance; AC: Anterior Cingulate Cortex; AI: Anterior Insula; PI: Posterior Insula; SS: Somatosensory Cortex; Glx: total glutamate and glutamine; Myo: myoinositol; tCho: total choline.

Same analysis as **Figure 5.3,** but with α corrected concentrations:

Figure C.1 *Univariate analyses of the statistically significant multivariate regression group interactions (from Table C.2) between A) MTS and Glx levels (mmol/L) in the posterior insular cortex, B) painDETECT and Glx levels (mmol/L) in the posterior insular cortex, C) CPM and myoinositol levels (mmol/L) in the anterior cingulate cortex, as well as D) CPM and myoinositol levels (mmol/L) in the anterior insular cortex for controls (circles, purple) and KOA patients (triangles, red). All values were adjusted so that higher values indicated higher pain sensitivity or more centralized pain likelihood. P-values indicate significance for group level univariate relationships between centralized pain and neurochemical concentrations.*

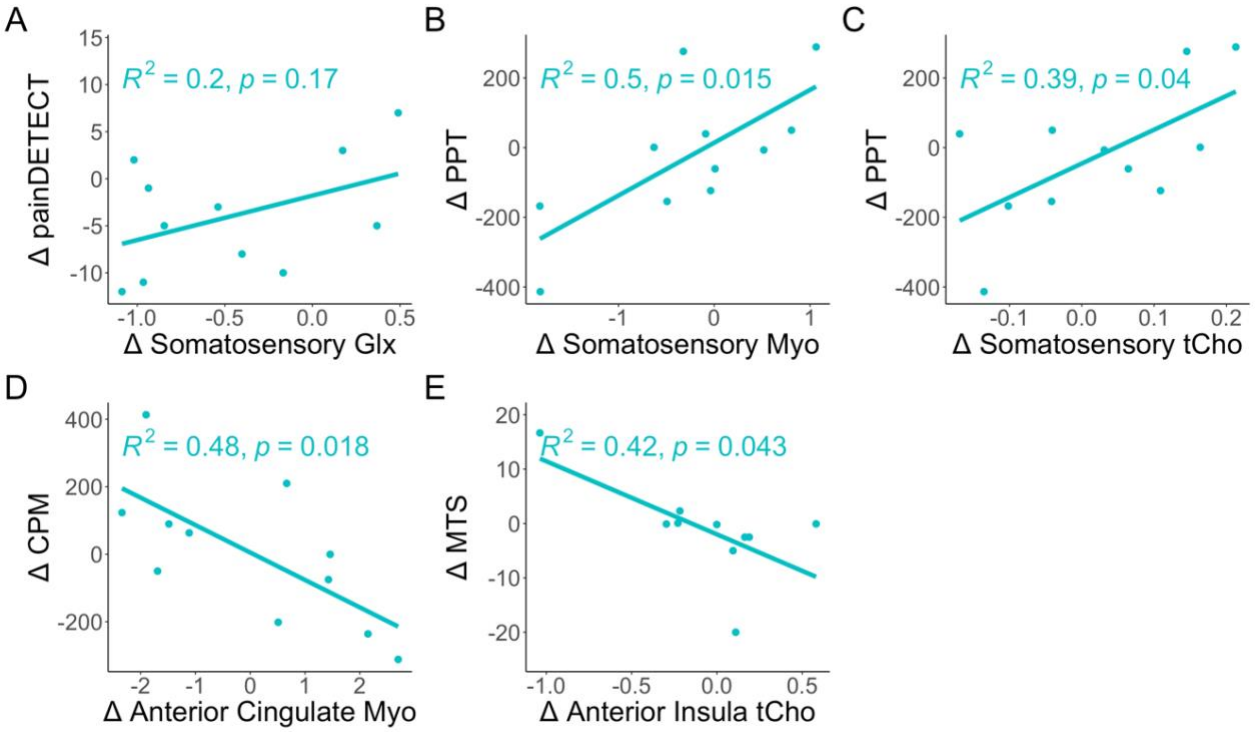

Same analysis as **Figure 5.4,** but with α corrected concentrations:

Figure C.2 *Correlation coefficients between changes in neurochemical levels (mmol/L) and changes in centralized pain metrics post-TKA. (Change calculated as post – pre for both). Red coefficients indicate a positive relationship (i.e., greater pain improvements associated with decreases in neurochemical levels post-TKA compared to pre-TKA). Blue coefficients indicate a negative relationship (i.e., greater pain improvements associated with higher neurochemical levels post-TKA). PPT: Pain Pressure Thresholds; CPM: Conditioned Pain Modulation; MTS: Mechanical Temporal Summation; CPT: Cold Pressor Tolerance; AC: Anterior Cingulate Cortex; AI: Anterior Insula; PI: Posterior Insula; SS: Somatosensory Cortex; Glx: total glutamate and glutamine; Myo: myoinositol; tCho: total choline.*

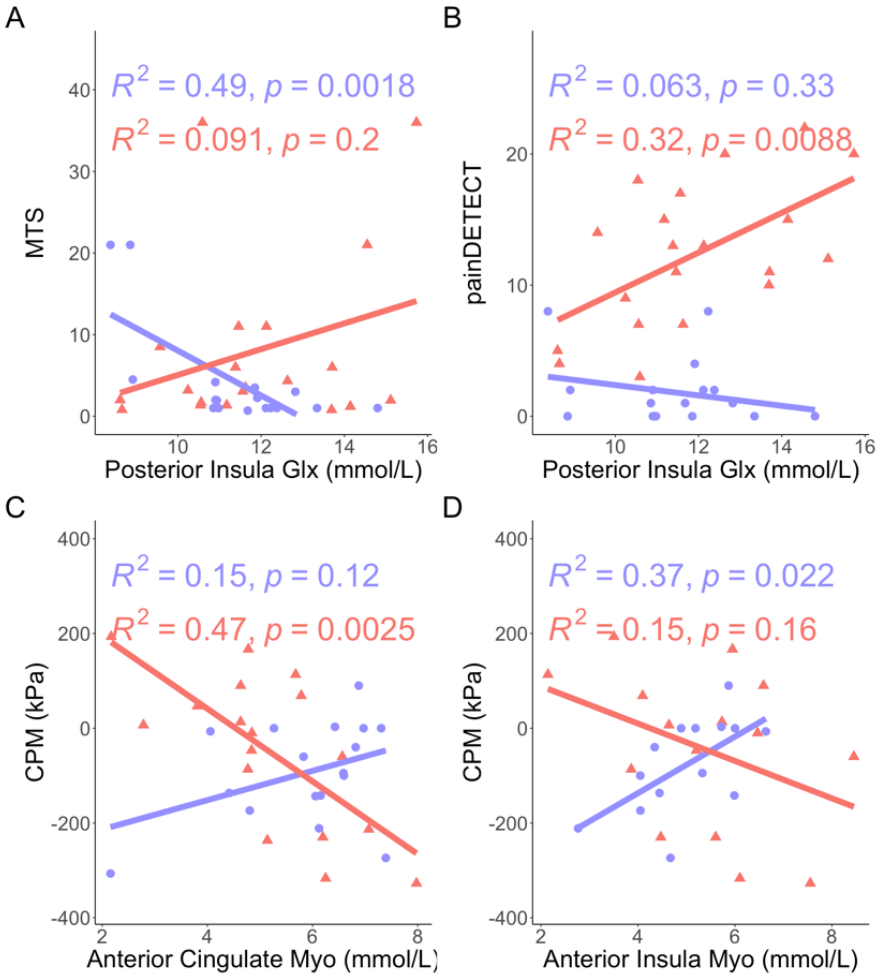

Same analysis as **Figure 5.5**, but with α corrected concentrations:

Figure C.3 *Significant Pearson correlations coefficients between changes in neurochemical levels (mmol/L) and changes in centralized pain measures before and after TKA. (Change calculated as post – pre). All pain measures were adjusted so that lower values indicated improvement in centralized pain measures post-TKA.*